

**Faculty of Science and Engineering  
School of Earth and Planetary Sciences**

**Integrating Zircon Grain Shape Analysis with Detrital Mineral  
Geochronology and Geochemical Fingerprinting, Eucla Basin,  
Australia**

**Gisela Gartmair  
0000-0002-9409-4006**

**This thesis is presented for the Degree of  
Master of Research (Earth and Planetary Sciences)  
of  
Curtin University**

**January 2022**

## **THESIS DECLARATION**

- 1) I, Gisela Sandra Gartmair, declare that this submitted thesis is a hybrid of published work and scientific findings to be submitted for peer review. All of the work presented is the product of my own words and ideas, unless otherwise stated.
- 2) To the best of my knowledge and belief this thesis contains no material previously published by any other person except where due acknowledgement has been made. Work from colleagues contributing to the research output and the completion of this thesis are stated in the author contribution list and meet university regulations for graduating.
- 3) I acknowledge that copyright of published works incorporated in this thesis resides with the copyright holders of those works. Copyrights of my own published work contained within this thesis are held by the journal publisher. I understand that permission to use my work in this thesis meets the journal's copyright policies to satisfy my degree-granting. I duly acknowledge the third-party copyrights of my own work and warrant that the original published journal article will not be made public with this thesis. I further acknowledge that the formatting of this thesis may differ to the format requirements of the publishing journal, and that my own published work incorporated in this thesis may vary in presentation to meet the thesis requirements.
- 4) No material incorporated in this thesis has been accepted for the award of any other degree or diploma in any university globally.

  
Gisela Sandra Gartmair

08/01/2022

\_\_\_\_\_  
Date

## THESIS ABSTRACT

The southern Australian Cenozoic Eucla Basin hosts major heavy mineral placer deposits along regressive palaeostrandlines. Non-unique U-Pb and Hf isotope compositions are identified for likely source regions contributing to the primary detrital zircon age spectra of placer deposits. This research aims to address ambiguities of the basin's detrital zircon sourcing through new heavy mineral compositional and detrital zircon U-Pb and Hf isotope data, with novel integration of zircon grain shape analysis. New detrital zircon data are comparable to published heavy mineral data. Polymodal detrital zircon age spectra express a dominant Mesoproterozoic sediment provenance, with secondary contributions from late Archean to the early Phanerozoic-aged sources. A distinct mineral system is identified for the western basin margin, indicative of restricted sediment supply and sediment reworking (Albany-Fraser Orogen and Yilgarn Craton). Northern and eastern shoreline margins are associated with a more complex mineral system of increased sediment source rock variability and multi-cycle reworking (Musgrave, Madura and Coompana provinces, Albany-Fraser Orogen, Yilgarn and Gawler cratons). Application of a Shannon-Weaver population diversity test quantifies detrital zircon source region heterogeneity which proxies progressive enrichment of beach placers along palaeoshorelines from west to east. Progressive enrichment is associated with proximal subordinate sediment contributions (Gawler Craton) and multi-sourced resistate mineral retention following increased sediment transportation and intermixing. Hf isotope data of Mesoproterozoic-aged detrital zircon grains of northern and eastern prospects highlight a dominant juvenile magmatic source (northern lying Musgrave Province or underlying Madura and Coompana provinces). Non-uniqueness in U-Pb and Hf isotope characteristics are resolved through zircon grain shape analysis. Eight shape parameters (*area, perimeter, major and minor axes, effective diameter, circularity, roundness, and aspect ratio*) are captured across a suite of Eucla Basin detrital zircon grains and Madura Province and Coompana Province crystalline zircon samples and are incorporated with published zircon grain shape data. Distinct zircon shape characteristics are identified for Eucla Basin Mesoproterozoic source regions, i.e., *perimeter* (Madura and Coompana provinces vs Musgrave Province), *major axis* (Madura and Coompana provinces vs Albany-Fraser Orogen), and *circularity* (Musgrave Province vs Albany-Fraser Orogen). Integrated filter analysis (U-Pb, Hf

isotope and grain shape analysis) of ~1400–1000 Ma-aged juvenile detrital zircon grains highlight the Madura and Coompana provinces as the dominant sediment sources for the northern and eastern Eucla Basin beach placers. Detrital reworking through intermediate sedimentary systems is implicated as an important mechanism for heavy mineral enrichment in sands. *Circularity* differentiates detrital versus crystalline zircon grains, a reflection of extensive transportational (re)working.

## ACKNOWLEDGEMENTS

I would like to thank several key individuals involved in the research journey and the completion of this thesis.

### *My Supervisors*

I truly thank *Milo Barham* and *Chris Kirkland* from the School of Earth & Planetary Sciences, Curtin University, for their guidance and support throughout the last years while working on this research project. You two introduced me to a whole new world that research is. Thank you for letting me learn from you and for boosting my confidence when I needed it. Your guidance and feedback were invaluable. Milo, special thanks for your late-night proof-reading, the countless phone calls you answered and for understanding that sometimes the only way forward is by heading to the trails first.

### *Contributors, Sponsors, Curtin University Staff and HDR Students*

I would like to express my gratitude to *Dr. Anthony Reid* from the Geological Survey of South Australia for providing transmitted light images that played an integral part of my research project. I also would like to acknowledge the *Mineral Research Institute of WA* (MRIWA) for providing the M551 grant, and *Curtin University* for the Master of Research (MRes) Stipend Scholarship. *Noreen Evans* and *Bradley McDonald* from the John de Laeter Centre (JdLC) at Curtin University are thanked for their laboratory help in conducting the laser ablation (LA-ICPMS) on my study samples. I would like to mention that the Tescan Mira3 TIMA at the JdLC was funded using the ARC LIEF grant LE140100150. The LA-ICPMS instrument in the JdLC, Curtin University, was funded via an Australian Geophysical Observing System grant provided to AuScope Pty Ltd. by the AQ44 *Australian* Education Investment Fund program. I further would like to thank my Master of Research course coordinator *Nick Timms* for his ongoing support in the last years, and students and professionals from the *Timescales of Mineral Systems Group* at Curtin University. Being part of this research team was a great motivator. I also would like to mention fellow HDR students *Taryn Scharf*, *Isabel Zutterkirch* and *Maximilian Dröllner*. Sharing cups of teas and coffees, bouncing off ideas, and getting support when I felt stuck was truly helpful. I

*G. Gartmair*

wish you all the best of luck in your research journey and I am looking forward to reading about your successes!

### **Iluka Resources Ltd.**

As a student I would like to acknowledge Iluka Resources Ltd. for the provision of sample material upon which this research project was based. Iluka representatives **Rohan Hine** and **David Sleigh** are thanked for their time and efforts to engage in regular meetings and for delivering constructive feedback. Now, as an employee at Iluka, I particularly thank my managers **Rohan Hine** and **Tess Reynolds** for giving me work flexibility and looking after me, especially during the stressful times of the thesis write-up. Your support and trust in me mean a lot.

### **My Family and Friends**

I am immensely grateful for my love **Stuart** for the ongoing support over the last 12 years. Especially in the last few months, when quality time was limited and the stress of working and studying occasionally became too overwhelming, your kind words and hugs kept me going. Thank you also for all the countless dinners you cooked, the emergency drives to town to find last-minute chocolates, and for taking care of our furry kids while I was working on this thesis. Thank you! I also would like to thank **my family** in Germany. Despite the distance I felt your love and support! My lovely neighbours **Jan** and **Joe** are thanked for everything they have done to help when time was not on my side. You are like parents to me! **Simon**, my trusted friend in Germany, is thanked for setting up an impromptu study for when I came to visit and needed to keep working on my research project, **Claire** for helping me out when I got stuck with software, and **Franzi** for being a true German friend here on the other side of the world! Thank you also to my two dogs, for (likely not) understanding why the walks have gotten shorter recently. I promise I will make up for it.

*Thank you to my mum – gone too early –  
for always being by my side and giving me comfort.*

## COPYRIGHT STATEMENT

Chapter Two of this thesis contains published work, titled *Detrital Zircon Perspectives on Heavy Mineral Sand Systems, Eucla Basin, Australia*, by the authors Gisela Gartmair, Milo Barham, and Christopher L. Kirkland.

A copyright agreement is signed by the lead author (myself) – Gisela Gartmair – on behalf of all authors. Any copyright privileges and rights of the published paper are held by the Society of Economic Geology (SEG).

The journal article is accessible through <https://doi.org/10.5382/econgeo.4871> and via SEG ([segweb.org](http://segweb.org)).




Violation of the copyright associated with the published journal article, in any form or media, is without my consent.

\_\_\_\_\_  
  
Gisela Sandra Gartmair




08/01/2022  
\_\_\_\_\_  
Date

## AUTHOR ATTRIBUTIONS

This hybrid thesis contains published work and work being prepared for publication. Chapter Two comprises the published journal article “Detrital Zircon Perspectives on Heavy Mineral Sand Systems, Eucla Basin, Australia”. Chapter Three contains the work of a second journal article currently undergoing final preparation for peer review, with the title “Refining Zircon Provenance Interpretation Via Integrated Grain Shape, Geochronology, and Hf Isotopes, a Case Study from the Eucla Basin, Australia”. Both articles were prepared and written by Gisela Gartmair (lead author), Dr. Milo Barham (principal supervisor), and Prof. Christopher L. Kirkland (second supervisor). Each author’s contributions to the final journal articles are listed.

<i>Detrital Zircon Perspectives on Heavy Mineral Sand Systems, Eucla Basin, Australia</i>									
	Project Conception and Design	Project Funding	Sample Acquisition	Sample Analyses	Data Analyses	Interpretation and Discussions	Writing – Original Drafts	Draft Proof-Reading and Corrections	Total % Contribution to Thesis
<b>First Author G. Gartmair</b>	0	0	0	35	90	80	93	0	75
Principal Author Acknowledgment: I acknowledge that these represent my contribution to the above research output									
Signed:  Date: 30 July 2021									
<b>Co-Author 1 Dr. M. Barham</b>	50	70	100	65	5	15	5	50	19
Principal Author Acknowledgment: I acknowledge that these represent my contribution to the above research output									
Signed:  Date: 30 July 2021									
<b>Co-Author 2 Prof. C. Kirkland</b>	50	30	0	0	5	5	2	50	6
Principal Author Acknowledgment: I acknowledge that these represent my contribution to the above research output									
Signed:  Date: 30 July 2021									
<b>Total Percentage (%)</b>	100	100	100	100	100	100	100	100	100



<i>Refining Zircon Provenance Interpretation via Integrated Grain Shape, Geochronology, and Hf Isotopes, a Case Study from the Eucla Basin, Australia</i>									
	Project Conception and Design	Project Funding	Sample Acquisition	Sample Analyses	Data Analyses	Interpretation and Discussions	Writing – Original Drafts	Draft Proof-Reading and Corrections	Total % Contribution to Thesis
First Author <b>G. Gartmair</b>	0	0	0	35	90	80	93	0	75
Principal Author Acknowledgment: I acknowledge that these represent my contribution to the above research output									
Signed:  Date: 31 December 2021									
Co-Author 1 <b>Dr. M. Barham</b>	50	70	100	65	5	15	5	75	20
Principal Author Acknowledgment: I acknowledge that these represent my contribution to the above research output									
Signed:  Date: 31 December 2021									
Co-Author 2 <b>Prof. C. Kirkland</b>	50	30	0	0	5	5	2	25	5
Principal Author Acknowledgment: I acknowledge that these represent my contribution to the above research output									
Signed:  Date: 31 December 2021									
<b>Total Percentage (%)</b>	<b>100</b>	<b>100</b>	<b>100</b>	<b>100</b>	<b>100</b>	<b>100</b>	<b>100</b>	<b>100</b>	<b>100</b>

## **ACKNOWLEDGEMENT OF COUNTRY**

As a student at the School of Earth and Planetary Sciences, I would like to acknowledge that Curtin University works across hundreds of traditional lands and custodial groups in Australia, and with First Nations people around the globe. We wish to pay our deepest respects to their ancestors and members of their communities, past, present, and to their emerging leaders. Our passion and commitment to work with all Australians and peoples from across the world, including our First Nations peoples are at the core of the work we do, reflective of our institutions' values and commitment to our role as leaders in the Reconciliation space in Australia.

## TABLE OF CONTENTS

THESIS DECLARATION.....	i
THESIS ABSTRACT .....	ii
ACKNOWLEDGEMENTS .....	iv
COPYRIGHT STATEMENT .....	vi
AUTHOR ATTRIBUTIONS.....	vii
ACKNOWLEDGEMENT OF COUNTRY .....	ix
TABLE OF CONTENTS.....	x
LIST OF FIGURES .....	xii
LIST OF TABLES .....	xvi
LIST OF SUPPLEMENTARY DATA.....	xviii
CHAPTER ONE .....	1
1. Introduction .....	1
2. Research Motivation, Aims and Objectives .....	3
3. Thesis Structure .....	4
Chapter One Reference List .....	7
CHAPTER TWO .....	9
Detrital Zircon Perspectives on Heavy Mineral Sand Systems, Eucla Basin, Australia .....	9
Abstract .....	9
1. Introduction .....	9
2. Geologic Background.....	15
2.1 Sedimentation and prospectivity of the Eucla Basin .....	15
3. Samples and Methods.....	16
3.1 Sample selection .....	16
3.2 Sample preparation .....	17
3.3 Analytical methodology.....	17
4. Results .....	18
4.1 Mineral composition.....	18
4.2 U-Pb geochronology .....	19
5. Discussion .....	21
5.1 Identification of source region lithology and source proximity using heavy mineral compositions.....	21
5.2 Detrital zircon provenance in the Eucla Basin.....	22

5.3 Provenance fingerprinting of Eucla Basin deposits.....	29
5.4 Characterising heavy mineral prospectivity and heavy mineral maturation through detrital zircon population analysis.....	35
5.5 Heavy mineral age spectra implications for exploration targeting.....	37
6. Conclusions .....	39
Acknowledgements .....	40
Chapter Two Reference List.....	41
CHAPTER THREE.....	54
Refining Zircon Provenance Interpretation via Integrated Grain Shape, Geochronology, and Hf Isotopes, a Case Study from the Eucla Basin, Australia .	54
Abstract .....	54
1. Introduction .....	55
2. Geologic Background.....	57
3. Samples and Methods.....	60
3.1 Sample selection .....	60
3.2 Sample preparation .....	62
3.3 Analytical methodology.....	62
4. Results .....	67
4.1 Detrital zircon Hf geochemistry of newly analysed prospect samples.....	67
4.2 Zircon grain shape analyses.....	69
5. Discussion .....	72
5.1 Hf isotope composition analysis of Eucla Basin heavy mineral samples.....	72
5.2 Zircon grain shape analysis for sediment provenance studies.....	74
5.3 Refined mineral system approach using integrated U-Pb, Hf isotopes and grain shape analysis .....	78
5.4 Implications for future sediment provenance studies and heavy mineral prospectivity models.....	86
6. Conclusions .....	87
Acknowledgements .....	88
Chapter Three Reference List.....	89
CHAPTER FOUR.....	98
Research Conclusions.....	98

## LIST OF FIGURES

The figures listed are ordered based on their occurrence in this thesis and are linked to the individual chapters. Figures from the journal article *Detrital Zircon Perspectives on Heavy Mineral Sand Systems, Eucla Basin, Australia* (Chapter Two) are numbered starting with 2. Figures relating to the second article *Refining Zircon Provenance Interpretation via Integrated Grain Shape, Geochronology, and Hf Isotopes, a Case Study from the Eucla Basin, Australia* (Chapter Three) are identified with the number 3. Tables and supplementary data follow the same convention throughout this thesis.

### Chapter Two

- Figure 2.1 Digital Elevation Model (a) and map (b) of the Eucla Basin with surrounding and underlying sediment source regions. Shoreline successions are shown (Hou et al., 2011; Reid et al., 2013b). Heavy mineral prospects sampled in this study shown in red font. Black prospect names denote previously published results (sample 1039436, Reid & Hou, 2006; sample 1688513, Hou et al., 2011; samples 1688514, 1688515, 1841639, 1924226, 1924258, 1924236, 1688510, 1688512 and 1688511, Reid et al., 2013a; App. Table 2.2). Colour coding of deposit markers consistent with Figure 2.6. Geologic boundaries based on Geoscience Australia (<http://www.ga.gov.au>). Onshore extent of Cenozoic Eucla Basin highlighted in yellow. AB = late Palaeozoic Arckaringa Basin, AFO = Mesoproterozoic Albany-Fraser Orogen, CP = Mesoproterozoic Coompana Province, DB = Permian Denman Basin, EB = Mesozoic Eromanga Basin, GC = Archean Gawler Craton, MGP = Mesoproterozoic Musgrave Province, MP = Mesoproterozoic Madura Province, MS = Cretaceous Madura Shelf, NT = Northern Territory, OB = Neoproterozoic Officer Basin, SA = South Australia, WA = Western Australia, YC = Archean Yilgarn Craton. .... 11
- Figure 2.2 Normalised mineral composition output from TESCAN integrated mineral analysis of the heavy mineral concentrates of eight newly dated samples. HM = heavy mineral. .... 19

Figure 2.3 Cumulative age distribution plot of concordant age data ( $\pm 10\%$ discordance) of the eight newly analysed heavy mineral samples. Multiple samples of a deposit are grouped by colour. ....	21
Figure 2.4 Stacked detrital zircon age spectra of Eucla Basin deposits analysed in this study. Deposit names in bold with grey fill spectra represent newly dated samples. Archived detrital zircon age data from the prospects Balladonia, Cyclone, Thar, Jacinth (sample 1924226), Atacama, Tripitaka (sample 1688510), Dromedary and Gullivers (Reid et al., 2013a), Jacinth (sample 1688513; Hou et al., 2011), and Notrab (Reid & Hou, 2006) are presented with white fill colour. Prospects with several samples (coloured age spectra lines) are combined to a single age spectrum (black age spectra lines). ....	24
Figure 2.5 Schematic mineral systems model of Eucla Basin palaeoshorelines indicating primary and secondary sediment supply and intermixing regimes from crystalline and intermediate reservoir sources. Increasing resistant heavy mineral maturation from west to east is associated with increased detrital age polymodality and heavy mineral grades of Eucla Basin beach placers. Colour coding of deposit markers consistent with Figure 2.6. HM = heavy mineral. ....	27
Figure 2.6 Pie charts (a) and multi-dimensional scaling (b) using detrital zircon age spectra of all prospects incorporated in this study. Pie charts representing percentages of zircon age ranges of the total zircon age population of Eucla Basin prospects identified through kernel density estimates (Fig. 2.4). Gobi background sample AD550079 excluded from the analysis. ....	34
Figure 2.7 Box plot of Shannon-Weaver diversity index coloured according to detrital zircon population similarities (Fig. 2.6). Peak and low heavy mineral grades of newly dated samples (highlighted in bold) from Table 2.1. Gobi background sample AD550079 excluded from the analysis. Amb = Ambrosia, Ata = Atacama, HM = heavy mineral, Trip = Tripitaka. ....	36

Chapter Three

Figure 3.1 Inset map with schematic overview of potential surrounding and underlying Eucla Basin sediment source regions (a) and satellite image with sample locations and overlain geological boundaries (b). Source region map modified after Gartmair et al. (2022). Deposits with heavy mineral samples analysed for Hf isotope characteristics shown in yellow (excluding Atacama). Published heavy mineral sample data from Reid & Hou (2006), Hou et al. (2011), Reid et al. (2013a, b) and Jagodzinski et al. (2018). AB = late Palaeozoic Arckaringa Basin, AFO = Mesoproterozoic Albany-Fraser Orogen, CP = Mesoproterozoic Coompana Province, DB = Permian Denman Basin, EB = Mesozoic Eromanga Basin, GC = Archean Gawler Craton, MGP = Mesoproterozoic Musgrave Province, MP = Mesoproterozoic Madura Province, MS = Cretaceous Madura Shelf, NT = Northern Territory, OB = Neoproterozoic Officer Basin, SA = South Australia, WA = Western Australia, YC = Archean Yilgarn Craton.....58

Figure 3.2 Hf isotope results from newly analysed heavy mineral samples (a-h). New Hf data overlain on published Eucla Basin heavy mineral Hf isotope data (i) (Reid et al., 2013b). Depleted mantle and chondritic uniform reference (CHUR) references from Spencer et al. (2020).....68

Figure 3.3 Detrital zircon Hf isotope data of Eucla Basin heavy mineral samples within the dominant age interval 1400-1000 Ma (this study; Reid et al., 2013b) overlain on published crystalline zircon Hf isotope data from the Albany-Fraser Orogen (Kirkland et al., 2011a; Spaggiari et al., 2015; Hartnady, 2019; Mole et al., 2019), the Musgrave Province (Kirkland et al., 2013), and the Madura and Coompana provinces (Kirkland et al., 2017; Hartnady et al., 2020). Regions (a - f) based on distinct U-Pb and Hf characteristics to distinguish source regions (Table 3.5).....73

Figure 3.4 Kolmogorov-Smirnov distance-based multidimensional scaling (MDS) analysis of *circularity* shape parameter analysed from detrital and crystalline zircon samples (Tables 3.1, 3.2, 3.3). Unfilled circles represent detrital zircon samples, red circles indicate crystalline Coompana Province

zircon grains. Amb\_228 = Ambrosia AD605228, Amb\_248 = Ambrosia AD605248, Amb\_251 = Ambrosia AD605251, Amb\_589 = Ambrosia AD605589, Ata\_236 = Atacama 1924236, Ata\_258 = Atacama 1924258, Ata\_711 = Atacama AD443711, Ata\_727 = Atacama AD443727, Ata\_731 = AD443731, Ata\_869 = Atacama AD458869, Ata\_878 = Atacama AD457878, Bal = Balladonia, Bun = Bunburra Suite (2423700, 2423705), Cyc = Cyclone, Gia = Giants Head Suite (2430064, 2498072), Gob\_079 = Gobi AD550079, Gob\_520 = Gobi AD550520, Jac = Jacinth, Koo = Koonalda Suite (2423713, 2423713\_534, 2423713\_828), Koom = Koomalboogurra Suite (2132936, 2425443, 2427076), Mer = Merdayerrah Shoshonite (2425514), Moo = Undifferentiated Moodini Supersuite (2132968, 2425514, 2427070), Noo = Noorina palaeochannel, Obs = Observatory Hill Beds, Tha = Thar, Tra = Trainor Hill Sandstone, Tri\_778 = Tripitaka AD376778, Wan = Wanna.....78

Figure 3.5 Box and whisker plots of grain shape parameters perimeter (a), major axis (b) and circularity (c) measured from 1400–1000 Ma dated crystalline zircon grains from Albany-Fraser Orogen (Makuluni et al., 2019), Musgrave Province (Markwitz & Kirkland, 2018) and Madura and Coompana provinces (this study; Makuluni et al., 2019). Box outlines show the 25 – 75 percentiles of shape data for each provenance-specific sample set. Median values of data are presented as horizontal lines inside the box. Short horizontal lines (‘whiskers’) outside the box outlines represent minimal and maximal values of data sets. Values from grain shape data (App. Table 3.5). Giants Head Suite samples (2430064 and 2498072) excluded from analysis.....80

Figure 3.6 Schematic summary figure and pie chart representation of dominant Mesoproterozoic source region contribution to Eucla Basin heavy mineral placer deposits based on integrated geochronology, Hf-isotope and grain shape filtering (Fig. 3,3; Table 3.5).....85



## LIST OF TABLES

### Chapter Two

Table 2.1 Summary of samples analysed in this study with overview of heavy mineral (HM) grade, mineralisation zones and sedimentary descriptions from reverse circulation and air core drilling assays .....	14
Table 2.2 Reinterpretation of Eucla Basin depositional shoreline settings of prospects analysed in this study from digital elevation model analysis.....	30
Table 2.3 Kolmogorov-Smirnov distance matrix with probability values of all heavy mineral prospects and deposits analysed. Matrix values calculated using ages of concordant zircon grains with corresponding error; varying text styles representing increasing differences among samples ( $D \leq 0.2$ = normal; $D > 0.2$ = <u>underlined</u> ); cells representing p-values of statistical significance between samples ( $p \leq 0.05$ ) highlighted in bold font .....	32

### Chapter Three

Table 3.1 Overview of heavy mineral samples analysed in this study for detrital zircon Lu-Hf geochemistry and detrital zircon grain morphology. Samples previously analysed for U-Pb geochronology in Gartmair et al. (2022). Atacama samples (marked in grey colour) analysed for grain shapes only. HM = heavy mineral.....	61
Table 3.2 Overview and description of shape parameters used for zircon grain shape analysis.....	66
Table 3.3 Schematic zircon representation of crystalline basement suites using grain shape median major and minor axes values of zircon grains analysed from Coompana Province samples. Values based on all grains analysed for the geological unit, including dated and non-dated grains. Age information and geological unit categorisation from Jagodzinski et al. (2018) and after Pawley et al. (2020).....	71

Table 3.4 Kolmogorov-Smirnov distance matrix comparing grain shape populations between source regions specifically for grains aged 1400–1000 Ma from the Albany-Fraser Orogen (Makuluni et al., 2019), the Musgrave Province (Markwitz & Kirkland, 2018) and the Madura and Coompana provinces (this study; Makuluni et al., 2019). Values in bold represent the most significant distance and probability values of distinct shape parameters to differentiate source regions. D = Distance values, p = Probability values. Giants Head Suite samples (2430064 and 2498072) excluded from analysis.....79

Table 3.5 Detrital provenance filter analysis using integrated U-Pb, Hf isotope and grain shape data. Filtering of data based on Fig. 3.3 and Table 3.4. Cells with bold text indicate detrital grains matching with data from Mesoproterozoic source regions. Percentages of grain contributions rounded to whole number. Filter = filter regions identified from integrated U-Pb, Hf isotope and grain shape filter analysis (Fig. 3.3). AFO = Albany-Fraser Orogen, Ci = circularity, MaA = major axis, MCP = Madura-Coompana provinces, MP = Musgrave Province, P = perimeter .....82

## LIST OF SUPPLEMENTARY DATA

Supplementary data of this thesis are provided electronically

<https://www.dropbox.com/sh/4d93xliy4q8791o/AADkbRiC36kfP0juX6HuNW5pa?dl=0>

### *Chapter Two*

App. 2.1 TESCAN integrated mineral analyser with integrated energy dispersive X-ray spectroscopy and backscattered electron imaging of the eight newly dated samples analysed in this study.

App. Fig. 2.1 Concordia diagrams of the eight LA-ICPMS U-Pb dated samples from the prospects Wanna, Ambrosia, Tripitaka, and Gobi. Data are filtered to  $\pm 10\%$  discordance. Green colour representing concordant data, red colour showing discordant ages.

App. Table 2.1 Dominant ages of crystalline regions and age modes within intermediate sedimentary reservoirs as likely detrital zircon sources for Eucla Basin heavy mineral sands. Yellow highlighted age intervals represent primary and secondary age modes observed in Eucla Basin heavy mineral prospect age spectra (Fig. 1.4). Geographically relevant lithologies that overlap in ages with detrital zircon ages of Eucla Basin prospect age spectra are highlighted. Ages in brackets indicate peak ages for the given interval.

App. Table 2.2 Previously U-Pb dated samples included in this study. Samples are geographically sorted from west to east using longitude coordinates.

App. Table 2.3 Summary of secondary zircon reference materials analysed from three different analytical sessions in this study.

App. Table 2.4 U-Pb geochronology data of the eight samples analysed in this study.

App. Table 2.5 Overview of minimum and maximum single grain ages and dominant age modes of the eight heavy mineral samples. Minimum and maximum single grain ages and modal ages were calculated using Age Pick Program (Gehrels, 2009). Age mode ranges were generated for populations  $\geq 5$  grains.

App. Table 2.6 Kolmogorov-Smirnov distance (D) matrix with probability values (p) of prospects with multiple intradeposit samples. Matrix values calculated using cumulative distribution function of concordant zircon grains with corresponding error. Varying text styles representing increasing differences among samples ( $D \leq 0.2$  = normal;  $D > 0.2$  = underlined); cells representing p-values of statistical significance between samples ( $p \leq 0.05$ ) highlighted in bold font. Amb. = Ambrosia, Ata. = Atacama, Gob. = Gobi, Jac. = Jacinth, Trip. = Tripitaka.

### Chapter Three

App. 3.1 TESCAN integrated mineral analyser with integrated energy dispersive X-ray spectroscopy and backscattered electron imaging of the eight newly analysed samples in this study.

App. Fig. 3.1 Grain shape extraction procedure applied to transmitted light images and filtered TIMA images from detrital and crystalline zircon samples analysed in this study (Tables 3.1, 3.2, 3.3). Grains were analysed using processing application Fiji (Schindelin et al., 2012), with shape descriptor plugin (Syverud et al., 2007) of the Image J software (Schneider et al., 2012; Rueden et al., 2017). Example provided from detrital heavy mineral sample Atacama 1924236 (Reid et al., 2013a). a = 8-bit binary image conversion, b = image thresholding, c = filling of grains, d = watershed segmentation, e = exclusion of unsuitable grains, f = outline drawings of zircon grain shapes.

App. Fig. 3.2 Bar chart representation of dominant shape characters identified through Principal Component Analysis (PCA) across zircon sample sets. High positive loadings represent dominant shape parameters that best describe the dispersion of data across zircon grain shape populations. Low positive and negative loadings represent zircon shape parameters of lesser importance. Bars showing principal component 1 with > 50% of the variance represented.

App. Fig. 3.3 Kolmogorov-Smirnov distance-based multidimensional scaling analysis of shape parameters analysed from detrital non-heavy mineral enriched, and heavy mineral enriched zircon samples. Amb\_228 = Ambrosia AD605228, Amb\_248 = Ambrosia AD605248, Amb\_251 = Ambrosia AD605251, Amb\_589 = Ambrosia AD605589, Ata\_236 = Atacama 1924236, Ata\_258 = Atacama 1924258, Ata\_711 = Atacama AD443711, Ata\_727 = Atacama AD443727, Ata\_731 = AD443731, Ata\_869 = Atacama AD458869, Ata\_878 = Atacama AD457878, Bal = Balladonia, Cyc = Cyclone, Gob\_079 = Gobi AD550079, Gob\_520 = Gobi AD550520, Jac = Jacinth, Noo = Noorina palaeochannel, Obs = Observatory Hill Beds, Tha = Thar, Tra = Trainor Hill Sandstone, Tri\_778 = Tripitaka AD376778, Wan = Wanna. Non-HM sample = detrital non-heavy mineral enriched sample, Generic HM sample = Heavy mineral sample with no known heavy mineral grade, Peak HM sample = heavy mineral peak sample, Low-grade HM sample = lower-grade heavy mineral sample.

App. Fig. 3.4 Kolmogorov-Smirnov distance-based multidimensional scaling (MDS) analysis of shape parameters analysed from all detrital and crystalline zircon samples (Tables 3.1, 3.2, 3.3). Unfilled circles represent detrital zircon samples, red circles indicate crystalline Coompana Province zircon grains. Amb\_228 = Ambrosia AD605228, Amb\_248 = Ambrosia AD605248, Amb\_251 = Ambrosia AD605251, Amb\_589 = Ambrosia AD605589, Ata\_236 = Atacama 1924236, Ata\_258 = Atacama 1924258, Ata\_711 = Atacama AD443711, Ata\_727 = Atacama AD443727, Ata\_731 = AD443731, Ata\_869 = Atacama AD458869, Ata\_878 = Atacama AD457878, Bal = Balladonia, Bun = Bunburra Suite (2423700, 2423705), Cyc = Cyclone, Gia = Giants Head Suite (2430064, 2498072), Gob\_079 = Gobi AD550079, Gob\_520 = Gobi AD550520, Jac = Jacinth, Koo = Koonalda Suite (2423713, 2423713\_534, 2423713\_828), Koom = Koomalboogurra Suite (2132936, 2425443, 2427076), Mer = Merdayerrah Shoshonite (2425514), Moo = Undifferentiated Moodini Supersuite (2132968, 2425514, 2427070), Noo = Noorina palaeochannel, Obs = Observatory

Hill Beds, Tha = Thar, Tra = Trainor Hill Sandstone, Tri\_778 = Tripitaka AD376778, Wan = Wanna.

App. Fig. 3.5 Box and whisker plots of grain shape parameters measured from crystalline zircon grains aged 1400–1000Ma from the Albany-Fraser Orogen (Makuluni et al., 2019), Musgrave Province (Markwitz & Kirkland, 2018) and Madura and Coompana provinces (this study; Makuluni et al., 2019). Box outlines show the 25 – 75 percentiles of shape data for each provenance-specific sample set. Median values of data are represented as horizontal lines inside the box. Short horizontal lines (‘whiskers’) outside the box outlines represent minimal and maximal values of data sets. Giants Head Suite samples (2430064 and 2498072) excluded from analysis.

App. Table 3.1 Overview of heavy mineral (HM) samples and sedimentary non-heavy mineral (non-HM) samples incorporated in this study. Detrital zircon grain shape analysis performed on highlighted samples.

App. Table 3.2 Overview of Coompana Province basement samples analysed for zircon grain shapes in this study. Zircon U-Pb geochronology analysed by Jagodzinski et al. (2018), zircon Lu-Hf geochemistry analysed by Hartnady et al. (2020). Stratigraphic units updated and newly defined by Pawley et al. (2020).

App. Table 3.3 Summary of secondary zircon Hf isotope reference materials analysed in this study.

App. Table 3.4 Hf isotope geochemical data of the eight heavy mineral samples analysed in this study. U-Pb ages from Gartmair et al. (2022).

App. Table 3.5 Shape data of detrital and crystalline zircon grains analysed from heavy mineral enriched and non-enriched samples, and from the Coompana Province. Samples analysed based on Table 3.1; App. Tables 3.1, 3.2.

App. Table 3.6 Summary statistics and normality testing of shape parameters of zircon grains sampled from heavy mineral, sedimentary non-heavy mineral and crystalline data sets analysed in this study (Table 3.1; App. Tables 3.1, 3.2). Sedimentary heavy mineral samples marked

with \* were bulk mounted. Unmarked sedimentary samples were hand-picked. Shapiro Wilk normality test p-values showing normal data distribution ( $p > 0.05$ ) are highlighted.

# CHAPTER ONE

## 1. Introduction

Southern Australia's Eucla Basin has become a heavy mineral sand exploration target, following the discovery of world-class placer deposits and the subsequent development of the world's largest operating zircon mine Jacinth-Ambrosia (Hou et al., 2011; Iluka Resources Limited, 2021; Fig. 2.1a). The Eucla Basin exhibits distinct regressive palaeoshorelines and barrier systems that host extensive heavy mineral accumulations, specifically along the basin's northern and north-eastern margins (Hou et al., 2011; Fig. 2.1a). Despite ongoing extensive exploratory drilling along the basin's palaeoshores, new large-scale deposits have not been identified in recent years. Research efforts on the basin's heavy mineral sand deposits and sediment provenance are limited and predate geological analysis of the underlying crystalline basement to the region (Madura Province and Coompana Province; Fig. 2.1b); thus, much of the basin's depositional history and sedimentary source to sink pathways remain poorly understood. A comprehensive understanding of the routing of Eucla Basin heavy minerals from source rock to final deposition and accumulation site is an important step in the success of future exploration targeting. Heavy mineral sand mineral exploration relies on an extensive understanding of the sedimentary system, to identify likely depositional settings of mineralisation and is becoming increasingly difficult as most near-surface deposits have already been exploited (Kullerud, 2003). Advances in research and technology are crucial to the success of future exploration efforts (in the Eucla Basin and globally) to help identify and process deeper lying mineral ore zones (Kullerud, 2003; Kesler, 2007). Research on heavy mineral systems often incorporate extensive sediment provenance studies which commonly apply detrital zircon geochronology to resolve source to sink histories through age-matching of detrital zircons with zircons grains from likely source regions (e.g., Sircombe & Freeman, 1999; Gehrels et al., 2011; Reid et al., 2013a). Difficulties in resolving sediment provenance across age-overlapping source regions can be addressed by additional application of zircon Hf isotope analyses to identify differences in geochemical signatures of grains (e.g., Reid et al., 2013b; Barham et al., 2018; Sundell & Saylor, 2021). Zircon grains are commonly utilised in sediment provenance investigations as



they are particularly suitable to reconstruct source to sink pathways because of their high resistance to chemical-mechanical alteration from weathering and erosion processes, and their ability to preserve age and geochemical characteristics through overprinting metamorphic events (Fedo et al., 2003). Previous sediment provenance analyses of detrital heavy mineral samples from the Eucla Basin were predominantly limited to U-Pb zircon geochronological studies (Reid & Hou, 2006; Hou et al., 2011; Reid et al., 2013a), with only one study additionally investigating the Hf isotope composition of zircon in these placer deposits (Reid et al., 2013b). Initial detrital zircon U-Pb investigation indicated a polymodal detrital zircon age spectra with a dominant Mesoproterozoic age mode of ~1300 - 1100 Ma across northern, north-eastern, and eastern deposits, and a slightly older dominant age mode population signature for far western mineral sand accumulations (Reid & Hou, 2006; Hou et al., 2011; Reid et al., 2013a). Preliminary sediment provenance interpretations based on geochronological data inferred a dominant Musgrave Province derived sediment supply intermixed with minor Albany-Fraser Orogen detritus to northern and eastern Eucla Basin placer deposits, while the far western Albany-Fraser Orogen was implicated as the primary sediment source for the western basin margin (Hou & Warland, 2005; Reid & Hou, 2006; Reid et al., 2013a; Fig. 2.1b). Secondary supply regions, i.e., the Yilgarn and Gawler cratons, and intermediate sediment reservoirs (e.g., Officer Basin; Fig. 2.1b), were also recognised to have contributed to the total Eucla Basin heavy mineral assemblages (Reid et al., 2013a). Hf isotope composition analysis on a selected group of Eucla Basin placer deposits (Reid et al., 2013b), supported the initial interpretation of a Musgrave Province dominated sediment provenance for northern and eastern beach placers based on a characteristic juvenile Hf signature of detrital deposit samples that match that of the northern crystalline basement region (Kirkland et al., 2013; Reid et al., 2013b). However, recent zircon analyses on the Eucla Basin's underlying crystalline basement, the Madura and Coompana provinces, revealed U-Pb and Hf isotope signatures that are largely indistinguishable from zircon grains of the Musgrave Province, pointing to a widespread juvenile zone of the Proterozoic Mirning Ocean (Kirkland et al., 2017; Jagodzinski et al., 2018; Hartnady et al., 2020). These new insights to the basin's crystalline sub-surface raises questions about previous interpretations of a Musgrave Province-dominant sediment supply and requires re-examination of the basin's detrital provenance histories utilising methodologies that go beyond conventional U-Pb and Hf isotope composition analyses. In recent years,

provenance studies investigating grain shape analysis suggested that the shape of detrital zircon grains may be correlated to that of zircon grains from likely source regions (e.g., Markwitz & Kirkland, 2018; Makuluni et al., 2019). The basis of the concept is built upon the knowledge that dominant grain morphologies are a function of the grain's unique crystal habit, ultimately affected by the growth-rate of its crystal faces as controlled by melt properties, that yield information on a given set of magmatic conditions and elemental concentrations (Pupin, 1980; Vavra, 1990; Benisek & Finger, 1993; Vavra et al., 1999). Sediment provenance studies incorporating grain shape analysis has demonstrated that some grain shape attributes may remain intact even after extensive transportation (Markwitz & Kirkland, 2018; Makuluni et al., 2019). Integrating zircon grain shape analysis with commonly applied U-Pb and Hf isotope composition analyses may therefore prove beneficial for resolving provenance ambiguities in detrital records where likely source regions express overlapping age and / or geochemical characteristics. The Eucla Basin is a prime study area to test the efficacy of this integrated approach given the non-unique age and geochemical signatures of the northern lying Musgrave Province and the underlying Madura and Coompana provinces.

## 2. Research Motivation, Aims and Objectives

The motivation behind this research project stems from an increased awareness that academic research is crucial in providing new answers to existing problems commonly encountered in the (mineral sands) industry. Through a collaboration of academia and the mineral industry, both entities will benefit by securing a demand for future research projects and by providing accessibility of technological advances to the exploration and mining industry that are usually only available to research professionals. This thesis aims to bridge the gap between academia and the industry by providing new perspectives on heavy mineral sand systems to help improve exploration targeting of placer deposits in the Eucla Basin and globally. The research project is specifically aimed to extend past conventional methodologies of U-Pb geochronology and Hf isotope geochemistry, previously applied in Eucla Basin provenance studies, to try and address limitations encountered. Several objectives were defined at the start of the research work to ensure the overarching aims would be met. Chapters of this thesis that address and fulfill the objectives are indicated in *parentheses*.

- 1) Provide novel detrital zircon U-Pb data for Eucla Basin heavy mineral samples and incorporate with published data; *Chapter Two*
- 2) Identify primary and secondary age mode variability across the basin's heavy mineral detrital zircon age spectra and re-examine potential sources; *Chapter Two*
- 3) Contextualise age-dis/similarities of Eucla Basin heavy mineral sand deposits and update depositional shoreline setting interpretations; *Chapter Two*
- 4) Establish a methodology to quantify heavy mineral enrichment and upgrading; *Chapter Two*
- 5) Provide an updated sediment provenance model for Eucla Basin heavy mineral sand deposits; *Chapter Two*
- 6) Provide new detrital zircon Hf isotope data for Eucla Basin placer samples and integrate with published data; *Chapter 3*
- 7) Establish and apply zircon grain shape analysis to Eucla Basin heavy mineral sands deposits and the basin's underlying basement, and incorporate with published zircon grain shape data; *Chapter 3*
- 8) Test the efficacy of grain shape analysis as a stand-alone method for sediment provenance investigations; *Chapter 3*
- 9) Investigate discrete zircon shape characteristics to distinguish across Eucla Basin Mesoproterozoic source regions; *Chapter 3*
- 10) Discern detrital zircon grains with overlapping U-Pb and Hf isotope characteristics and identify dominant Eucla Basin sediment provenance; *Chapter 3*

### 3. Thesis Structure

This thesis is structured into chapters that logically build upon each other. Chapters Two and Three present individual journal articles (published and prepared for peer review, respectively) that each include separate background literature reviews and methodological information. Consequently, some repetition across the journal articles may be present. A separate literature review has been omitted from this thesis as it is inherent to Chapters Two and Three. Chapter Four synthesises the research work with final conclusions.

Chapter Two:*Detrital Zircon Perspectives on Heavy Mineral Sand Systems, Eucla Basin, Australia*

This research article focusses on an in-depth U-Pb geochronology analysis of detrital zircon grains sampled from Eucla Basin heavy mineral placer deposits. Mineral composition and detrital zircon U-Pb geochronology data of newly acquired heavy mineral concentrates are incorporated with published Eucla Basin heavy mineral data. The combined detrital zircon data are contextualised with respect to recently revised regional crystalline basement (in particular the basin's underlying Madura and Coompana provinces; Jagodzinski et al., 2018) in a re-examination of sediment provenances. A primary sediment supply from Mesoproterozoic-aged source rocks is identified, implicating the underlying Madura and Coompana provinces as potential heavy mineral source regions in addition to the previously highlighted Musgrave Province and Albany-Fraser Orogen (e.g., Reid et al., 2013a). The study further re-evaluates the likely timing and shoreline highstand association of beach placer formation using age spectra similarity analysis and provides a revised depositional shoreline model for Eucla Basin prospects. Progressive heavy mineral prospectivity and heavy mineral maturation of Eucla Basin palaeoshorelines are known to increase with distance to the east (Hou et al., 2011) and are now quantifiable through detrital zircon age spectra heterogeneity analysis. The efficacy of integrating traditional geochronology studies with statistical age similarity and heterogeneity analyses are highlighted in a mineral systems model.

Chapter Three:*Refining Zircon Provenance Interpretation Via Integrated Grain Shape, Geochronology, and Hf Isotopes, a Case Study from the Eucla Basin, Australia*

This chapter, although presented as a stand-alone paper, continues the Eucla Basin sediment provenance investigation. In this work, new Hf isotope data of the newly U-Pb dated Eucla Basin heavy mineral samples (Chapter Two) are presented and incorporated with published Hf isotope data. The dominant Mesoproterozoic age mode of Eucla Basin heavy mineral prospect samples indicate derivation from a compositionally juvenile magmatic source. Previous interpretations of a significant Musgrave Province sediment supply to Eucla Basin palaeoshorelines are re-examined as integration of recently published Hf isotope data from the basin's underlying

Madura and Coompana provinces reveal similar age- and geochemical characteristics. Focussing on zircon grains with overlapping U-Pb and Hf isotope signatures in likely Eucla Basin sediment source regions, zircon grain shape analysis is incorporated and its efficacy for resolving ambiguities in the detrital zircon record is tested. Grain shape analysis is applied to zircon grains from crystalline Madura and Coompana province samples and incorporated with published zircon shape data from the Musgrave Province and the Albany-Fraser Orogen (Markwitz & Kirkland, 2018; Makuluni et al., 2019). Concentrating on the dominant age mode of Eucla Basin heavy mineral age spectra, distinguishing shape characteristics are statistically identified for zircon grains aged ~1400–1000 Ma across each potential Eucla Basin Mesoproterozoic source region. Eucla Basin detrital zircon grains with overlapping U-Pb and Hf isotope characteristics are able to be associated with a specific source region based on distinct grain shape attributes. The integrated analysis identifies a significant sediment contribution from the basin's underlying Madura and Coompana provinces to Eucla Basin beach placers and highlights the significance of sediment reworking through intermediate basins given the lack of direct pathways from source to sink.

## Chapter One Reference List

- Barham, M., Reynolds, S., Kirkland, C. L., O'Leary, M. J., Evans, N. J., Allen, H. J., . . . McDonald, B. J. (2018). Sediment routing and basin evolution in Proterozoic to Mesozoic east Gondwana: A case study from southern Australia. *Gondwana Research*, 58, 122-140.  
<https://doi.org/10.1016/j.gr.2018.03.006>
- Benisek, A., & Finger, F. (1993). Factors controlling the development of prism faces in granite zircons: a microprobe study. *Contributions to mineralogy and petrology*, 114(4), 441-451. <https://doi.org/10.1007/bf00321749>
- Fedo, C. M., Sircombe, K. N., & Rainbird, R. H. (2003). Detrital zircon analysis of the sedimentary record. *Reviews in Mineralogy and Geochemistry*, 53(1), 277-303. <https://doi.org/10.2113/0530277>
- Gehrels, G. E., Blakey, R., Karlstrom, K. E., Timmons, J. M., Dickinson, B., & Pecha, M. (2011). Detrital zircon U-Pb geochronology of Paleozoic strata in the Grand Canyon, Arizona. *Lithosphere*, 3(3), 183-200.  
<https://doi.org/10.1130/L121.1>
- Hartnady, M. I. H., Kirkland, C. L., Dutch, R. A., Bodorkos, S., & Jagodzinski, E. A. (2020). Evaluating zircon initial Hf isotopic composition using a combined SIMS–MC–LASS–ICP–MS approach: A case study from the Coompana Province in South Australia. *Chemical geology*, 558, 119870.  
<https://doi.org/10.1016/j.chemgeo.2020.119870>
- Hou, B., Keeling, J., Reid, A., Fairclough, M., Warland, I., Belousova, E., . . . Hocking, R. (2011). Heavy mineral sands in the Eucla Basin, southern Australia: deposition and province-scale prospectivity. *Economic Geology*, 106(4), 687-712. <https://doi.org/10.2113/econgeo.106.4.687>
- Hou, B., & Warland, I. (2005). Heavy mineral sands potential of the Eucla Basin in South Australia—a world-class palaeobeach placer province. *MESA Journal*, 37, 4-12.
- Iluka Resources Limited. (2021). Jacinth-Ambrosia Overview.  
<https://iluka.com/operations-resource-development/operations/jacinth-ambrosia>. Retrieved from <https://www.iluka.com/operations-resource-636-development/operations/jacinth-ambrosia>
- Jagodzinski, E. A., Bodorkos, S., & Crowley, J. L. (2018). PACE Copper Coompana Drilling Project: U-Pb Dating of Basement and Cover Rocks. *Department for Energy and Mining, South Australia, Report Book 2018/00028*, 211.
- Kesler, S. E. (2007). Mineral supply and demand into the 21st century. In: *Briskey, J. A. and Schulz, K. J., (Eds.) US Geological Survey circular 1294. Proceedings for a workshop on deposit modeling, mineral resource assessment, and their role in sustainable development. Reston, VA, USA. Geological Survey*, 55-62.
- Kirkland, C. L., Smithies, R. H., Spaggiari, C., Wingate, M., De Gromard, R. Q., Clark, C., . . . Belousova, E. A. (2017). Proterozoic crustal evolution of the Eucla basement, Australia: Implications for destruction of oceanic crust during emergence of Nuna. *Lithos*, 278, 427-444.  
<https://doi.org/10.1016/j.lithos.2017.01.029>

- Kirkland, C. L., Smithies, R. H., Woodhouse, A. J., Howard, H. M., Wingate, M. T., Belousova, E. A., . . . Spaggiari, C. V. (2013). Constraints and deception in the isotopic record; the crustal evolution of the west Musgrave Province, central Australia. *Gondwana Research*, 23(2), 759-781. <https://doi.org/10.1016/j.gr.2012.06.001>
- Kullerud, G. (2003). Ore Petrology. In: R. A. Meyers (Ed.), *Encyclopedia of Physical Science and Technology (Third Edition)* (pp. 411-433). New York: Academic Press.
- Makuluni, P., Kirkland, C., & Barham, M. (2019). Zircon grain shape holds provenance information: a case study from southwestern Australia. *Geological Journal*, 54(3), 1279-1293. <https://doi.org/10.1002/gj.3225>
- Markwitz, V., & Kirkland, C. (2018). Source to sink zircon grain shape: Constraints on selective preservation and significance for Western Australian Proterozoic basin provenance. *Geoscience Frontiers*, 9(2), 415-430. <https://doi.org/10.1016/j.gsf.2017.04.004>
- Pupin, J. (1980). Zircon and granite petrology. *Contributions to mineralogy and petrology*, 73(3), 207-220. <https://doi.org/10.1007/BF00381441>
- Reid, A. J., & Hou, B. (2006). Source of heavy minerals in the Eucla Basin palaeobeach placer province, South Australia: age data from detrital zircons. *MESA Journal*, 42, 10-14.
- Reid, A. J., Keeling, J. L., & Belousova, E. A. (2013b). Hf isotopic investigation into the provenance of zircons in heavy mineral sands of the Eucla Basin. *MESA Journal*, 68, 17-24.
- Reid, A. J., Keeling, J., Boyd, D., Belousova, E., & Hou, B. (2013a). Source of zircon in world-class heavy mineral placer deposits of the Cenozoic Eucla Basin, southern Australia from LA-ICPMS U–Pb geochronology. *Sedimentary Geology*, 286-287, 1-19. <https://doi.org/10.1016/j.sedgeo.2012.10.008>
- Sircombe, K., & Freeman, M. (1999). Provenance of detrital zircons on the Western Australia coastline—Implications for the geologic history of the Perth basin and denudation of the Yilgarn craton. *Geology*, 27(10), 879-882. [https://doi.org/10.1130/0091-7613\(1999\)027<0879:PODZOT>2.3.CO;2](https://doi.org/10.1130/0091-7613(1999)027<0879:PODZOT>2.3.CO;2)
- Sundell, K. E., & Saylor, J. E. (2021). Two-Dimensional Quantitative Comparison of Density Distributions in Detrital Geochronology and Geochemistry. *Geochemistry, Geophysics, Geosystems*, 22(4), e2020GC009559. <https://doi.org/10.1029/2020GC009559>
- Vavra, G. (1990). On the kinematics of zircon growth and its petrogenetic significance: a cathodoluminescence study. *Contributions to mineralogy and petrology*, 106(1), 90-99. <https://doi.org/10.1007/BF00306410>
- Vavra, G., Schmid, R., & Gebauer, D. (1999). Internal morphology, habit and U-Th-Pb microanalysis of amphibolite-to-granulite facies zircons: geochronology of the Ivrea Zone (Southern Alps). *Contributions to mineralogy and petrology*, 134(4), 380-404. <https://doi.org/10.1007/s004100050492>

## CHAPTER TWO

### **Detrital Zircon Perspectives on Heavy Mineral Sand Systems, Eucla Basin, Australia**

Gisela Gartmair<sup>1</sup>, Milo Barham<sup>1</sup>, Christopher L. Kirkland<sup>1</sup>

(gisela.gartmair@postgrad.curtin.edu.au)

<sup>1</sup> Timescales of Mineral Systems Group, School of Earth and Planetary Sciences, Curtin University, GPO Box U1987, Perth, WA 6845, Australia

#### **Abstract**

Southern Australia's Cenozoic Eucla Basin contains world-class strandline heavy mineral deposits. This study links detrital zircon U-Pb geochronology and heavy mineral compositions from four mineral sand prospects, and published results from a suite of other deposits to bounding Archean to Neoproterozoic crustal areas. A variable number of distinct sediment sources is recorded from each prospect's detrital zircon age spectrum. This variability in zircon ages, quantified using a Shannon-Weaver test, serves as a metric of source region heterogeneity. Greater zircon age heterogeneity correlates with heavy mineral enrichment. Enhanced heavy mineral yields reflect retention of resistate over labile minerals — a function of greater sediment transport, reworking, and upgrading processes, that parallel those, that result in detrital zircon age polymodality. In this case study, greater reworking in intermediate storage sites and transport by longshore processes, eastward along the ~1,000 km spanned by the study sites, corresponds to the direction of progressive heavy mineral enrichment identified in zircon ages and mineral compositions. This approach is a proxy for the duration minerals have spent in the sedimentary system and provides an important perspective for understanding heavy mineral sands.

#### **1. Introduction**

The Eucla Basin in southern Australia is one of Australia's major heavy mineral sand provinces, which together with the south-eastern Murray Basin and the western lying



Perth and Canning basins host the continent's major zircon, rutile, and ilmenite resources (Senior et al., 2020). Australia's supply of critical minerals (i.e., zirconium and titanium) to the global economy is substantial, with the country ranked among the most significant producers of rutile (leader in global production with 29% in 2019), zircon (second highest global production rate with 25% in 2018), and ilmenite (third highest global production with 15% in 2018; Australian Government, 2020). Specifically, the Eucla Basin has gained global attention for its world-class heavy mineral resources following discoveries of significant deposits along its north-eastern and eastern palaeostrandlines (Hou et al., 2011; Fig. 2.1a). Covering an area of approximately 250,000 km<sup>2</sup> and extending over 2,000 km in length from Western Australia to South Australia, the Eucla Basin is considered the largest onshore Cenozoic marine sedimentary basin (Benbow, 1990; Clarke et al., 2003; Li et al., 2003; Hou et al., 2006). The discovery of the Jacinth-Ambrosia deposit in 2004 on the Eucla Basin's eastern margin, and its subsequent development into the world's largest operating zircon mine (Iluka Resources Limited, 2021; Fig. 2.1a), has spurred extensive exploration efforts across the basin. In particular, the well-preserved coastal barrier systems, the middle-upper Eocene Ooldea Barrier and the upper Eocene Barton Barrier (Fig. 2.1a), are of significant interest for mineral sand exploration in this region.

Heavy minerals such as zircon, rutile, garnet, and ilmenite have a density of  $\geq 2.90$  g/cm<sup>3</sup>. Because of their density and recalcitrance, heavy minerals may become concentrated in nearshore environments to form beach placer deposits through hydraulic fractionation processes caused by wave and current action during transgression and highstand sea phases (Roy, 1999; Garzanti & Andò, 2019). Understanding the generation, transport, deposition, concentration, and preservation of heavy minerals in sands relies on a comprehensive knowledge of the mineral system, including the basin's crystalline source regions, likely sediment routing pathways and transport duration, and intermediate storage systems on the route from primary source to ultimate sink. A powerful approach in investigating sediment systems and the genesis of heavy mineral deposits is the application of provenance geochronology to detrital zircon (Sircombe & Freeman, 1999; Gehrels et al., 2011).

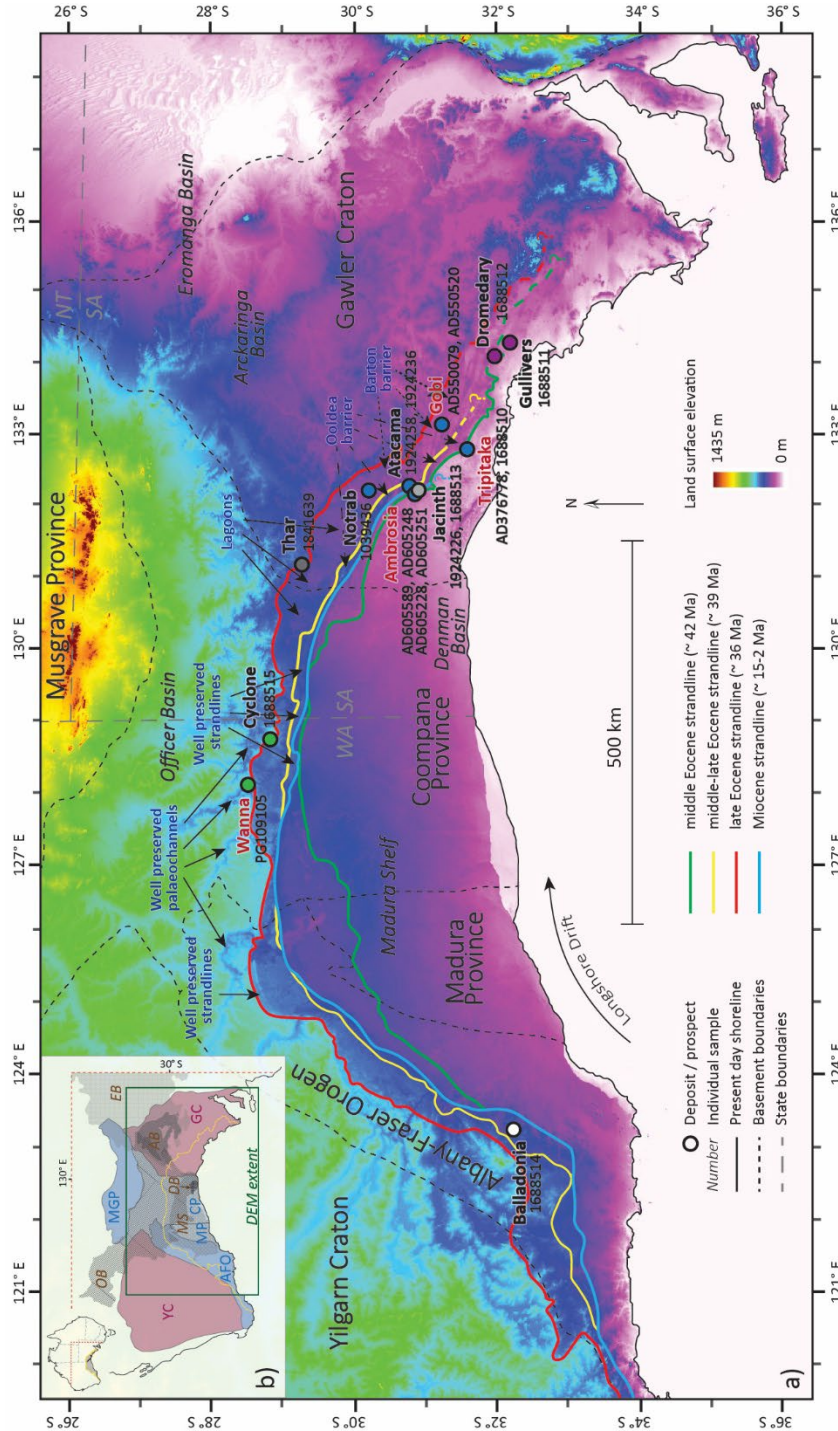


Figure 2.1 Digital Elevation Model (a) and map (b) of the Eucla Basin with surrounding and underlying sediment source regions. Shoreline successions are shown (Hou et al., 2011; Reid et al., 2013b). Heavy mineral prospects sampled in this study shown in red font. Black prospect names denote previously published results (sample I039436, Reid & Hou, 2006; sample 1688513, Hou et al., 2011; samples 1688514, 1688515, 1841639, 1924226, 1924258, 1924236, 1688510, 1688512 and 1688511, Reid et al., 2013a; App. Table 1.2). Colour coding of deposit markers consistent with Table 1.6. Geologic boundaries based on Geoscience Australia (<http://www.ga.gov.au>). Onshore extent of Cenozoic Eucla Basin highlighted in yellow. AB = late Palaeozoic Arkaringa Basin, AFO = Mesoproterozoic Albany-Fraser Orogen, CP = Mesoproterozoic Coompana Province, DB = Permian Denman Basin, EB = Mesozoic Eromanga Basin, GC = Archean Gawler Craton, MGP = Mesoproterozoic Musgrave Province, MP = Mesoproterozoic Madura Province, MS = Cretaceous Madura Shelf, NT = Northern Territory, OB = Neoproterozoic Officer Basin, SA = South Australia, WA = Western Australia, YC = Archean Yilgarn Craton.

Zircon grains are highly suitable for reconstructing sediment routing from crystalline source regions and intermediate sediment reservoirs because of their ability to preserve characteristic age and geochemical information through low grade metamorphism and prolonged chemical and mechanical attack during weathering and erosion (Fedo et al., 2003). This approach is dependent on established concepts of distinctive ages of rock-forming events within specific crystalline regions, as well as climatic, tectonic, and geographic factors, influencing sediment migration regimes within the basin (Gehrels, 2014; Helland-Hansen et al., 2016).

The Eucla Basin is surrounded and underlain by a variety of crystalline basement ranging in age from the Archean (Yilgarn and Gawler cratons) to Proterozoic (Albany-Fraser Orogen, Musgrave Province and Madura and Coompana provinces; Fig. 2.1b; App. Table 2.1). Previous detrital zircon geochronology studies on the formation of the Eucla Basin and its palaeostrandlines inferred a dominant magmatic source region of Mesoproterozoic age from the basin's hinterland (Reid & Hou, 2006; Hou et al., 2011; Reid et al., 2013a). Sediment reworking has also been identified as an important factor for heavy mineral enrichment (Hou & Keeling, 2008; Hou et al., 2011). Even though these studies enhanced understanding of the basin's depositional history, new world-class deposits have not been discovered in the region. Since 2004, only economically small-scale prospects have been identified, with Jacinth-Ambrosia remaining a one-of-its-kind tier-1 deposit to date (total resource of ~208.5 million tonnes [Mt], ~5.7 Mt in situ heavy minerals, and ~48.7% zircon concentration; Government of South Australia - Department for Energy and Mining, 2020). This reflects the global challenges of modern-day mineral exploration, as many near-surface high-grade ore reserves are already discovered and (actively being) exploited, while new discoveries of easily detectable deposits exhibit decreasing ore concentrations (Kullerud, 2003). Exploration efforts increasingly rely on more intensive research, new technologies, and analytical methodologies to ensure the rising global demand for minerals can be sustainably met through time- and cost-efficient targeting of new near-surface and undercover ore deposits (Kullerud, 2003; Kesler, 2007). Although exploratory drilling has substantially expanded across the Eucla Basin, geochronological analyses have not been performed on newly acquired samples. Furthermore, undercover sampling has led to new insights of the Eucla Basin's underlying crystalline basement lithologies, the Mesoproterozoic Madura and

Coompana provinces (Fraser & Neumann, 2016; Kirkland et al., 2017; Jagodzinski et al., 2018; Fig. 2.1b; App. Table 2.1), which have been implicated as alternative potential sediment source regions for overlying clastic sequences (Makuluni et al., 2019; Barham & Kirkland, 2020).

Here, we provide compositional and zircon U-Pb geochronology data from eight new heavy mineral samples from four prospects in the northern and eastern Eucla Basin (Table 2.1). Zircon grains from the Ambrosia deposit are dated for the first time, as are zircon grains from the recently drilled Wanna and Gobi prospects. Published results from U-Pb dated samples from the Eucla Basin's palaeoshorelines (Reid & Hou, 2006; Hou et al., 2011; Reid et al., 2013a; App. Table 2.2) are incorporated in the broader analysis of this study. Integrating all samples, we attempt to characterise Eucla Basin palaeoshoreline sequences and provide novel information on the basin's heavy mineral deposits. Using our study site as an example, we present a new metric that aids in identifying depositional similarities and trends in mineral endowment of beach placers that may benefit global exploration targeting and prospectivity modelling.

Table 2.1 Summary of samples analysed in this study with overview of heavy mineral (HM) grade, mineralisation zones and sedimentary descriptions from reverse circulation and air core drilling assays

Sample ID	Prospect/ Deposit	Latitude	Longitude	Drill Hole ID	Collar Depth (m)	RSL (m)	HM Grade* (%)	Zircon (%)	Mineralisation Zone & Sediment Description
PG109105	Wanna prospect**	-28.5116	128.0969	WE0191	27.0 - 28.5	311.6 - 310.1	2.5	26.8	HM mineralisation peak*** medium sized, moderately well-sorted sand
AD605589	Ambrosia deposit	-30.8624	132.2178	AM1100	18.0 - 19.0	120.5 - 119.5	0.8	61.2	Upper low-grade HM**** well-sorted, clay dominated
AD605228	Ambrosia deposit	-30.8600	132.2218	AM1089	3.0 - 4.0	139.0 - 138.0	0.9	58.6	Upper low-grade HM fine-grained, well-sorted sand
AD605248	Ambrosia deposit	-30.8600	132.2218	AM1089	22.0 - 23.0	120.0 - 119.0	21.9	66.8	HM mineralisation peak fine-grained, well-sorted sand
AD605251	Ambrosia deposit	-30.8600	132.2218	AM1089	25.0 - 26.0	117.0 - 116.0	1.6	58.1	Lower low-grade HM***** fine-grained, well-sorted sand
AD376778	Tripitaka prospect	-31.5481	132.8048	TR1078	23.0 - 24.0	101.0 - 100.0	9.1	83.7	HM mineralisation peak medium-sized, moderately well-sorted sand
AD550079	Gobi prospect	-31.2267	133.1277	YE16687	24.0 - 25.5	110.0 - 108.5	0.3	87.7	Background HM medium-grained, well sorted sand
AD550520	Gobi prospect	-31.2285	133.1392	YE16708	11.0 - 12.0	114.0 - 113.0	14.2	27.6	HM mineralisation peak fine-grained, very well sorted sand

\* received heavy mineral (HM) grade

\*\* also referred to as Western Eucla prospect

\*\*\* highest recorded HM grade observed in drill hole

\*\*\*\* low-grade proportion of HM mineralisation zone found above peak mineralisation of drill hole

\*\*\*\*\* low-grade portion of HM mineralisation zone found below peak mineralisation of drill hole

## 2. Geologic Background

### 2.1 Sedimentation and prospectivity of the Eucla Basin

Limited sedimentary sequences appear to have been preserved along the present-day southern margin of Australia prior to the formation of the passive margin during the final Mesozoic Australia-Antarctica rifting (Brown et al., 2003). However, stability of these sedimentary systems has been inferred from detrital zircon geochronology of the Officer Basin and Madura Shelf (Fig. 2.1b), reflecting the longer-term history of coherent East Gondwana (Barham et al., 2018; Barham & Kirkland, 2020). Following the complete Cenozoic opening of the Australia-Antarctica seaway, deposition of carbonates and the formation of several distinct palaeoshorelines with beach placer deposits occurred across the Eucla Basin during major transgressive highstands (Hou et al., 2011). Terrigenous clastic sedimentation was restricted to the coastal margins (Lowry, 1970) and derived from an extensive inherited palaeodrainage system penetrating the adjacent Precambrian hinterland (de Broekert & Sandiford, 2005; Hou & Warland, 2005; Hou & Keeling, 2008; Hou et al., 2008).

During the Eocene, marine transgressions gradually increased in magnitude, leading to the formation of terraced palaeoshorelines further inland (Li et al., 2003). Following a period of relative sea level stability and nondeposition of sediments in the Oligocene, coastal sedimentation abruptly shifted to a long-term regressive phase during the Miocene-Pliocene (Hou et al., 2003a, 2011). Cenozoic regressive palaeoshoreline sedimentation is difficult to resolve in the eastern Eucla Basin because of a significant west-up, east-down elevation difference across the region, associated with Australia's rapid northward migration over a mantle anomaly (Gurnis, 2001; Sandiford, 2007). The resulting vertical differential of ~150 m caused deeper marine flooding and stratigraphically thicker marine sedimentation in the eastern Eucla Basin (Jones, 1990; Hou et al., 2001; de Broekert & Sandiford, 2005). Prevailing winds further facilitated a predominant west to east longshore drift (Kemp, 1978; Beard, 1998) that enabled the progressive enrichment of beach barriers along the eastern basin margin during transgressional highstands (Hou et al., 2008).

Heavy mineral prospectivity varies across individual Eucla Basin palaeoshoreline sequences and is considered highest along the eastern, and to a lesser degree, north-eastern margin (Hou et al., 2011). Zircon concentrations found in the basin's north-

eastern and eastern deposits are considerably higher (~10 – 65%) compared to the basin's west (Balladonia, ~1.5%; Pownceby et al., 2008; Hou et al., 2011). Heavy mineral concentrations and zircon percentages found in beach placers of the Ooldea Barrier system of the middle-late Eocene palaeoshoreline (Fig. 2.1a) are considered the highest across all Eucla Basin placer deposits (Hou et al., 2011). Other significant heavy mineral accumulations are found in the upper Eocene Barton Barrier system, which overprints the Ooldea Barrier in the basin's north-east (Fig. 2.1a). The development of a Miocene palaeoshoreline (Fig. 2.1a) extensively reworked Eocene sediments and facilitated the development of enriched beach placers in the basin's east (e.g., Hou et al., 2011; Reid et al., 2013a).

### 3. Samples and Methods

#### 3.1 Sample selection

Heavy mineral samples from recent exploratory drilling undertaken by Iluka Resources Limited were obtained from reverse circulation and air core drilling assays of unconsolidated sediment across four drill sites, Wanna, Tripitaka, and Gobi prospects, and the Ambrosia deposit, from the Eucla Basin's northern and eastern margins (Fig. 2.1a; Table 2.1). A single sample was obtained from a high-grade part of the Wanna prospect along the basin's northern margin (Fig. 2.1a; Table 2.1). In the east, four samples with varying heavy mineral percentages (high-grade and low-grade heavy mineral sediment) were chosen from two drill holes from the Ambrosia deposit (Fig. 2.1a; Table 2.1). A single high-grade heavy mineral rich sample from Tripitaka (Fig. 2.1a; Table 2.1) was obtained from the northern part of the prospect. From the Gobi prospect, two samples from two drill holes were taken (one from the high-grade part of the mineralisation zone and another outside of the heavy mineral orebody; Fig. 2.1a; Table 2.1). Heavy mineral samples were categorised into peak heavy mineral samples, referring to the highest heavy mineral grade observed in a drill hole, and low-grade heavy mineral samples, denoting lower heavy mineral grade proportions of a prospect's mineralisation zone (Table 2.1). The Gobi background sample (AD550079) was chosen from a drill hole outside the prospect's mineralisation zone at a similar relative sea level to the heavy mineral peak sample AD550520 (Table 2.1).

### 3.2 Sample preparation

Drill sample splitting and heavy mineral separation was performed through the Iluka Resources Limited Narngulu mineral separation plant in Western Australia. Samples were sieved to >53- to 1,000- $\mu\text{m}$  sands and density separated to extract heavy minerals of  $\geq 2.86 \text{ g/cm}^3$  using heavy liquid concentration. Representative heavy mineral concentrates were bulk mounted on double-sided tape affixed to glass plates and set in 25 mm-diameter Epofix resin discs at the School of Earth and Planetary Sciences, Curtin University, in Western Australia. Bulk mounting was performed to avoid unwanted bias from selective handpicking of zircon grains (Sláma & Košler, 2012; Dröllner et al., 2021) and is highlighted in recent sediment provenance studies as a valuable method for analysing comprehensive data sets without the need for incorporating traditional petrographic analyses of hand-selected grains (Akinlotan & Rogers, 2021; Akinlotan et al., 2021). Grain-mount surfaces were then manually polished with successively finer abrasive paper (up to 2,000 grit), diamond-embedded lapping film (9, 6, and 3  $\mu\text{m}$ ), and diamond suspension (1  $\mu\text{m}$ ) to expose grain interiors. A final coat of carbon (2,000 ms =  $\sim 20 \text{ nm}$ ) was applied to all samples using an Emitech 950x evaporative carbon coater to facilitate scanning electron microscopy imaging.

### 3.3 Analytical methodology

Mineralogical and geochronological analyses of the selected heavy mineral concentrates were performed at the John de Laeter Centre, at Curtin University in Western Australia. Mineralogical dot-mapping of all eight prepared samples was performed based on a sample's elemental composition using the TESCAN integrated mineral analyser (TIMA), with integrated energy dispersive X-ray spectroscopy (EDS) and backscattered electron imaging (App. 2.1). TIMA mineral classification rules employed for distinguishing the Fe-Ti oxides (elemental peak intensities for iron [Fe-K]) were incapable of distinguishing leucogenised ilmenite and rutile. Mineral phase maps, in conjunction with light microscopy and backscattered imaging were used to guide point selection.

Uranium-lead geochronology was performed on cores of zircon grains targeting single primary growth phases using laser ablation-inductively coupled plasma mass spectrometry (LA-ICPMS). Using TIMA generated zircon mineral phase maps (App.



2.1), representative zircon grains with nonfractured, nonincluded areas  $>50\ \mu\text{m}$  were randomly selected to capture true zircon core ages. Time-resolved isotopic signals for  $^{204}\text{Pb}$ ,  $^{206}\text{Pb}$ ,  $^{207}\text{Pb}$ ,  $^{208}\text{Pb}$ ,  $^{232}\text{Th}$ , and  $^{238}\text{U}$  were obtained with a laser spot size of  $50\ \mu\text{m}$  and a 10-Hz dynamic repetition time. Two cleaning laser pulses were fired, with 35 s of ablation and 60 s of background capture per analysis. Geochronology data were reduced using Iolite v3 running in Igor Pro 6.37. Calibration of U-Pb fractionation and data monitoring were achieved with the 91500 zircon reference material ( $1062.4 \pm 0.4$  Ma; Wiedenbeck et al., 1995). Secondary zircon reference materials GJ-1 ( $608.5 \pm 0.4$  Ma; Jackson et al., 2004) and Man ( $3008.7 \pm 0.7$  Ma; Marsh et al., 2019) were used for monitoring accuracy and precision of data. Samples were split into three analytical sessions with zircon reference materials GJ1 ( $606 \pm 1$ ,  $605 \pm 2$ , and  $607 \pm 1$  Ma) and Man ( $3007 \pm 3$ ,  $3015 \pm 4$ , and  $3006 \pm 6$  Ma; App. Table 2.3) all within 1% of published values. Primary and secondary reference materials were run at the start and end of each analytical session and every 20 to 24 unknowns to assess and correct for instrument drift.

Concordia ages were calculated using IsoplotR (Vermeesch, 2018a) and filtered to a  $\pm 10\%$  discordance level (App. Fig. 2.1; App. Table 2.4). The nonradiogenic  $^{204}\text{Pb}$  isotope was monitored but no corrections were deemed necessary in the age calculations of the selected samples due to low count rates. Concordia ages from previously published U-Pb analyses were also calculated from their isotopic ratios and filtered at an equivalent 10% discordance threshold for comparison (Reid & Hou, 2006; Hou et al., 2011; Reid et al., 2013a; App. Table 2.2).

## 4. Results

### 4.1 Mineral composition

Five principal heavy minerals occur within each of the eight heavy mineral concentrate samples (Fig. 2.2). Zircon and rutile comprise the dominant mineral phases across all samples ( $\sim 85\text{-}98\%$  of a sample's total heavy mineral composition), followed by ilmenite, with minor contributions from anhydrous aluminium silicate (kyanite, andalusite and sillimanite) and tourmaline (Fig. 2.2). Zircon mass percentages range between  $\sim 27$  and  $88\%$  of each sample's heavy mineral concentrate (Fig. 2.2; Table 2.1). The highest and lowest zircon contents are found in the Gobi background sample

AD550079 (87.7%) and at Wanna (26.8%), respectively (Fig. 2.2; Table 2.1). The highest rutile contents of 70.6% are recorded in the peak mineralisation samples of Wanna and Gobi, with the lowest calculated percentage of 9.1% present in the Gobi background sample (Fig. 2.2). Highest and lowest ilmenite concentrations are found in Ambrosia's low-grade sample AD605228 (10.5%) and the Gobi background sample (0.1%), respectively (Fig. 2.2).

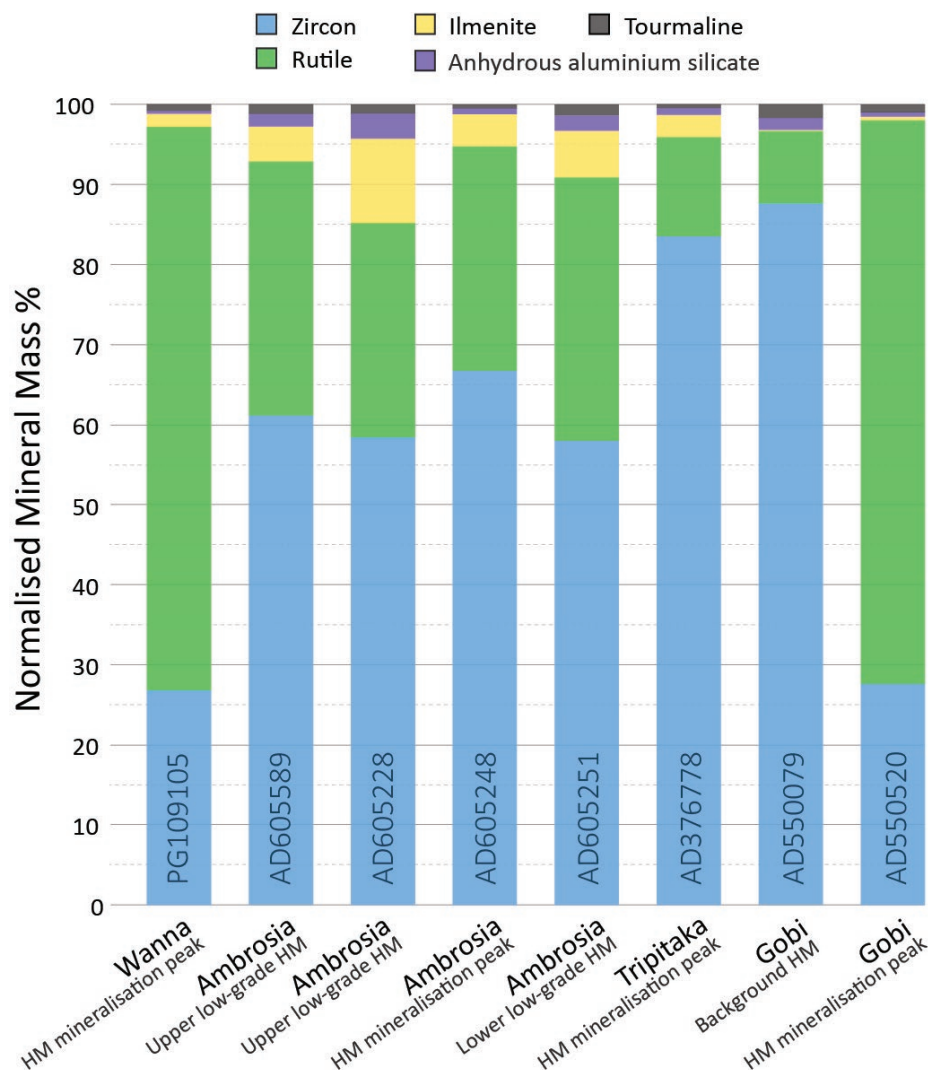


Figure 2.2 Normalised mineral composition output from TESCAN integrated mineral analysis of the heavy mineral concentrates of eight newly dated samples. HM = heavy mineral.

#### 4.2 U-Pb geochronology

Detrital zircon age spectra from the newly dated samples (Table 2.1) are plotted using a cumulative age distribution function (Fig. 2.3; Vermeesch, 2007) from the online program IsoplotR (Vermeesch, 2018a) and visually compared to published data (Reid & Hou, 2006; Hou et al., 2011; Reid et al., 2013a; App. Table 2.2) using kernel density

estimates (KDE; Fig. 2.4; Vermeesch, 2012) from the R-based Provenance package (Vermeesch et al., 2016). KDE were generated using adaptive estimation, area normalisation, and uniform bandwidth across all samples. For the eight newly analysed samples (Table 2.1) the Age Pick Excel package (Gehrels, 2009) was used to determine the sample's youngest single grain and the number of grains comprising principal, shoulder and subordinate age modes (App. Table 2.5). Subordinate age modes representing ~5% ( $\geq 5$  overlapping grain ages) of the concordant sample population were deemed significant and resolvable with >80% confidence based on the number of measurements undertaken (Vermeesch, 2004). Here, we only present results for the eight newly U-Pb analysed samples (Table 2.1).

Uranium-lead measurements of zircon grains from the eight heavy mineral samples show broadly similar polymodal age spectra (Figs. 2.3, 2.4), irrespective of their mineralisation grade (Table 2.1) or geographic locality (Fig. 2.1a). All eight samples exhibit a dominant Mesoproterozoic age mode of ~1300 to 1000 Ma (Figs. 2.3, 2.4; App. Table 2.5) and exhibit youngest detrital single grain ages between  $353 \pm 2$  Ma (Gobi AD550520; App. Table 2.5) and  $560 \pm 5$  Ma (Ambrosia AD605248; App. Table 2.5). With the exception of the Ambrosia low-grade sample AD605251, the remaining seven samples show a prominent, although varying secondary late Mesoproterozoic to early Neoproterozoic age mode between ~1100 and 800 Ma (Figs. 2.3, 2.4). Grains dated to the late Palaeoproterozoic to early Mesoproterozoic (~1800–1500 Ma) and late Proterozoic to early Palaeozoic (~650–500 Ma) are present in all eight heavy mineral samples (Figs. 2.3, 2.4). Ambrosia samples and the Gobi background sample AD550079 indicate a less distinct zircon age mode of late Proterozoic to early Palaeozoic age (~650–500 Ma) compared to heavy mineral peak assemblages of Gobi (AD550520), Tripitaka (AD376778) and Wanna (PG109105; Figs. 2.3, 2.4). Overall, Archean to early Proterozoic-aged zircon grains are typically minor across the newly dated samples (Figs. 2.3, 2.4). Archean zircon contributions are entirely absent in Wanna (Figs. 2.3, 2.4). A summary of the U-Pb results is presented in Appendix Table 2.4.

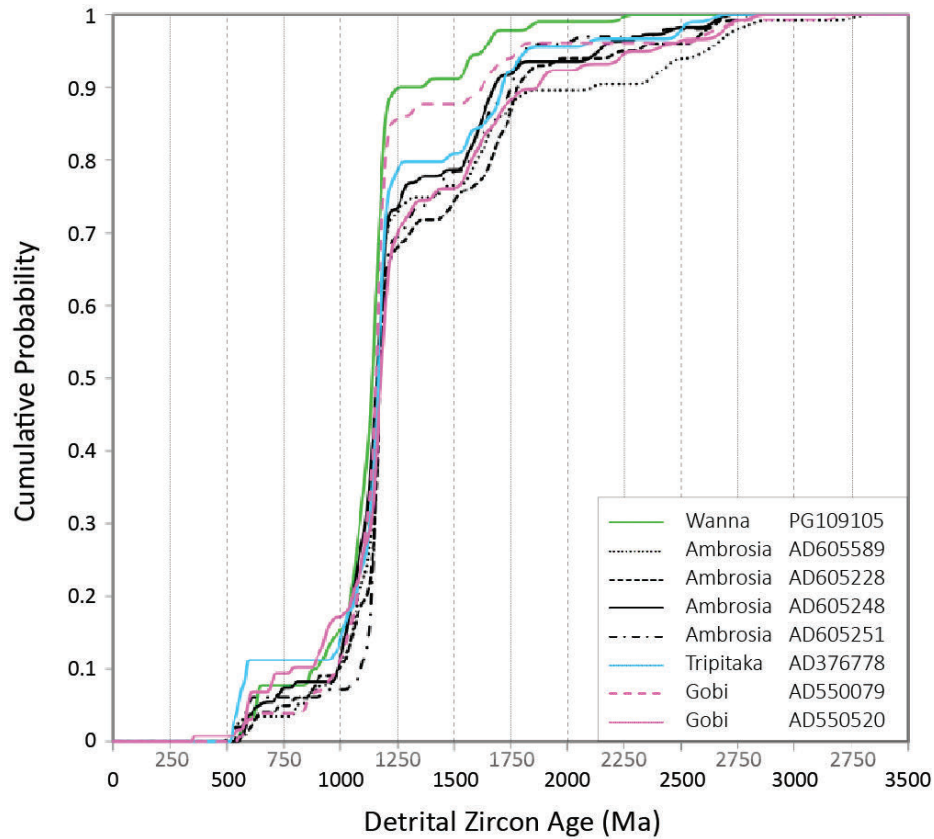


Figure 2.3 Cumulative age distribution plot of concordant age data ( $\pm 10\%$  discordance) of the eight newly analysed heavy mineral samples. Multiple samples of a deposit are grouped by colour.

## 5. Discussion

### 5.1 Identification of source region lithology and source proximity using heavy mineral compositions

Heavy mineral compositions are important indicators for sediment provenance and transport (e.g., Morton, 1991; Morton & Hallsworth, 1994; Hegde et al., 2006; Garzanti & Andò, 2007; Dill & Skoda, 2017; Poon et al., 2020). Although the TIMA mineral composition output (Fig. 2.2) may overestimate pure rutile concentrations and differ from reported mineralogical compositional data of Eucla Basin prospects (e.g., Australian Securities Exchange reports), the underlying trends in stable titanium-bearing oxide phases retain geologic relevance.

The high concentrations of stable - ultrastable mineral phases (zircon and rutile/pseudorutile/leucoxenised ilmenite) across all eight newly dated samples from the northern and eastern basin margins (Figs. 2.1a, 2.2; Table 2.1) indicate a prolonged transportation mode and/or diagenetic modification with a reduction in more labile mineral phases through high degrees of weathering during temporary storage and

attrition during active recycling (Force, 1980; Ejeh et al., 2015; Caracciolo, 2020; Caracciolo et al., 2020). Concentrations of the less stable mineral ilmenite across the eight heavy mineral assemblages are overall much lower (~0.1–10.5%; Fig. 2.2). The northern and eastern basin margins may have either experienced minor sediment supply from a proximal basic or acidic igneous source (Force, 1980; Shalini et al., 2020), undergone greater rates of hydrodynamic separation (Le Roux, 1990; McIntyre et al., 2020) compared to ilmenite-rich areas, or experienced increased alteration of ilmenite to pseudorutile and leucoxene as a result of prolonged exposure to weathering during sea-level lowstands (Mücke & Chaudhuri, 1991; Nair et al., 2006). Samples from Ambrosia, Tripitaka, and Gobi (background sample AD550079) exhibit zircon contents greater than 50% (Fig. 2.2; Table 2.1), irrespective of the heavy mineral grade (0.3–21.9%; Table 2.1). The observed zircon dominance supports previous interpretations of a zircon-rich eastern basin (up to 65% of the total heavy mineral mass in eastern and north-eastern deposits; Hou et al., 2011) and indicates sourcing predominantly originated from a felsic igneous source or from upgrading of detrital zircon from sedimentary reservoirs (Thomas, 2011). Intradeposit mineral composition analysis of the Gobi prospect indicates that extensive reworking of sediments and residual accumulation of resistant phases is not restricted to economic heavy mineral deposits, based on the zircon-rich nature of the overall heavy mineral-poor assemblage of the Gobi background sample AD550079 (~88% zircon; 0.3% heavy mineral grade; Fig. 2.2; Table 2.1). This highlights the significance of adequate sediment trapping for the development of placer deposits.

## **5.2 Detrital zircon provenance in the Eucla Basin**

We exclude the Gobi prospect background sample AD550079 from the following discussion because of its extremely low heavy mineral grade, its position outside a defined resource zone and a potentially distinct generation process and focus our analysis on 18 heavy mineral samples from 12 deposits (Fig. 2.1a; Table 2.1; App. Table 2.2; Reid & Hou, 2006; Hou et al., 2011; Reid et al., 2013a). Data from the newly analysed Tripitaka sample AD376778, are comparable to published data from the same deposit (sample 1688510; Reid et al., 2013a), supporting their combination in a representative age spectrum, as well as justifying direct comparison of newly acquired and published data. Composite age spectra are considered for heavy mineral

placer deposits with more than one heavy mineral sample (Table 2.1; App. Table 2.2) to capture the overall detrital zircon provenance of the deposit (Fig. 2.4).

The newly dated samples express great similarity to that of published Eucla Basin prospect samples (Fig. 2.4; Table 2.1; App. Table 2.2). All 12 deposits exhibit polymodal detrital zircon age spectra with a dominant Mesoproterozoic age mode of ~1300–1100 Ma and several subordinate age modes of late Archean to early Palaeoproterozoic, middle-late Palaeoproterozoic to early Mesoproterozoic, and Neoproterozoic to early Phanerozoic ages (Fig. 2.4; Reid & Hou, 2006; Hou et al., 2011; Reid et al., 2013a).

### 5.2.1 Primary zircon provenance

Magmatic and metamorphic events matching the principal Mesoproterozoic detrital zircon age modes of the deposits are found in most bounding and underlying geologic terranes of the Eucla Basin but are not recorded in the Archean Yilgarn or Gawler cratons (Fanning et al., 2007; Hand et al., 2007; Fig. 2.1b; App. Table 2.1). Balladonia expresses a subtly distinct primary age mode of ~1300–1200 Ma (Fig. 2.4) that corresponds well with ages recorded for the proximal Albany-Fraser Orogen (stage I thermo-tectonic phase, ~1345–1260 Ma; Recherche Supersuite, ~1330–1283 Ma; Fraser Range metamorphic rocks, ~1304–1291 Ma; Clark et al., 2000; Spaggiari et al., 2009; Clark et al., 2014; Kirkland et al., 2015a; App. Table 2.1).

Slightly younger primary age modes of ~1250–1100 Ma are recorded in northern and eastern deposits (Fig. 2.4) that overlap with Balladonia's younger shoulder mode of ~1200–1100 Ma (Fig. 2.4). Both intervals coincide with ages recorded for Stage II of the Albany-Fraser Orogeny (~1214–1140 Ma; App. Table 2.1), including the orogen's Esperance Supersuite (~1198–1138 Ma; Spaggiari et al., 2009; Kirkland et al., 2015a; App. Table 2.1). For northern and eastern prospects, significant rock-forming events of the Musgrave Province's Pitjantjatjara Supersuite (~1219–1121 Ma; Edgoose et al., 2004; Howard, H., et al., 2011; App. Table 2.1), appear to have contributed to the Mesoproterozoic age spectra (Fig. 2.4), likely via palaeodrainage networks directly from the craton or through intermediate storage in older basins (e.g., Officer and Eromanga basins; Hou et al., 2008; Reid et al., 2009; Fig. 2.5). The Musgrave Province was previously implicated as a dominant sediment source based on both U-Pb detrital zircon age and Hf isotope analysis (matching juvenile Hf isotope signature; Hou et al.,

2011; Kirkland et al., 2011, 2013; Reid et al., 2013a, b), while Balladonia's U-Pb and Hf signatures are more closely associated with the Albany-Fraser Orogen (Reid et al., 2013a, b).

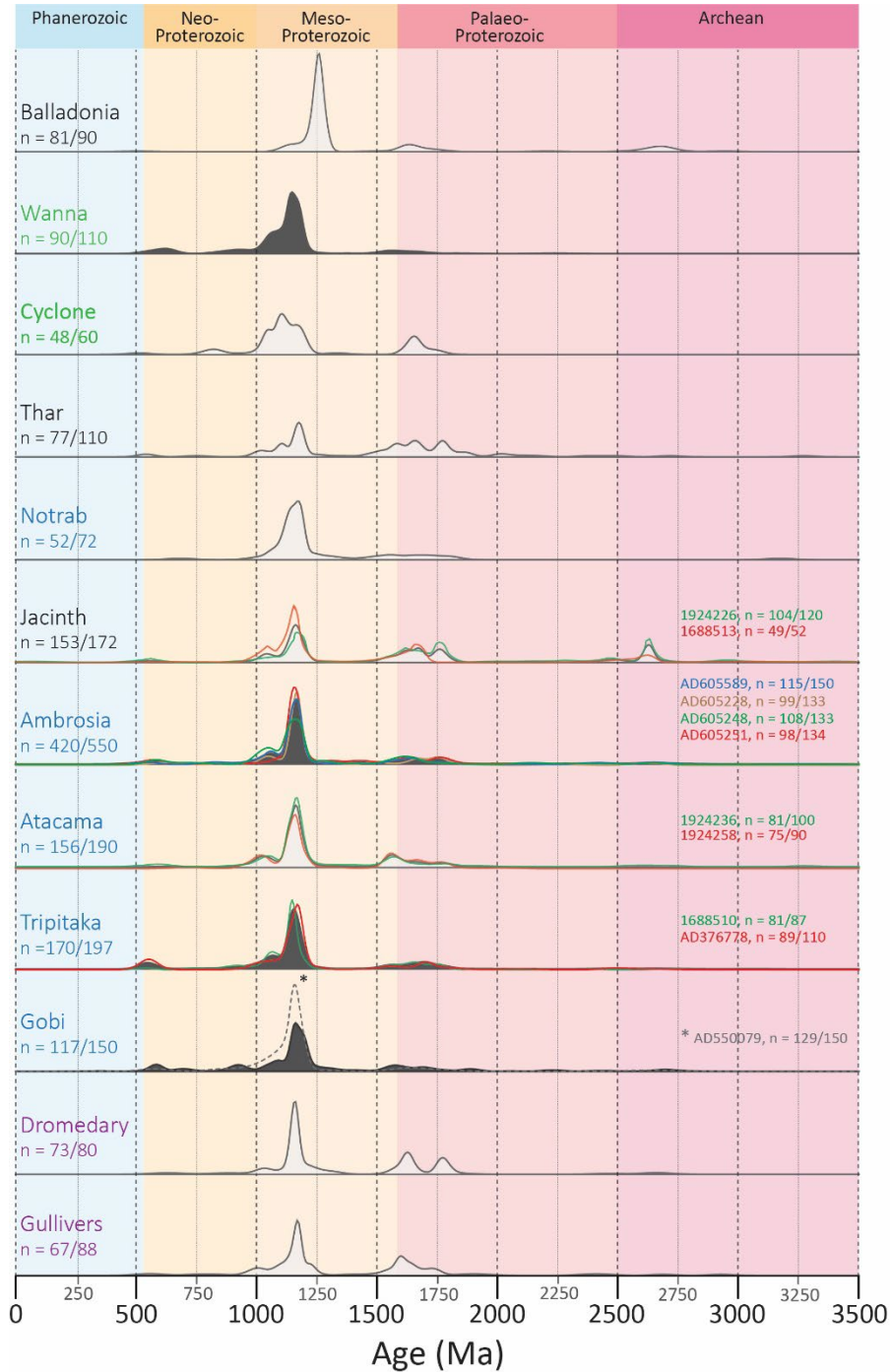


Figure 2.4 Stacked detrital zircon age spectra of Eucla Basin deposits analysed in this study. Deposit names in bold with grey fill spectra represent newly dated samples. Archived detrital zircon age data from the prospects Balladonia, Cyclone, Thar, Jacinth (sample 1924226), Atacama, Tripitaka (sample 1688510), Dromedary and Gullivers (Reid et al., 2013a), Jacinth (sample 1688513; Hou et al., 2011), and Notrab (Reid & Hou, 2006) are presented with white fill colour. Prospects with several samples (coloured age spectra lines) are combined to a single age spectrum (black age spectra lines).

Rock-forming events within the recently defined late Mesoproterozoic Madura and Coompana provinces (Moodini Supersuite, ~1181–1125 Ma, and metamorphic episodes of the Toolgana and Undawidgi supersuites, ~1179, ~1167, ~1150, and ~1174 Ma; Neumann & Korsch, 2014; Wingate et al., 2015; de Gromard et al., 2016; Jagodzinski et al., 2018; App. Table 2.1) underlying the Eucla Basin and older sedimentary basins (i.e., Mesozoic Madura Shelf and Neoproterozoic-Palaeozoic Officer Basin; Fig. 2.1B) are also potential sediment sources (Kirkland et al., 2017; Jagodzinski et al., 2018; Hartnady et al., 2020; Fig. 2.5). Similar dominant Mesoproterozoic detrital zircon age modes (~1250–1100 Ma) exist within Officer Basin and lower Madura Shelf age spectra (Barham et al., 2018), as well as with the Permian Denman Basin (Bendall et al., 2016; Fig. 2.1b), suggesting detritus from Mesoproterozoic sources (Musgrave, Madura and Coompana provinces) may have been supplied to Eucla Basin shorelines through recycling of intermediate sedimentary basins (Fig. 2.5). Given the extensive onshore carbonate cover of the central Eucla Basin exceeding the extent of the Madura Shelf (Lowry, 1970), Madura and Coompana province derived detrital zircons are more likely to have been supplied through intermediate storage in Officer Basin sediments, which are exposed or directly underlie the Eucla Basin's northern margin (Figs. 2.1b, 2.5). Recent analysis on the Hf isotope signature of the basin's underlying Coompana Province also revealed a juvenile magmatic composition (similar to that of the Musgrave Province; Hartnady et al., 2020), further implicating the underlying basement as a plausible sediment supplier for Eucla Basin heavy mineral sands consistent with age and isotopic constraints. The dominant, yet subtly varying Mesoproterozoic detrital zircon age modes in northern and eastern prospects (Fig. 2.4) is thus likely the product of recycling and intermixing of detrital material from several Mesoproterozoic sources (Musgrave, Madura and Coompana provinces and Albany-Fraser Orogen; Fig. 2.5).

### 5.2.2 Secondary zircon sources

Only two of the 12 analysed heavy mineral placers exhibit significant contributions of Archean detrital zircons (~2750–2600 Ma; >10% of total age spectrum; Balladonia and Jacinth; Figs. 2.4, 2.6a; Hou et al., 2011; Reid et al., 2013a, b). The age interval corresponds well to ages of granites and gneisses of the Yilgarn Craton (Cassidy et al., 2006; App. Table 2.1) and inherited material within Albany-Fraser Orogen gneisses, reflecting modification of the Yilgarn Craton (Hercules, Munglinup, and Tropicana



gneisses; Spaggiari et al., 2009, 2011; Doyle et al., 2015; Kirkland et al., 2015b; Smithies et al., 2015; App. Table 2.1). Sediments from western crystalline sources were likely supplied to Balladonia and the western Eucla margin via palaeodrainage and further transported along the basin's palaeoshorelines via predominant W- to E-directed longshore drift to Jacinth in the east (Fig. 2.5).

Although varying in magnitude and age spread, strong secondary zircon age modes spanning between ~1900 and 1500 Ma occur across all samples (Fig. 2.4). The late Palaeoproterozoic secondary age modes coincide with rock forming events of the Albany-Fraser Orogen (Kirkland et al., 2011; App. Table 2.1), the Musgrave Province (Kirkland et al., 2013; App. Table 2.1), and the Coompana and Madura provinces (Hartnady et al., 2020; App. Table 2.1), as well as detrital zircon ages in intermediate sediment reservoirs such as the newly defined Decoration Sandstone of the southern Officer Basin (Barham et al., 2018; App. Table 2.1). Such a diversity of potential primary and secondary source regions for specific age modes highlights the difficulty in sediment provenance interpretations where there are overlapping zircon ages in potential source rocks. However, secondary detrital zircon age modes of most prospects can be matched to rock-forming events of proximal source regions.

The geographic positions of Thar, Jacinth and Ambrosia with a secondary ~1800–1700 Ma age mode (Figs. 2.1a, 2.4) coincide with palaeodrainage systems (Hou et al., 2008) capturing metasedimentary and metaigneous rocks dated to ~1790–1740 Ma in the north-western Gawler Craton (Myola volcanic rocks, Peake metamorphic rocks, Moonta Porphyry and Mc Gregor volcanic rocks; Parker et al., 1993; Cowley et al., 2003; App. Table 2.1), as well as the craton's Fowler Domain (~1790–1720 Ma; Fanning et al., 2007; Howard, K.E., et al., 2011; Jagodzinski et al., 2019; App. Table 2.1). Dromedary and Gullivers are positioned further south-east (Fig. 2.1a) and likely received detritus from more varied Gawler Craton sources directly and via sediment reworking and longshore drift (Fig. 2.5; App. Table 2.1). The distinct secondary age mode of ~1650 Ma present in Cyclone, Thar, and Jacinth (and less strongly in Ambrosia; Fig. 2.4) may be related to recycled components through the Officer Basin Decoration Sandstone (~1650 Ma; Barham et al., 2018; Fig. 2.5; App. Table 2.1), while Balladonia's slightly younger Palaeoproterozoic secondary age mode (~1620 Ma; Fig. 2.4) is most likely associated with the Albany-Fraser Orogen's Biranup Orogeny (~1700–1600; Kirkland et al., 2011; Fig. 2.5; App. Table 2.1). Resolvable

zircon enrichment from the Gawler Craton to the eastern basin margin is implied by Dromedary's ~1620 Ma secondary age mode (Figs. 2.4, 2.5) that matches with the craton's St Peter Suite (~1620 Ma; Jagodzinski, 2005; Hand et al., 2007; Reid et al., 2020; App. Table 2.1). Additional sediment supply from the Gawler Craton's Hiltaba Suite and volcanic rocks (both ~1595–1575 Ma; e.g., Daly, 1998; Hand et al., 2007; Allen et al., 2008; Courtney-Davies et al., 2020; App. Table 2.1) is identified by Gullivers' ~1600 Ma secondary age mode and the presence of ~1600–1500 Ma zircon grains that are only found in Thar, Atacama and Gobi (Figs. 2.4, 2.5). Although the Musgrave's Warlawurru Supersuite (~1607–1575 Ma; Howard et al., 2015; Kirkland et al., 2015a; de Gromard et al., 2016; App. Table 2.1) coincides with the ~1580 Ma centred age mode observed in some eastern deposits (Fig. 2.4), it is only known from a few thrust sheets in the province's west (de Gromard et al., 2016).

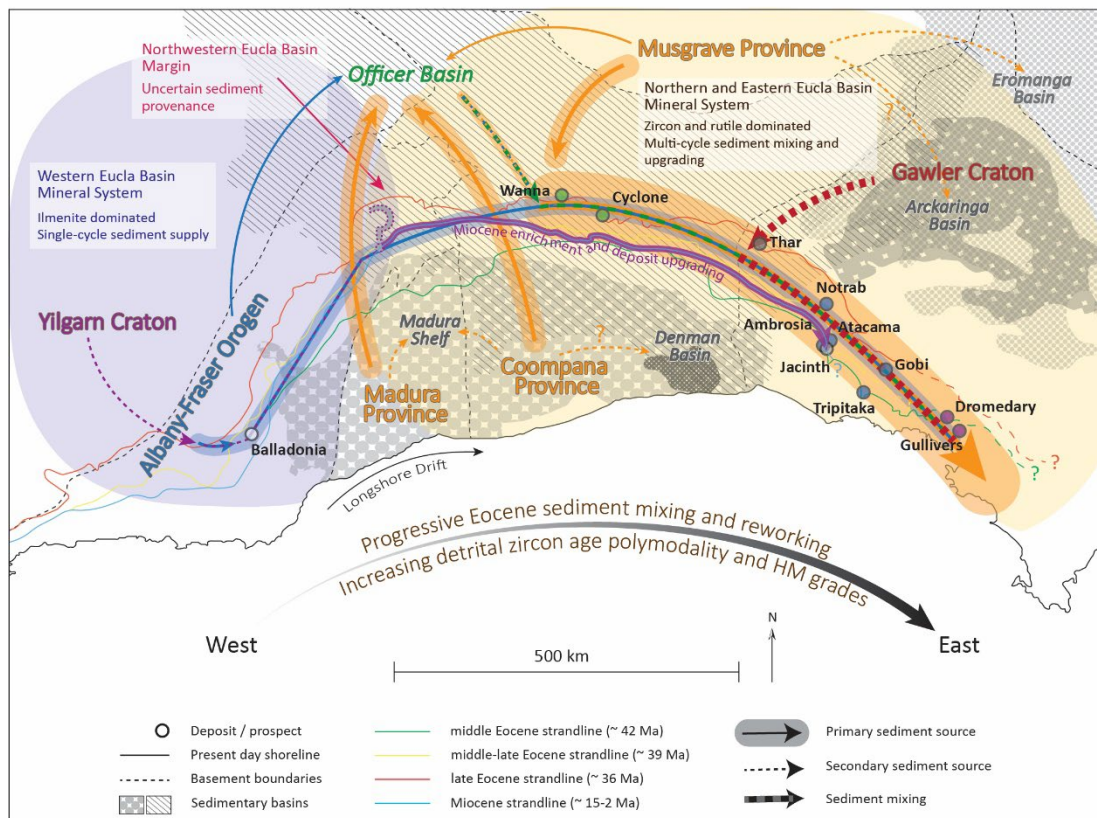


Figure 2.5 Schematic mineral systems model of Eucla Basin palaeoshorelines indicating primary and secondary sediment supply and intermixing regimes from crystalline and intermediate reservoir sources. Increasing resistant heavy mineral maturation from west to east is associated with increased detrital age polymodality and heavy mineral grades of Eucla Basin beach placers. Colour coding of deposit markers consistent with Figure 2.6. HM = heavy mineral.

Additional secondary age modes of late- to post-Mesoproterozoic ages are recorded in northern and eastern prospects. All eastern prospects (excluding Nortab) exhibit secondary age modes of ~1100–900 Ma (Fig. 2.4) that correspond in parts to ages of the Musgrave Province's Giles Complex (~1078–1052 Ma; Sun et al., 1996; App. Table 2.1) and the Warakurna Supersuite (~1074 Ma; Wise et al., 2018; App. Table 2.1) intruding the Madura and Coompana provinces. A distinct ~900–700 Ma secondary age mode is only observed in Cyclone, while Wanna, Tripitaka, Gobi and to a lesser degree Thar, express detrital contributions between ~650 and 500 Ma (Fig. 2.4). The younger Neoproterozoic age mode of ~650–500 Ma demonstrates age similarities with zircon grains associated with Officer Basin sediments (Lennis Sandstone, ~600–500 Ma, and Wanna Formation, ~600–500 Ma; Wingate et al., 2013a, 2013b; App. Table 2.1) or detritus derived from the Kuunga Orogen in Antarctica (~700–500 Ma; Haines et al., 2013; Morón et al., 2019; App. Table 2.1). Cyclone's Neoproterozoic detrital contributions may be related to more evolved components of the Willouran Large Igneous Province (~825 Ma; Wang et al., 2010; App. Table 2.1) or the Gunbarrel mafic magmatic event (~780 Ma; Harlan et al., 2003; Mackinder et al., 2019; App. Table 2.1), both of which are associated with the continental rifting of Rodinia.

Previous U-Pb analysis of prospect samples incorporated in this study identified the eastern Mesozoic Eromanga Basin (Fig. 2.1b) as an additional potential sediment contributor for zircon grains dated ~ <480 Ma (Reid et al., 2013a; App. Table 2.2). Although these relatively young ages were derived from a limited number of zircon grains and are not highlighted in our KDE analysis (Fig. 2.4), it was suggested that Musgrave Province-derived sediments (aged ~1300–1100 Ma) may have been supplied to the Eromanga Basin (Fig. 2.5), mixed with Phanerozoic eastern Australia-derived grains, and subsequently transported to Eucla Basin palaeoshorelines via palaeodrainage (Garford channel; Reid et al., 2009, 2013a). It is possible that other eastern sedimentary basins (e.g., the late Palaeozoic Arckaringa Basin; Fig. 2.1b) are also intermediate reservoirs for Musgrave Province detritus that was later supplied to north-eastern heavy mineral prospects. However, given the limited number of characteristic <500 Ma zircon populations in our samples (Fig. 2.4), we do not consider the far eastern sedimentary basins (Eromanga Basin or Arckaringa Basin) as significant intermediate reservoirs for Eucla Basin heavy mineral sands (Fig. 2.5). This

separation from eastern Australian sources has been previously recognised in older Mesozoic Madura Shelf sequences (Barham et al., 2018) and Cenozoic offshore sediments (Barham & Kirkland, 2020).

### **5.3 Provenance fingerprinting of Eucla Basin deposits**

Previous palaeoshoreline interpretations in the Eucla Basin have varied (e.g., Hou & Warland, 2005; Hou et al., 2011; Reid et al., 2013b), and depositional ages for beach placer deposits are largely derived from interpreted associations with more biostratigraphically amenable facies (e.g., Hou et al., 2011). However, exploratory drill samples in the basin's east are often difficult to assign to specific depositional shoreline settings (i.e., Barton or Ooldea barriers; Exploration Team, Iluka Resources Limited, pers. commun., 2021), and interpretations of the depositional ages of beach placers remain speculative. Here, we investigate whether the age spectra of heavy mineral samples can aid in determining the likely timing of deposition and reworking of placer deposits. We interpreted individual Cenozoic palaeoshorelines using digital elevation model (DEM) imagery of the Eucla Basin and superimposed the geographic position of all 12 prospects analysed in this study (Fig. 2.1a; Table 2.1; App. Table 2.2). DEM analysis was performed using Shuttle Radar Topography Mission (SRTM) derived 1 second (~30m) smoothed imagery (Gallant et al., 2011). Identification of preserved shoreline features and the corresponding depositional shoreline setting for each of the Eucla Basin prospects is based on visual interpretation of digital elevation data, tracking individual shorelines as linear topographic features. Ages of strandlines and the order of transgressive and regressive phases follow published work (Hou et al., 2011; Reid et al., 2013b). Our DEM analysis reveals well-developed shoreline features along the basin's western and northern margins that become increasingly difficult to resolve toward the east (Fig. 2.1a; Table 2.2). Although the eastern basin margin is associated with reworking during the Miocene (e.g., Hou et al., 2003a, b, c), a reported Miocene shoreline in the basin's far east could not be resolved in our DEM analysis (Fig. 2.1a).

Table 2.2 Reinterpretation of Eucla Basin depositional shoreline settings of prospects analysed in this study from digital elevation model analysis

Prospect/ Deposit	This analysis	Previous interpretations	Reference
Balladonia	middle-late Eocene	? Miocene	Hou et al , 2011; Reid et al , 2013a
Wanna	late Eocene	N/A	this study
Cyclone	late Eocene	late Eocene	Hou et al , 2011; Reid et al , 2013a
Thar	late Eocene	late Eocene	Reid et al , 2013a
Notrab	late Eocene	late Eocene	Reid and Hou, 2006; Hou et al , 2011
Jacinth	middle Eocene & Miocene	middle-late Eocene	Hou and Warland, 2005; Hou et al , 2011; Reid et al , 2013a
Ambrosia	middle Eocene	middle-late Eocene	Hou et al , 2011; Reid et al , 2013a
Atacama	middle-late Eocene	middle-late Eocene	Hou et al , 2011; Reid et al , 2013a
Tripitaka	middle Eocene	middle-late Eocene	Hou et al , 2011; Reid et al , 2013a
Gobi	late Eocene	N/A	this study
Dromedary	middle Eocene	? Miocene	Hou et al , 2011; Reid et al , 2013a
Gullivers	middle Eocene	? Miocene	Hou et al , 2011; Reid et al , 2013a

### 5.3.1 Provenance grouping of Eucla Basin prospects

Applying detrital zircon geochronology data to heavy mineral prospects indicates that age spectra cannot be used to uniquely fingerprint particular Cenozoic shorelines (Figs. 2.1a, 2.4; Table 2.2). This implies that sediment provenance during the Cenozoic was not temporally restricted to specific sources or defined depositional pathways. However, application of Kolmogorov-Smirnov distance-based multidimensional scaling of detrital zircon age populations (Vermeesch, 2013) identifies distinct provenance groups among Eucla Basin prospects (Figs. 2.1a, 2.6b; Table 2.3). Clusters of deposits are based on a goodness of fit method by statistically evaluating the maximum distance between the populations in cumulative distribution space; hence, the lower the distance value (D), the more closely related the age populations of the deposits are (Fig. 2.6b; Table 2.3). For this analysis, we focused on interdeposit variation across the 12 beach placers and combined age spectra of all heavy mineral samples of a deposit (excluding background sample Gobi AD550079), as detrital zircon age spectra of intradeposit samples express statistical similarity (App. Table 2.6). Despite greater dissimilarity in age spectra of the two Jacinth samples (1924226 and 1688513;  $D = 0.330$ ;  $p = <0.05$ ; App. Table 2.6) we decided to combine the two data sets for consistency across the analysis and discuss the dissimilarity found within the Jacinth deposit below.

Three clusters were identified across the 12 prospects (Figs. 2.1a, 2.4, 2.6b; Table 2.3), with additional ungrouped samples expressing more unique age characteristics (Balladonia, Thar, and Jacinth). Detrital zircon age grouping is strongly influenced by

secondary age modes and subtle variation in the primary age modes (Vermeesch, 2018b; Figs. 2.4, 2.6a). Prospect groupings are associated with proximity along the same shoreline setting, i.e., Wanna and Cyclone (late Eocene strandline,  $D = 0.153$ ;  $p = 0.460$ ; Figs. 2.1a, 2.4, 2.6b; Tables 2.2, 2.3) and Dromedary and Gullivers (middle Eocene strandline,  $D = 0.081$ ;  $p = 0.975$ ; Figs. 2.1a, 2.4, 2.6b; Tables 2.2, 2.3). Grouping of Notrab, Ambrosia, Atacama, Tripitaka and Gobi can be correlated to geographic proximity of prospects irrespective of their depositional shoreline settings (i.e., Ambrosia and Atacama; middle Eocene shoreline and middle-late Eocene shoreline; ~10 km apart;  $D = 0.051$ ;  $p = 0.925$ ; Figs. 2.1a, 2.4, 2.6b; Tables 2.2, 2.3) and to distal prospects on the same palaeostrandline (i.e., Ambrosia and Tripitaka; middle Eocene strandline; ~94 km apart;  $D = 0.079$ ;  $p = 0.442$ ; Figs. 2.1a, 2.4, 2.6b; Tables 2.2, 2.3). Age spectra of prospects associated with the Barton Barrier (late Eocene strandline; Notrab and Gobi; Hou et al., 2011; Table 2.2) group with prospects identified in the Ooldea Barrier (middle-late Eocene strandline; Atacama;  $0.089 < D < 0.117$ ;  $0.323 < p < 0.914$ ; Figs. 2.1a, 2.4, 2.6b; Tables 2.2, 2.3). This suggests that the middle Eocene and middle-late Eocene strandlines exhibit some shared age signatures of proximal sources (i.e., a distinct Gawler Craton detrital signature) and similarity in sediment regimes (i.e., primary crystalline and intermediate sedimentary sources, time spent in a sedimentary system, and degree and mode of detrital transport and reworking; Fig. 2.5). These underlying fundamental sedimentary system similarities occur despite differences in shoreline geomorphology, lithology, and biostratigraphy (Hou & Warland, 2005; Hou et al., 2006, 2011; Hou & Keeling, 2008).



Balladonia, Thar, and Jacinth exhibit distinct zircon spectra that do not clearly correspond to any particular strandline or to age spectra of proximal prospects (Figs. 2.1a, 2.4, 2.6b; Tables 2.2, 2.3). Jacinth is the only prospect that expresses a similarly high Archean grain contribution (16%) as the far western Balladonia prospect (11%; Figs. 2.1a, 2.4, 2.6a). A crossover of (middle) Eocene and Miocene strandlines in the vicinity of Jacinth is identified from past strandline interpretations and within this study (Hou et al., 2008; Reid et al., 2013a; Fig. 2.1a), and a Neogene enrichment phase may explain the enhanced late Archean Yilgarn Craton signature observed in the Jacinth deposit (Figs. 2.4, 2.5, 2.6a; App. Table 2.1). Sediment enrichment with Yilgarn Craton-derived detrital zircons along the Miocene strandline may be linked to Australia-Antarctica separation and the accelerated spreading of the Australian continent during the Neogene (Veevers et al., 1991). A resulting increase in the fetch of the Southern Ocean and dominance of north-east directed winds likely enhanced i) erosion of the basin's western hinterland regions and the reworking of western Yilgarn Craton detritus-rich Eocene shorelines (e.g., middle-late Eocene strandline with Balladonia) via ocean swells, and ii) eastward transport of material via predominant west to east directed longshore drift (Kemp, 1978; Beard, 1998; Fig. 2.5). Heavy mineral enrichment of Jacinth was likely favoured because of a well-developed sediment trapping site preserved during the Neogene (Hou et al., 2011). The multicycle upgrading of the Jacinth deposit may have occurred inconsistently across the deposit and may explain the greater detrital zircon age variability observed in the age spectra sampled from the deposit (App. Table 2.6). Support for reworking of the middle Eocene strandline by the Miocene shore at Jacinth is found in similarities of middle-late Palaeoproterozoic to early Mesoproterozoic secondary age peaks in Jacinth, Dromedary, and Gullivers (Fig. 2.4; Table 2.3), indicating that all three deposits likely developed on the same middle Eocene shoreline, with Jacinth later becoming upgraded during the Miocene transgression (Fig. 2.5).



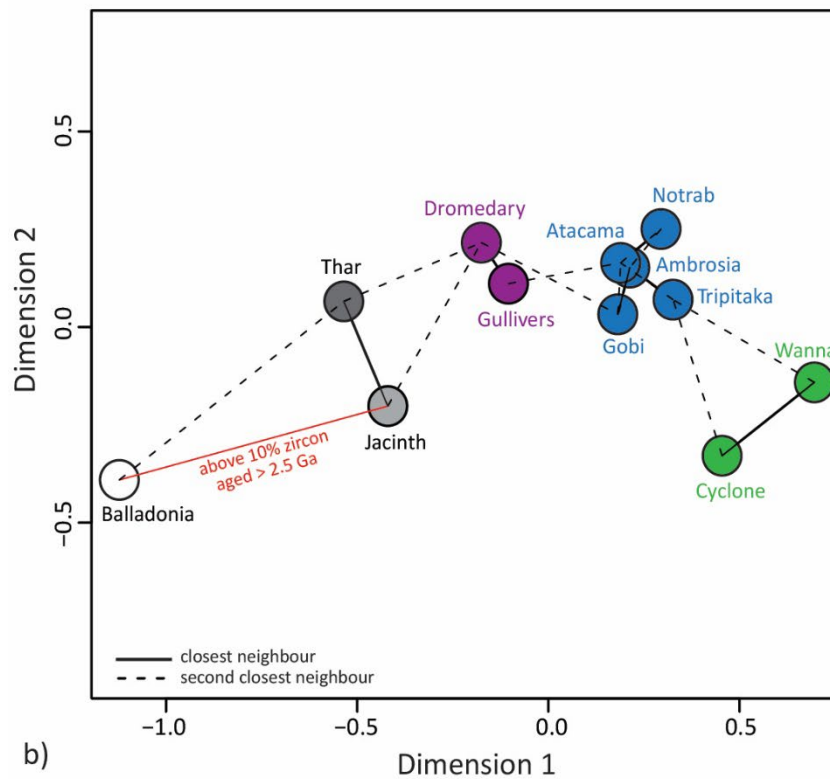
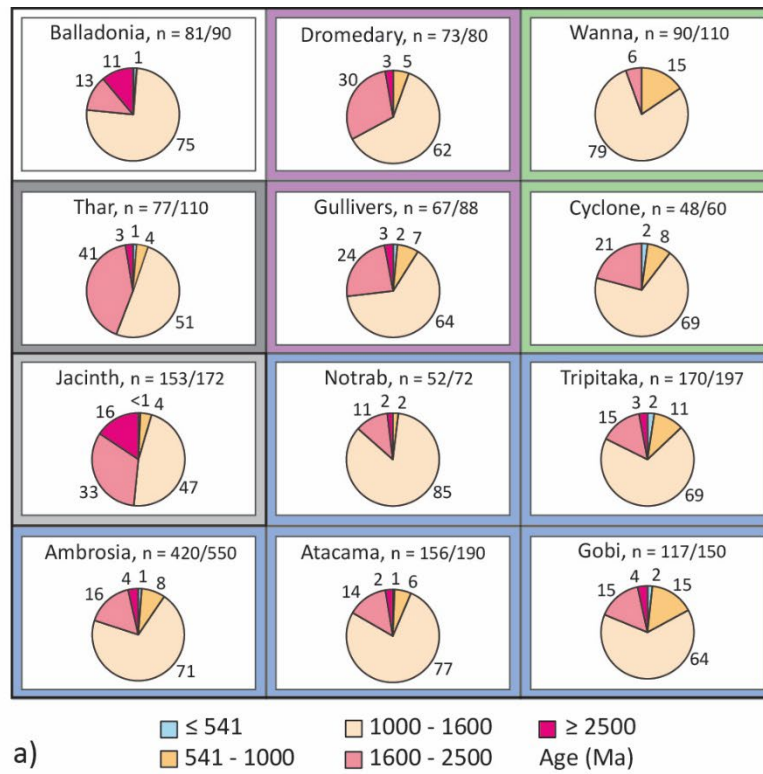


Figure 2.6 Pie charts (a) and multi-dimensional scaling (b) using detrital zircon age spectra of all prospects incorporated in this study. Pie charts representing percentages of zircon age ranges of the total zircon age population of Eucla Basin prospects identified through kernel density estimates (Fig. 2.4). Gobi background sample AD550079 excluded from the analysis.

#### **5.4 Characterising heavy mineral prospectivity and heavy mineral maturation through detrital zircon population analysis**

Previous Eucla Basin publications interpreted intermixing and recycling of primary and secondary sediment sources as the driving factor for prospective beach placer formations in the basin's east (e.g., Hou et al., 2008; Reid et al., 2013a). Here we extend sedimentary provenance regime analysis (i.e., source to sink transportation, routing and reworking, and overall time of detritus spent in a sedimentary system) and test whether U-Pb age data can be further used to directly infer prospectivity of a given region within a mineral sand province.

We incorporated all U-Pb dated samples analysed in this study (Fig. 2.1a; Table 2.1; App. Table 2.2) to show that the degree of sediment source heterogeneity (as a proxy for transport- and recycling-induced maturity via hydraulic segregation and chemical and mechanical selective concentration of stable mineral phases) can be quantified using the Shannon-Weaver diversity index (Shannon & Weaver, 1964) applied to detrital zircon age population data (Fig. 2.7). The test follows the principles of heterogeneity analysis as previously applied to rock compositions (Smosna et al., 1999) and enables a quantitative measure of the degree of sediment mixing/maturation based on the number and distribution of different zircon ages of a detrital age spectrum. Shannon-Weaver heterogeneity is calculated using the equation  $H^* = -\sum p_i \ln p_i$  where  $H^*$  describes the heterogeneity's absolute value and  $p_i$  represents the proportion of an age constituent ( $i$ ). While heavy mineral grades were only available for the newly dated samples, our analysis shows that greater Shannon-Weaver index values (implying greater heterogeneity of the population; Figs. 2.4, 2.7) coincide with greater heavy mineral grades within deposits (Ambrosia and Gobi; Table 2.1). This indicates a relationship between detrital zircon age polymodality, sediment mixing/reworking/maturation and compositional evolution, and heavy mineral enrichment (Figs. 2.4, 2.5, 2.7; Table 2.1).

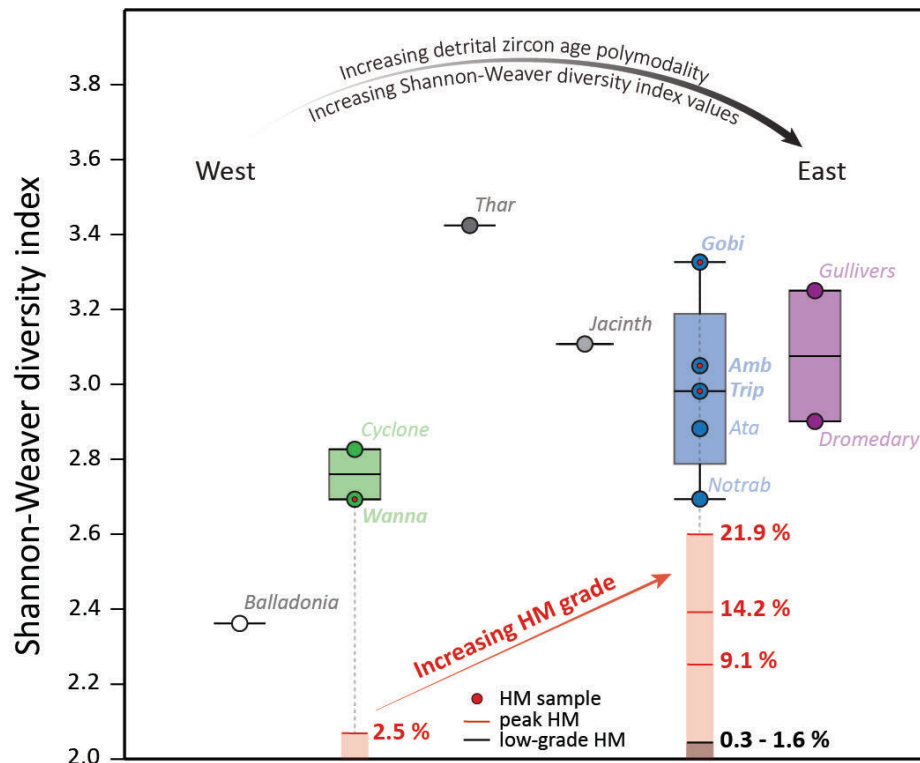


Figure 2.7 Box plot of Shannon-Weaver diversity index coloured according to detrital zircon population similarities (Fig. 2.6). Peak and low heavy mineral grades of newly dated samples (highlighted in bold) from Table 2.1. Gobi background sample AD550079 excluded from the analysis. Amb = Ambrosia, Ata = Atacama, HM = heavy mineral, Trip = Tripitaka.

Integrating mineral compositions, heavy mineral grades, detrital zircon geochronology and heterogeneity analyses to the Eucla Basin more broadly indicates at least two distinct sediment systems may be operating in the basin (Fig. 2.5). The lowest Shannon-Weaver diversity index is observed in Balladonia (~2.4; Figs. 2.1a, 2.7) and corresponds with a weakly polymodal age spectrum correlating with local sources in the Albany-Fraser Orogen (Fig. 2.4; App. Table 2.1), indicating that the degree of sediment working/maturation (i.e., degree of transportation, recycling, attrition and intermixing of resistant minerals from various sources) along the western Eucla Basin margin was minor (Fig. 2.5). The interpretation of a proximal and single-cycle sediment provenance is consistent with the prospect's low heavy mineral grade (~1.4%) and heavy mineral assemblage with a high concentration of more labile (relative to ultrastable zircon and rutile) ilmenite (~82%; <3.5% for zircon and rutile; Hou et al., 2011; Fig. 2.5). It is therefore likely that the western Eucla Basin expresses high contributions of Archean-aged detritus across differently aged Cenozoic shorelines with overall lower heavy mineral grades compared to deposits on the northern and eastern basin margins.

A higher Shannon-Weaver diversity index is observed in the northern prospects Wanna and Cyclone (~2.8; Figs. 2.1a, 2.7) and further increases for prospects positioned in the basin's east (~3.0 – 3.4; Figs. 2.1a, 2.7). The rising diversity index corresponds with increasing detrital zircon age polymodality (Fig. 2.4) and highlights zircon ages that are more similar to age spectra of the Officer Basin and ages associated with the Gawler Craton (Fig. 2.4; App. Table 2.1). All northern and eastern deposits exhibit heavy mineral grades that exceed those observed in the western basin (~2.5 - 21.9% for northern and eastern prospects; Hou et al., 2011; Table 2.1). The higher heavy mineral grades appear associated with multicycle sediment maturation, intermixing, and upgrading from various aged sources (Figs. 2.4, 2.5; App. Table 2.1). Heavy mineral assemblages of northern and eastern prospects (excluding Atacama, Dromedary, and Gullivers) are mainly dominated by the ultrastable mineral phases zircon and rutile (up to 98%; Hou et al., 2011; Fig. 2.2), indicating extensive sediment transport, diagenesis, and reworking with associated destruction of labile phases (Fig. 2.5). Intermixing of sediments from distal and proximal sources is associated with increased ilmenite concentrations observed in the heavy mineral assemblages from Atacama, Dromedary, and Gullivers (~57–75%; ~15–21% zircon; ~2% rutile; Hou et al., 2011), highlighting the significance of continued less mature heavy mineral supplies from more proximal sources (e.g., Gawler Craton; Fig. 2.5). The importance of sediment contributions from proximal sources to Eucla Basin beach placers has been identified previously with monazite, another less resistant mineral phase (Jacinth deposit; Reid et al., 2013a), further supporting our interpretations. Sedimentary trapping (e.g., J-shaped bay formation at Jacinth; Hou et al., 2011) is crucial for final heavy mineral endowment, as (eastern) deposits may express polymodal age spectra (i.e., enhanced sediment mixing through extensive transportation and recycling of resistant heavy minerals from varying sources) without proportionally increased heavy mineral grades (i.e., Thar and Gobi deposits; Fig. 2.1a; Table 2.1).

### **5.5 Heavy mineral age spectra implications for exploration targeting**

Exploration targeting for mineral deposits in global settings relies on a wide range of data. In recent decades, the concept of mineral systems analysis, an approach to understanding the complex geologic processes involved in the formation and preservation of mineral deposits, has become increasingly adopted in industry and academia (e.g., Wyborn et al., 1994; Barnicoat, 2007; Blewett et al., 2009; Barnes et

al., 2016; Wei et al., 2020). The mineral systems model applies a comprehensive analysis of the source to sink pathways and the energy and fluid flow involved in the generation and preservation of ore deposits to reduce exploration risk (e.g., Wyborn et al., 1994; Porwal et al., 2010; McCuaig & Hronsky, 2014; Joly et al., 2015; Li et al., 2018; Mao et al., 2019). The main goal of a mineral systems approach is to link scientific knowledge of ore formation to its practical application in exploration field work (McCuaig et al., 2010).

Integrating traditional detrital zircon U-Pb geochronology (to infer sediment provenance and resource source) with statistical similarity and heterogeneity analyses (e.g., Kolmogorov-Smirnov distance-based multidimensional scaling and Shannon-Weaver heterogeneity testing) helps improve the understanding of important deeper geologic controls on heavy minerals in sands (Garzanti & Andò, 2007). This more mineral systems-based approach to heavy minerals is relevant for better targeting of exploration efforts and prospectivity evaluations in global sedimentary basins. Enhanced statistical interrogation of large detrital zircon geochronology data sets (as are increasingly available via the proliferation of LA-ICPMS and now available for the Eucla Basin) enables more nuanced differentiation of age modes crucial for understanding localised sediment routing and recycling controls on deposit makeup. Further, we believe detrital zircon age spectra heterogeneity testing is a valuable method to efficiently quantify the heavy mineral maturity of sediment reservoirs for prospectivity models. By integrating a Shannon-Weaver heterogeneity test of U-Pb detrital zircon age spectra with heavy mineral compositional analysis, the source heterogeneity of resistant minerals (as a proxy for catchment scale, degree of transportation and recycling, and overall active time in the sediment system) can be estimated. Such an understanding can be directly linked to processes of economic mineral enrichment due to progressive recalcitrant mineral concentration associated with enhanced sediment compositional maturity (destruction of labile phases through diagenesis and physical modification, as well as fractionation during transport; Weissbrod & Nachmias, 1986; Dinis & Soares, 2007; Garzanti & Andò, 2007). A comprehensive understanding of the primary crystalline source regions, the ability to define intermediate storage and quantify sediment evolution through the sediment cycle, and recognition of ultimate in-situ upgrading are all necessary in the identification of economically valuable beach placer deposits. In-depth understanding

of these deeper controls is critical for identifying broader prospectivity beyond the final fractionation processes at the ultimate trap site and may prove particularly useful for the global mineral sector concerned with prospectivity analyses of sedimentary settings in greenfield basins.

## **6. Conclusions**

Detrital zircon age spectra from Cenozoic heavy mineral prospects across the Eucla Basin margins indicate dominant Mesoproterozoic ages with variable secondary age components. Subtle variations within primary and secondary detrital zircon age modes highlight unique geographical and temporal controls on sediment provenance. Two distinct heavy mineral systems are identified. Sediment supply to the western region of the Eucla Basin is restricted (Albany-Fraser Orogen and Yilgarn Craton), while northern and eastern basin margins evidence detritus derived from several Mesoproterozoic sources (Musgrave, Madura and Coompana provinces and Albany-Fraser Orogen) and secondary Archean sources (Yilgarn Craton and Gawler Craton) likely via intermediate sedimentary basins. The significance of subordinate local age signatures, regionally specific sediment regimes (relating to detrital source, transportation, and recycling variability), and enrichment of beach placers is highlighted by a dominant geographic influence of the palaeoshoreline detrital zircon age signatures. Quantification of time within the sediment system (transport, mixing and recycling), critical to heavy mineral upgrading, within a sedimentary basin can be achieved using a Shannon-Weaver diversity test of U-Pb detrital zircon ages. With distance to the basin's east, increased sediment recycling and compositional maturation is expressed in greater detrital zircon age polymodality, higher heavy mineral grades and elevated zircon-rutile mass percentages. Detrital zircon analysis assists in the understanding of underlying geologic processes related to heavy mineral endowment and the prospectivity of sedimentary basins prior to ultimate trap identification.

## **Acknowledgements**

The authors thank the editors and two anonymous reviewers for their constructive feedback that helped improve the original paper draft. We would like to acknowledge Iluka Resources Ltd. for the provision of sample material. Iluka Resources Ltd. representatives Rohan Hine and David Sleight, as well as Paul Smith and Nickolas Northcott are thanked for helpful discussions, assistance, and support. Noreen Evans and Bradley McDonald from the John de Laeter Centre at Curtin University facilitated laser ablation measurements. We gratefully acknowledge the Mineral Research Institute of Western Australia (MRIWA) grant M551, and Curtin University for a Master of Research Stipend Scholarship that enabled this work.

## Chapter Two Reference List

- Akinlotan, O. O., & Rogers, G. H. (2021). Heavy mineral constraints on the provenance evolution of the English Lower Cretaceous (Wessex Basin). *Marine and Petroleum Geology*, *127*, 104952. <https://doi.org/10.1016/j.marpetgeo.2021.104952>
- Akinlotan, O. O., Rogers, G. H., & Okunuwadije, S. E. (2021). Provenance evolution of the English Lower Cretaceous Weald Basin and implications for palaeogeography of the northwest European massifs: constraints from heavy mineral assemblages. *Marine and Petroleum Geology*, *127*, 104953. <https://doi.org/10.1016/j.marpetgeo.2021.104953>
- Allen, S., McPhie, J., Ferris, G., & Simpson, C. (2008). Evolution and architecture of a large felsic igneous province in western Laurentia: The 1.6 Ga Gawler Range Volcanics, South Australia. *Journal of Volcanology and Geothermal Research*, *172*(1-2), 132-147. <https://doi.org/10.1016/j.jvolgeores.2005.09.027>
- Australian Critical Minerals Prospectus. (2020). Australian Government, Australian Trade and Investment Commission, Geoscience Australia, Department of Industry, Science, Energy and Resources. Retrieved from <https://www.austrade.gov.au/International/Invest/Opportunities/Resources-and-energy>
- Barham, M., & Kirkland, C. L. (2020). Changing of the guards: Detrital zircon provenance tracking sedimentological reorganization of a post-Gondwanan rift margin. *Basin Research*, *32*, 854-874. <https://doi.org/10.1111/bre.12403>
- Barham, M., Reynolds, S., Kirkland, C. L., O'Leary, M. J., Evans, N. J., Allen, H. J., . . . McDonald, B. J. (2018). Sediment routing and basin evolution in Proterozoic to Mesozoic east Gondwana: A case study from southern Australia. *Gondwana Research*, *58*, 122-140. <https://doi.org/10.1016/j.gr.2018.03.006>
- Barnes, S. J., Cruden, A. R., Arndt, N., & Saumur, B. M. (2016). The mineral system approach applied to magmatic Ni–Cu–PGE sulphide deposits. *Ore Geology Reviews*, *76*, 296-316. <https://doi.org/10.1016/j.oregeorev.2015.06.012>
- Barnicoat, A. (2007). Mineral systems and exploration science: linking fundamental controls on ore deposition with the exploration process. In: Andrew, C. J. et al., (Eds.), 2007, *Digging Deeper: Proceedings of the Ninth Biannual SGA Meeting, Dublin, Ireland, 20th-23rd August 2007*, 1407-1410.
- Beard, J. (1998). Position and developmental history of the central watershed of the Western Shield, Western Australia. *Journal of the Royal Society of Western Australia*, *81*, 157-164.
- Benbow, M. (1990). Tertiary coastal dunes of the Eucla Basin, Australia. *Geomorphology*, *3*(1), 9-29.
- Bendall, B., Jensen-Schmidt, B., Holford, S., Dutch, R., & Pawley, M. (2016). Insights into the nature and extent of sedimentary basins underlying the Eucla Basin from reprocessing and interpretation of the 13GA-EG1 Eucla-Gawler



- Seismic Survey. *Australian Earth Sciences Convention, Adelaide, South Australia, June 26<sup>th</sup>-30<sup>th</sup>, 2016.*
- Benisek, A., & Finger, F. (1993). Factors controlling the development of prism faces in granite zircons: a microprobe study. *Contributions to mineralogy and petrology*, 114(4), 441-451. <https://doi.org/10.1007/bf00321749>
- Blewett, R., Champion, D., Czarnota, K., Henson, P., Goscombe, B., Halley, S., . . . Roache, T. (2009). Five answers to five questions: a scale-integrated mineral systems study of the East Yilgarn Craton. In: *Williams, et al. (Eds.), 2009, Smart Science for Exploration and Mining, Proceedings of the 10th Biennial SGA Meeting of the Society for Geology Applied to Mineral Deposits, Townsville Australia, p. 84-86.*
- Brown, B., Müller, R., Gaina, C., Struckmeyer, H., Stagg, H., & Symonds, P. (2003). Formation and evolution of Australian passive margins: Implications for locating the boundary between continental and oceanic crust. *Special Papers - Geological Society of America*, 372, 223-243. <https://doi.org/10.1130/0-8137-2372-8.223>
- Caracciolo, L. (2020). Sediment generation and sediment routing systems from a quantitative provenance analysis perspective: Review, application and future development. *Earth-Science Reviews*, 209, 103226. <https://doi.org/10.1016/j.earscirev.2020.103226>
- Caracciolo, L., Chew, D., & Andò, S. (2020). Sediment Generation and Sediment Routing Systems. *Earth-Science Reviews*, 207, 103221. <https://doi.org/10.1016/j.earscirev.2020.103221>
- Cassidy, K., Champion, D., Krapez, B., Barley, M., Brown, S., Blewett, R., . . . Tyler, I. (2006). A revised geological framework for the Yilgarn Craton, Western Australia. *Geological Survey of Western Australia, Record 2006/8*, 8.
- Clark, C., Kirkland, C. L., Spaggiari, C. V., Oorschot, C., Wingate, M. T., & Taylor, R. J. (2014). Proterozoic granulite formation driven by mafic magmatism: an example from the Fraser Range Metamorphics, Western Australia. *Precambrian Research*, 240, 1-21. <https://doi.org/10.1016/j.precamres.2013.07.024>
- Clark, D. J., Hensen, B. J., & Kinny, P. D. (2000). Geochronological constraints for a two-stage history of the Albany–Fraser Orogen, Western Australia. *Precambrian Research*, 102(3), 155-183. [https://doi.org/10.1016/S0301-9268\(00\)00063-2](https://doi.org/10.1016/S0301-9268(00)00063-2)
- Clarke, J. D., Gammon, P. R., Hou, B., & Gallagher, S. J. (2003). Middle to Upper Eocene stratigraphic nomenclature and deposition in the Eucla Basin. *Australian Journal of Earth Sciences*, 50(2), 231-248. <https://doi.org/10.1046/j.1440-0952.2003.00995.x>
- Courtney-Davies, L., Ciobanu, C. L., Tapster, S. R., Cook, N. J., Ehrig, K., Crowley, J. L., . . . Condon, D. J. (2020). Opening the magmatic-hydrothermal window: High-precision U-Pb geochronology of the Mesoproterozoic Olympic Dam Cu-U-Au-Ag deposit, South Australia. *Economic Geology*, 115(8), 1855-1870. <https://doi.org/10.5382/econgeo.4772>

- Cowley, W., Conor, C., & Zang, W. (2003). New and revised Proterozoic stratigraphic units on northern Yorke Peninsula. *MESA Journal*, 29, 46-58.
- Daly, S. (1998). Tectonic evolution and exploration potential of the Gawler Craton, South Australia. *AGSO Journal of Australian Geology Geophysics*, 17, 145-168.
- de Broekert, P., & Sandiford, M. (2005). Buried inset-valleys in the Eastern Yilgarn Craton, Western Australia: geomorphology, age, and allogenic control. *The Journal of Geology*, 113(4), 471-493. <https://doi.org/10.1086/430244>
- de Gromard, R. Q., Wingate, M. T. D., Kirkland, C., Smithies, R., & Howard, H. (2016). Geology and U-Pb Geochronology of the Warlawurru Supersuite and MacDougall Formation in the Mitika and Wanarn Areas, West Musgrave Province. *Geological Survey of Western Australia, Record 2016/4*, 29. Retrieved from <http://hdl.handle.net/20.500.11937/55206>
- Dill, H. G., & Skoda, R. (2017). Provenance analysis of heavy minerals in beach sands (Falkland Islands/Islas Malvinas) – A view to mineral deposits and the geodynamics of the South Atlantic Ocean. *Journal of South American Earth Sciences*, 78, 17-37. <https://doi.org/10.1016/j.jsames.2017.06.005>
- Dinis, P. A., & Soares, A. F. (2007). Stable and ultrastable heavy minerals of alluvial to nearshore marine sediments from Central Portugal: Facies related trends. *Sedimentary Geology*, 201(1-2), 1-20. <https://doi.org/10.1016/j.sedgeo.2007.04.004>
- Doyle, M. G., Fletcher, I. R., Foster, J., Large, R. R., Mathur, R., McNaughton, N. J., . . . Rasmussen, B. (2015). Geochronological constraints on the Tropicana gold deposit and Albany-Fraser orogen, Western Australia. *Economic Geology*, 110(2), 355-386. <https://doi.org/10.2113/econgeo.110.2.355>
- Dröllner, M., Barham, M., Kirkland, C., & Ware, B. (2021). Every zircon deserves a date: selection bias in detrital geochronology. *Geological Magazine*, 158, 1-8. <https://doi.org/10.1017/S0016756821000145>
- Edgoose, C., Scrimgeour, I., & Close, D. (2004). Geology of the Musgrave Block, Northern Territory. *Northern Territory Geological Survey, Report 15*, 48.
- Ejeh, O. I., Akpoborie, I. A., & Etobro, A. A. I. (2015). Heavy minerals and geochemical characteristics of sandstones as indices of provenance and source area tectonics of the Ogwashi-Asaba Formation, Niger Delta Basin. *Open Journal of Geology*, 5(08), 562-576. <https://doi.org/10.4236/ojg.2015.58051>
- Fanning, C., Reid, A., & Teale, G. S. (2007). A geochronological framework for the Gawler Craton, South Australia. *South Australia Geological Survey. Bulletin* 55, 258.
- Fedo, C. M., Sircombe, K. N., & Rainbird, R. H. (2003). Detrital zircon analysis of the sedimentary record. *Reviews in Mineralogy and Geochemistry*, 53(1), 277-303. <https://doi.org/10.2113/0530277>
- Ferris, G., & Schwarz, M. (2004). Definition of the Tunkillia Suite, western Gawler craton. *MESA Journal*, 34, 32-41.

- Force, E. R. (1980). The provenance of rutile. *Journal of Sedimentary Research*, 50(2), 485-488. <https://doi.org/10.1306/212F7A31-2B24-11D7-8648000102C1865D>
- Fraser, G., & Neumann, N. (2016). Under the Nullarbor: New SHRIMP U-Pb zircon ages from the Coompana, Madura and Albany-Fraser Provinces, and Officer Basin, western South Australia and eastern Western Australia. *Geoscience Australia, Record 2016/16*, 70. <http://dx.doi.org/10.11636/Record.2016.016>
- Gallant, J., Wilson, N., Dowling, T., Read, A., & Inskip, C. (2011). SRTM-derived 1 Second Digital Elevation Models Version 1.0. Record 1. *Geoscience Australia, Canberra*. <http://pid.geoscience.gov.au/dataset/ga/72759>
- Garzanti, E., & Andò, S. (2007). Heavy mineral concentration in modern sands: implications for provenance interpretation. *Developments in Sedimentology*, 58, 517-545. [https://doi.org/10.1016/S0070-4571\(07\)58020-9](https://doi.org/10.1016/S0070-4571(07)58020-9)
- Garzanti, E., & Andò, S. (2019). Heavy minerals for junior woodchucks. *Minerals*, 9(3), 148. <https://doi.org/10.3390/min9030148>
- Gehrels, G. (2009). Age pick program. *University of Arizona Laserchron Center, Tucson, AZ*.
- Gehrels, G. (2014). Detrital zircon U-Pb geochronology applied to tectonics. *Annual Review of Earth and Planetary Sciences*, 42, 127-149. <https://doi.org/10.1146/annurev-earth-050212-124012>
- Gehrels, G. E., Blakey, R., Karlstrom, K. E., Timmons, J. M., Dickinson, B., & Pecha, M. (2011). Detrital zircon U-Pb geochronology of Paleozoic strata in the Grand Canyon, Arizona. *Lithosphere*, 3(3), 183-200. <https://doi.org/10.1130/L121.1>
- Government of South Australia - Department for Energy and Mining. (2020). South Australia's major operating/approved mines. Resource estimates and production statistics. <https://map.sarig.sa.gov.au/CrystalRunner/Report/Export/1?exportName=MajorProjects>
- Gurnis, M. (2001). Sculpting the Earth from inside out. *Scientific American*, 284(3), 40-47. Retrieved from <https://www.jstor.org/stable/10.2307/26059128>
- Haines, P., Wingate, M., & Kirkland, C. (2013). Detrital Zircon U-Pb Ages from the Paleozoic of the Canning and Officer basins, Western Australia: implications for provenance and interbasin connections. *Proceedings of the West Australian Basins Symposium, Perth, Western Australia, 2013*, 18.
- Hand, M., Reid, A., & Jagodzinski, L. (2007). Tectonic framework and evolution of the Gawler Craton, Southern Australia. *Economic Geology*, 102(8), 1377-1395. <https://doi.org/10.2113/gsecongeo.102.8.1377>
- Harlan, S. S., Heaman, L., LeCheminant, A. N., & Premo, W. R. (2003). Gunbarrel mafic magmatic event: A key 780 Ma time marker for Rodinia plate reconstructions. *Geology*, 31(12), 1053-1056. <https://doi.org/10.1130/G19944.1>
- Hartnady, M. I. H., Kirkland, C. L., Dutch, R. A., Bodorkos, S., & Jagodzinski, E. A. (2020). Evaluating zircon initial Hf isotopic composition using a combined SIMS–MC–LASS–ICP–MS approach: A case study from the Coompana

- Province in South Australia. *Chemical geology*, 558, 119870.  
<https://doi.org/10.1016/j.chemgeo.2020.119870>
- Hegde, V. S., Shalini, G., & Kanchanagouri, D. G. (2006). Provenance of heavy minerals with special reference to ilmenite of the Honnavar beach, central west coast of India. *Current Science*, 91(5), 644-648. Retrieved from <http://www.jstor.org.dbgw.lis.curtin.edu.au/stable/24094372>
- Helland-Hansen, W., Sømme, T. O., Martinsen, O. J., Lunt, I., & Thurmond, J. (2016). Deciphering Earth's natural hourglasses: perspectives on source-to-sink analysis. *Journal of Sedimentary Research*, 86(9), 1008-1033.  
<https://doi.org/10.2110/jsr.2016.56>
- Hou, B., Alley, N., Frakes, L., Gammon, P. R., & Clarke, J. (2003c). Facies and sequence stratigraphy of Eocene palaeovalley fills in the eastern Eucla Basin, South Australia. *Sedimentary Geology*, 163(1-2), 111-130.  
[https://doi.org/10.1016/S0037-0738\(03\)00175-1](https://doi.org/10.1016/S0037-0738(03)00175-1)
- Hou, B., Alley, N., Frakes, L., Stoian, L., & Cowley, W. (2006). Eocene stratigraphic succession in the Eucla Basin of South Australia and correlation to major regional sea-level events. *Sedimentary Geology*, 183(3-4), 297-319.  
<https://doi.org/10.1016/j.sedgeo.2005.10.007>
- Hou, B., Frakes, L., & Alley, N. (2001). Development of geoscientific models for the exploration in Tertiary palaeochannels draining the Gawler Craton, SA. *South Australia, Minerals and Energy Resources. Geoscientific Report Book 2001/021*, 133.
- Hou, B., Frakes, L., Alley, N., & Clarke, J. (2003b). Characteristics and evolution of the Tertiary palaeovalleys in the northwest Gawler Craton, South Australia. *Australian Journal of Earth Sciences*, 50(2), 215-230.  
<https://doi.org/10.1046/j.1440-0952.2003.00987.x>
- Hou, B., Frakes, L., Alley, N., & Heithersay, P. (2003a). Evolution of beach placer shorelines and heavy-mineral deposition in the eastern Eucla Basin, South Australia. *Australian Journal of Earth Sciences*, 50(6), 955-965. <https://doi.org/10.1111/j.1400-0952.2003.01036.x>
- Hou, B., Frakes, L., Sandiford, M., Worrall, L., Keeling, J., & Alley, N. (2008). Cenozoic Eucla Basin and associated palaeovalleys, southern Australia—climatic and tectonic influences on landscape evolution, sedimentation and heavy mineral accumulation. *Sedimentary Geology*, 203(1-2), 112-130.  
<https://doi.org/10.1016/j.sedgeo.2007.11.005>
- Hou, B., & Keeling, J. (2008). Eucla basin, emerging as a new heavy mineral province of global significance: Old province—new ideas. *MESA Journal*, 49, 20-26.
- Hou, B., Keeling, J., Reid, A., Fairclough, M., Warland, I., Belousova, E., . . . Hocking, R. (2011). Heavy mineral sands in the Eucla Basin, southern Australia: deposition and province-scale prospectivity. *Economic Geology*, 106(4), 687-712. <https://doi.org/10.2113/econgeo.106.4.687>
- Hou, B., & Warland, I. (2005). Heavy mineral sands potential of the Eucla Basin in South Australia—a world-class palaeobeach placer province. *MESA Journal*, 37, 4-12.

- Howard, H., Smithies, R., Evins, P., Kirkland, C., Werner, M., Wingate, M., & Pirajno, F. (2011). Explanatory notes for the west Musgrave Province. *Geological Survey of Western Australia, Record 2011/4*, 349.
- Howard, H., Smithies, R., Kirkland, C., Kelsey, D., Aitken, A., Wingate, M., . . . Maier, W. D. (2015). The burning heart—the Proterozoic geology and geological evolution of the west Musgrave Region, central Australia. *Gondwana Research*, 27(1), 64-94. <https://doi.org/10.1016/j.gr.2014.09.001>
- Howard, K. E., Hand, M., Barovich, K. M., Payne, J. L., & Belousova, E. A. (2011). U–Pb, Lu–Hf and Sm–Nd isotopic constraints on provenance and depositional timing of metasedimentary rocks in the western Gawler Craton: Implications for Proterozoic reconstruction models. *Precambrian Research*, 184(1-4), 43-62. <https://doi.org/10.1016/j.precamres.2010.10.002>
- Iluka Resources Limited. (2021). Jacinth-Ambrosia Overview. <https://iluka.com/operations-resource-development/operations/jacinth-ambrosia>. Retrieved from <https://www.iluka.com/operations-resource-636-development/operations/jacinth-ambrosia>
- Jackson, S. E., Pearson, N. J., Griffin, W. L., & Belousova, E. A. (2004). The application of laser ablation-inductively coupled plasma-mass spectrometry to in situ U–Pb zircon geochronology. *Chemical geology*, 211(1-2), 47-69. <https://doi.org/10.1016/j.chemgeo.2004.06.017>
- Jagodzinski, E. (2005). Compilation of SHRIMP U-Pb geochronological data, Olympic Domain, Gawler Craton, South Australia, 2001-2003. *Geoscience Australia Record*, 20, 197.
- Jagodzinski, E. A., Bodorkos, S., & Crowley, J. L. (2018). PACE Copper Coompana Drilling Project: U-Pb Dating of Basement and Cover Rocks. *Department for Energy and Mining, South Australia, Report Book 2018/00028*, 211.
- Jagodzinski, E. A., Reid, A., & Gribbin, G. (2019). U-Pb geochronological data from the Fowler Domain, western Gawler Craton. *Department for Energy and Mining, Adelaide, South Australia, Report Book 2019/00018*, 58.
- Joly, A., Porwal, A., McCuaig, T. C., Chudasama, B., Dentith, M. C., & Aitken, A. R. (2015). Mineral systems approach applied to GIS-based 2D-prospectivity modelling of geological regions: Insights from Western Australia. *Ore Geology Reviews*, 71, 673-702. <https://doi.org/10.1016/j.oregeorev.2015.06.007>
- Jones, B. (1990). Cretaceous and Tertiary sedimentation on the western margin of the Eucla Basin. *Australian Journal of Earth Sciences*, 37(3), 317-329. <https://doi.org/10.1080/08120099008727930>
- Kemp, E. M. (1978). Tertiary climatic evolution and vegetation history in the southeast Indian Ocean region. *Palaeogeography, Palaeoclimatology, Palaeoecology*, 24(3), 169-208. [https://doi.org/10.1016/0031-0182\(78\)90042-1](https://doi.org/10.1016/0031-0182(78)90042-1)
- Kesler, S. E. (2007). Mineral supply and demand into the 21st century. In: *Briskey, J. A. and Schulz, K. J., (Eds.) US Geological Survey circular 1294. Proceedings for a workshop on deposit modeling, mineral resource assessment, and their role in sustainable development. Reston, VA, USA. Geological Survey*, 55-62.

- Kinny, P. D., & Nutman, A.P. (1996). Zirconology of the Meeberrie gneiss, Yilgarn craton, Western Australia: An early Archaean migmatite. *Precambrian Research*, 78, 165-178. [https://doi.org/10.1016/0301-9268\(95\)00076-3](https://doi.org/10.1016/0301-9268(95)00076-3)
- Kinny, P. D., Wijbrans, J., Froude, D., Williams, I., & Compston, W. (1990). Age constraints on the geological evolution of the Narryer Gneiss Complex, Western Australia. *Australian Journal of Earth Sciences*, 37, 51-69. <https://doi.org/10.1080/08120099008727905>
- Kirkland, C. L., Smithies, R., & Spaggiari, C. (2015a). Foreign contemporaries—Unravelling disparate isotopic signatures from Mesoproterozoic Central and Western Australia. *Precambrian Research*, 265, 218-231. <https://doi.org/10.1016/j.precamres.2014.12.001>
- Kirkland, C. L., Smithies, R. H., Spaggiari, C., Wingate, M., De Gromard, R. Q., Clark, C., . . . Belousova, E. A. (2017). Proterozoic crustal evolution of the Eucla basement, Australia: Implications for destruction of oceanic crust during emergence of Nuna. *Lithos*, 278, 427-444. <https://doi.org/10.1016/j.lithos.2017.01.029>
- Kirkland, C. L., Smithies, R. H., Woodhouse, A. J., Howard, H. M., Wingate, M. T., Belousova, E. A., . . . Spaggiari, C. V. (2013). Constraints and deception in the isotopic record; the crustal evolution of the west Musgrave Province, central Australia. *Gondwana Research*, 23(2), 759-781. <https://doi.org/10.1016/j.gr.2012.06.001>
- Kirkland, C. L., Spaggiari, C. V., Pawley, M., Wingate, M., Smithies, R. H., Howard, H., . . . Poujol, M. (2011). On the edge: U–Pb, Lu–Hf, and Sm–Nd data suggests reworking of the Yilgarn craton margin during formation of the Albany-Fraser Orogen. *Precambrian Research*, 187(3-4), 223-247. <https://doi.org/10.1016/j.precamres.2011.03.002>
- Kirkland, C. L., Spaggiari, C. V., Smithies, R. H., Wingate, M. T. D., Belousova, E. A., Gréau, Y., . . . Creaser, R. (2015b). The affinity of Archean crust on the Yilgarn—Albany—Fraser Orogen boundary: Implications for gold mineralisation in the Tropicana Zone. *Precambrian Research*, 266, 260-281. <https://doi.org/10.1016/j.precamres.2015.05.023>
- Kullerud, G. (2003). Ore Petrology. In: R. A. Meyers (Ed.), *Encyclopedia of Physical Science and Technology (Third Edition)* (pp. 411-433). New York: Academic Press.
- Le Roux, J. P. (1990). Flume study on the concentration of ilmenite in fine-grained sand and implications concerning uranium mineralization in the Beaufort Group. *South African Journal of Geology*, 93(5/6), 785-794. Retrieved from [http://inis.iaea.org/search/search.aspx?orig\\_q=RN:23014145](http://inis.iaea.org/search/search.aspx?orig_q=RN:23014145)
- Li, N., Xiao, K., Sun, L., Li, S., Zi, J., Wang, K., . . . Li, C. (2018). Part I: A resource estimation based on mineral system modelling prospectivity approaches and analogical analysis: A case study of the MVT Pb-Zn deposits in Huayuan district, China. *Ore Geology Reviews*, 101, 966-984. <https://doi.org/10.1016/j.oregeorev.2018.02.014>
- Li, Q., James, N., & McGowran, B. (2003). Middle and Late Eocene Great Australian Bight lithobiostatigraphy and stepwise evolution of the southern

- Australian continental margin. *Australian Journal of Earth Sciences*, 50(1), 113-128. <https://doi.org/10.1046/j.1440-0952.2003.00978.x>
- Lowry, D. C. (1970). Geology of the Western Australian part of the Eucla Basin. *Geological Survey of Western Australia. Bulletin 122*, 201.
- Mackinder, A., Cousens, B. L., Ernst, R. E., & Chamberlain, K. R. (2019). Geochemical, isotopic, and U–Pb zircon study of the central and southern portions of the 780 Ma Gunbarrel Large Igneous Province in western Laurentia. *Canadian Journal of Earth Sciences*, 56(7), 738-755. <https://doi.org/10.1139/cjes-2018-0083>
- Makuluni, P., Kirkland, C., & Barham, M. (2019). Zircon grain shape holds provenance information: a case study from southwestern Australia. *Geological Journal*, 54(3), 1279-1293. <https://doi.org/10.1002/gj.3225>
- Mao, X., Ren, J., Liu, Z., Chen, J., Tang, L., Deng, H., . . . Liu, C. (2019). Three-dimensional prospectivity modeling of the Jiaojia-type gold deposit, Jiaodong Peninsula, Eastern China: A case study of the Dayingezhuang deposit. *Journal of Geochemical Exploration*, 203, 27-44. <https://doi.org/10.1016/j.gexplo.2019.04.002>
- Markwitz, V., & Kirkland, C. (2018). Source to sink zircon grain shape: Constraints on selective preservation and significance for Western Australian Proterozoic basin provenance. *Geoscience Frontiers*, 9(2), 415-430. <https://doi.org/10.1016/j.gsf.2017.04.004>
- Marsh, J. H., Jørgensen, T. R. C., Petrus, J. A., Hamilton, M. A., & Mole, D. R. (2019). U-Pb, trace element, and hafnium isotope composition of the Maniitsoq zircon: A potential new Archean zircon reference material. *Goldschmidt, Barcelona, 18-23 August, 2019*, p. 2161. Retrieved from <https://goldschmidtabstracts.info/2019/2161.pdf>
- McCuaig, T. C., Beresford, S., & Hronsky, J. (2010). Translating the mineral systems approach into an effective exploration targeting system. *Ore Geology Reviews*, 38(3), 128-138. <https://doi.org/10.1016/j.oregeorev.2010.05.008>
- McCuaig, T. C., & Hronsky, J. M. (2014). The mineral system concept: the key to exploration targeting. *Society of Economic Geologists Special Publication*, 18, 153-175. <https://doi.org/10.5382/SP.18.08>
- McIntyre, C. J., Symonds, R. T., Lu, D. Y., Champagne, S., Macchi, A., & Mehrani, P. (2020). Experimental evaluation of hydrodynamics and tube-to-bed heat transfer of fluidized Ilmenite ore particles at elevated pressures. *Powder Technology*, 376, 697-707. <https://doi.org/10.1016/j.powtec.2020.08.062>
- Morón, S., Cawood, P. A., Haines, P. W., Gallagher, S. J., Zahirovic, S., Lewis, C. J., & Moresi, L. (2019). Long-lived transcontinental sediment transport pathways of East Gondwana. *Geology*, 47(6), 513-516. <https://doi.org/10.1130/G45915.1>
- Morton, A. C. (1991). Geochemical studies of detrital heavy minerals and their application to provenance research. *Geological Society, London, Special Publications*, 57(1), 31-45. <https://doi.org/10.1144/GSL.SP.1991.057.01.04>

- Morton, A. C., & Hallsworth, C. (1994). Identifying provenance-specific features of detrital heavy mineral assemblages in sandstones. *Sedimentary Geology*, 90(3), 241-256. [https://doi.org/10.1016/0037-0738\(94\)90041-8](https://doi.org/10.1016/0037-0738(94)90041-8)
- Mücke, A., & Chaudhuri, J. N. B. (1991). The continuous alteration of ilmenite through pseudorutile to leucoxene. *Ore Geology Reviews*, 6(1), 25-44. [https://doi.org/10.1016/0169-1368\(91\)90030-B](https://doi.org/10.1016/0169-1368(91)90030-B)
- Nair, A. G., Babu, D. S. L., Vivekanandan, K., & Vlach, S. R. (2006). Differential alteration of ilmenite in a tropical beach placer, southern India: microscopic and electron probe evidences. *Resource Geology*, 56(1), 75-81. <https://doi.org/10.1111/j.1751-3928.2006.tb00270.x>
- Neumann, N., & Korsch, R. J. (2014). SHRIMP U-Pb zircon ages for Kutjara 1 and Mulyawara 1, Northwestern South Australia. *Geoscience Australia, Canberra, Record 2014/5*, 18.
- Parker, A., Daly, S., Flint, D., Flint, R., Preiss, W., & Teale, G. (1993). Palaeoproterozoic. *The Geology of South Australia*, 1, 50-105.
- Poon, P., Graham, I. T., Liepa, E. A. C., Cohen, D. R., Pringle, I. J., Burkett, D. A., & Privat, K. (2020). Mineral distribution and provenance of heavy mineral sands (zircon, ilmenite, rutile) deposits from the NW Murray Basin, far western NSW, Australia. *Australian Journal of Earth Sciences*, 67(4), 575-590. <https://doi.org/10.1080/08120099.2020.1703813>
- Porwal, A., González-Álvarez, I., Markwitz, V., McCuaig, T., & Mamuse, A. (2010). Weights-of-evidence and logistic regression modeling of magmatic nickel sulfide prospectivity in the Yilgarn Craton, Western Australia. *Ore Geology Reviews*, 38(3), 184-196. <https://doi.org/10.1016/j.oregeorev.2010.04.002>
- Pownceby, M. I., Sparrow, G. J., & Fisher-White, M. J. (2008). Mineralogical characterisation of Eucla Basin ilmenite concentrates: First results from a new global resource. *Minerals engineering*, 21(8), 587-597. <https://doi.org/10.1016/j.mineng.2007.11.011>
- Pupin, J. (1980). Zircon and granite petrology. *Contributions to mineralogy and petrology*, 73(3), 207-220. <https://doi.org/10.1007/BF00381441>
- Reid, A. J. (2019). The Olympic Cu-Au province, Gawler craton: A review of the lithospheric architecture, geodynamic setting, alteration systems, cover successions and prospectivity. *Minerals*, 9, 371. <https://doi.org/10.3390/min9060371>
- Reid, A. J., Hand, M., Jagodzinski, E., Kelsey, D., & Pearson, N. (2008). Paleoproterozoic orogenesis in the southeastern Gawler craton, South Australia. *Australian Journal of Earth Sciences*, 55, 449-471. <https://doi.org/10.1080/08120090801888594>
- Reid, A. J., & Hou, B. (2006). Source of heavy minerals in the Eucla Basin palaeobeach placer province, South Australia: age data from detrital zircons. *MESA Journal*, 42, 10-14.
- Reid, A. J., Jagodzinski, E.A., Fraser, G.L., & Pawley, M.J. (2014). SHRIMP U-Pb zircon age constraints on the tectonics of the Neoproterozoic to early Paleoproterozoic transition within the Mulgathing Complex, Gawler craton,



- South Australia. *Precambrian Research*, 250, 27-49.  
<https://doi.org/10.1016/j.precamres.2014.05.013>
- Reid, A. J., Keeling, J. L., & Belousova, E. A. (2013b). Hf isotopic investigation into the provenance of zircons in heavy mineral sands of the Eucla Basin. *MESA Journal*, 68, 17-24.
- Reid, A. J., Keeling, J., Boyd, D., Belousova, E., & Hou, B. (2013a). Source of zircon in world-class heavy mineral placer deposits of the Cenozoic Eucla Basin, southern Australia from LA-ICPMS U–Pb geochronology. *Sedimentary Geology*, 286-287, 1-19.  
<https://doi.org/10.1016/j.sedgeo.2012.10.008>
- Reid, A. J., Korsch, R., Hou, B., & Black, L. (2009). Sources of sediment in the Eocene Garford paleovalley, South Australia, from detrital-zircon geochronology. *Australian Journal of Earth Sciences*, 56(S1), S125-S137.  
<https://doi.org/10.1080/08120090902871168>
- Reid, A. J., Pawley, M., Wade, C., Jagodzinski, E., Dutch, R., & Armstrong, R. (2020). Resolving tectonic settings of ancient magmatic suites using structural, geochemical and isotopic constraints: the example of the St Peter Suite, southern Australia. *Australian Journal of Earth Sciences*, 67(1), 31-58.  
<https://doi.org/10.1080/08120099.2019.1632224>
- Roy, P. S. (1999). Heavy mineral beach placers in southeastern Australia; their nature and genesis. *Economic Geology*, 94(4), 567-588.  
<https://doi.org/10.2113/gsecongeo.94.4.567>
- Sandiford, M. (2007). The tilting continent: a new constraint on the dynamic topographic field from Australia. *Earth and Planetary Science Letters*, 261(1-2), 152-163. <https://doi.org/10.1016/j.epsl.2007.06.023>
- Senior, A., Britt, A., Summerfield, D., Hughes, A., Hitchman, A., Cross, A., . . . Schofield, A. (2020). Australia's Identified Mineral Resources 2019. *Geoscience Australia, Canberra, AU*, 67.
- Shalini, G., Hegde, V. S., Soumya, M., & Korkoppa, M. M. (2020). Provenance and implications of heavy minerals in the beach sands of India's Central West Coast. *Journal of Coastal Research*, 36(2), 353-361.  
<https://doi.org/10.2112/JCOASTRES-D-19-00046.1>
- Shannon, C. E., & Weaver, W. (1964). The mathematical theory of communication. *Urbana: The University of Illinois Press*, p. 125.
- Sircombe, K., & Freeman, M. (1999). Provenance of detrital zircons on the Western Australia coastline—Implications for the geologic history of the Perth basin and denudation of the Yilgarn craton. *Geology*, 27(10), 879-882.  
[https://doi.org/10.1130/0091-7613\(1999\)027<0879:PODZOT>2.3.CO;2](https://doi.org/10.1130/0091-7613(1999)027<0879:PODZOT>2.3.CO;2)
- Sláma, J., & Košler, J. (2012). Effects of sampling and mineral separation on accuracy of detrital zircon studies. *Geochemistry, Geophysics, Geosystems*, 13(5), 1525-2027. <https://doi.org/10.1029/2012GC004106>
- Smithies, R., Spaggiari, C., & Kirkland, C. (2015). Building the crust of the Albany-Fraser Orogen; constraints from granite geochemistry. *Geological Survey of Western Australia, Report 150*, 49.

- Smosna, R., Bruner, K. R., & Burns, A. (1999). Numerical analysis of sandstone composition, provenance, and paleogeography. *Journal of Sedimentary Research*, 69(5), 1063-1070. <https://doi.org/10.2110/jsr.69.1063>
- Spaggiari, C., Bodorkos, S., Barquero-Molina, M., Tyler, I., & Wingate, M. (2009). Interpreted bedrock geology of the south Yilgarn and central Albany-Fraser orogen, Western Australia. *Geological Survey of Western Australia, Record*, 2009/10, 84.
- Spaggiari, C., Kirkland, C., Pawley, M., Smithies, R., Wingate, M., Doyle, M., . . . Fox, L. (2011). The geology of the east Albany-Fraser Orogen—a field guide. *Geological Survey of Western Australia, Record*, 2009/10, 97.
- Sun, S., Sheraton, J., Glikson, A., & Stewart, A. (1996). A major magmatic event during 1050–1080 Ma in central Australia, and an emplacement age for the Giles Complex. *AGSO Research Newsletter*, 24, 13-15.
- Sundell, K. E., & Saylor, J. E. (2021). Two-Dimensional Quantitative Comparison of Density Distributions in Detrital Geochronology and Geochemistry. *Geochemistry, Geophysics, Geosystems*, 22(4), e2020GC009559. <https://doi.org/10.1029/2020GC009559>
- Szpunar, M., Hand, M., Barovich, K., Jagodzinski, E., & Belousova, E. (2011). Isotopic and geochemical constraints on the Paleoproterozoic Hutchison Group, southern Australia: Implications for Paleoproterozoic continental reconstructions. *Precambrian Research*, 187, 99-126. <https://doi.org/10.1016/j.precamres.2011.02.006>
- Thomas, W. A. (2011). Detrital-zircon geochronology and sedimentary provenance. *Lithosphere*, 3(4), 304-308. <https://doi.org/10.1130/RF.L001.1>
- Vavra, G. (1990). On the kinematics of zircon growth and its petrogenetic significance: a cathodoluminescence study. *Contributions to mineralogy and petrology*, 106(1), 90-99. <https://doi.org/10.1007/BF00306410>
- Vavra, G., Schmid, R., & Gebauer, D. (1999). Internal morphology, habit and U-Th-Pb microanalysis of amphibolite-to-granulite facies zircons: geochronology of the Ivrea Zone (Southern Alps). *Contributions to mineralogy and petrology*, 134(4), 380-404. <https://doi.org/10.1007/s004100050492>
- Veevers, J. J., Powell, C. M., & Roots, S. R. (1991). Review of seafloor spreading around Australia. I. synthesis of the patterns of spreading. *Australian Journal of Earth Sciences*, 38(4), 373-389. <https://doi.org/10.1080/08120099108727979>
- Vermeesch, P. (2004). How many grains are needed for a provenance study? *Earth and Planetary Science Letters*, 224(3-4), 441-451. <https://doi.org/10.1016/j.epsl.2004.05.037>
- Vermeesch, P. (2007). Quantitative geomorphology of the White Mountains (California) using detrital apatite fission track thermochronology. *Journal of Geophysical Research: Earth Surface*, 112(F3), 3004. <https://doi.org/10.1029/2006JF000671>
- Vermeesch, P. (2012). On the visualisation of detrital age distributions. *Chemical geology*, 312-313, 190-194. <https://doi.org/10.1016/j.chemgeo.2012.04.021>

- Vermeesch, P. (2013). Multi-sample comparison of detrital age distributions. *Chemical geology*, 341, 140-146.  
<https://doi.org/10.1016/j.chemgeo.2013.01.010>
- Vermeesch, P. (2018a). IsoplotR: A free and open toolbox for geochronology. *Geoscience Frontiers*, 9(5), 1479-1493.  
<https://doi.org/10.1016/j.gsf.2018.04.001>
- Vermeesch, P. (2018b). Dissimilarity measures in detrital geochronology. *Earth-Science Reviews*, 178, 310-321.  
<https://doi.org/10.1016/j.earscirev.2017.11.027>
- Vermeesch, P., Resentini, A., & Garzanti, E. (2016). An R package for statistical provenance analysis. *Sedimentary Geology*, 336, 14-25.  
<https://doi.org/10.1016/j.sedgeo.2016.01.009>
- Wade, C.E., Reid, A.J., Wingate, M.T., Jagodzinski, E.A., & Barovich, K. (2012). Geochemistry and geochronology of the c. 1585 Ma Benagerie Volcanic Suite, southern Australia: Relationship to the Gawler Range volcanics and implications for the petrogenesis of a Mesoproterozoic silicic large igneous province. *Precambrian Research*, 206-207, 17–35.  
<https://doi.org/10.1016/j.precamres.2012.02.020>
- Wade, C.E., Payne, J.L., Barovich, K.M., & Reid, A.J. (2019). Heterogeneity of the sub-continental lithospheric mantle and “non-juvenile” mantle additions to a Proterozoic silicic large igneous province. *Lithos*, 340–341, 87-107.  
<https://doi.org/10.1016/j.lithos.2019.05.005>
- Wang, X.-C., Li, X.-H., Li, Z.-X., Liu, Y., & Yang, Y.-H. (2010). The Willouran basic province of South Australia: Its relation to the Guibei large igneous province in South China and the breakup of Rodinia. *Lithos*, 119(3), 569-584.  
<https://doi.org/10.1016/j.lithos.2010.08.011>
- Wei, H., Xiao, K., Shao, Y., Kong, H., Zhang, S., Wang, K., . . . Wen, C. (2020). Modeling-based mineral system approach to prospectivity mapping of stratabound hydrothermal deposits: A case study of MVT Pb-Zn deposits in the Huayuan area, northwestern Hunan Province, China. *Ore Geology Reviews*, 120, 103368. <https://doi.org/10.1016/j.oregeorev.2020.103368>
- Weissbrod, T., & Nachmias, J. (1986). Stratigraphic significance of heavy minerals in the Late Precambrian-Mesozoic clastic sequence (“Nubian Sandstone”) in the Near East. *Sedimentary Geology*, 47(3), 263-291.  
[https://doi.org/10.1016/0037-0738\(86\)90086-2](https://doi.org/10.1016/0037-0738(86)90086-2)
- Wiedenbeck, M., Allé, P., Corfu, F., Griffin, W., Meier, M., Oberli, F., . . . Spiegel, W. (1995). Three natural zircon standards for U-Th-Pb, Lu-Hf, trace element and REE analyses. *Geostandards newsletter*, 19(1), 1-23.  
<https://doi.org/10.1111/j.1751-908X.1995.tb00147.x>
- Wilde, S. (2001). Jimperding and Chittering metamorphic belts, southwestern Yilgarn craton, Western Australia: A field guide. *Geological Survey of Western Australia, Record 2001/12*, 24.
- Wingate, M., Kirkland, C., Haines, P., & Hocking, R. (2013a). 199423: Sandstone, Empress 1A. *Geological Survey of Western Australia, Geochronology Record 1112*, 1-6.

- Wingate, M., Kirkland, C., Haines, P., & Hocking, R. (2013b). 199424: Sandstone, Empress 1. *Geological Survey of Western Australia, Geochronology Record 1113*, 1-6.
- Wingate, M., Kirkland, C., Spaggiari, C., & Smithies, R. (2015). U–Pb geochronology of the Forrest Zone of the Coompana Province. *Eucla basement stratigraphic drilling results release workshop: extended abstracts compiled by CV Spaggiari and RH Smithies: Geological Survey of Western Australia, Record 2015/10*, 37-40.
- Wise, T., Dutch, R., Pawley, M., Foss, C., & Thiel, S. (2018). Building the Coompana Province. *MESA Journal*, 88, 25-37.
- Wyborn, L., Heinrich, C., & Jaques, A. (1994). Australian Proterozoic mineral systems: essential ingredients and mappable criteria. *Australasian Institute of Mining and Metallurgy Publication Series 5/94*, 109-115.

## CHAPTER THREE

### **Refining Zircon Provenance Interpretation via Integrated Grain Shape, Geochronology, and Hf Isotopes, a Case Study from the Eucla Basin, Australia**

#### **Abstract**

Sediment provenance studies commonly utilise isotopic and geochemical analyses to resolve detrital mineral sources and routing. Non-unique ages and geochemical characteristics across geographically distinct crystalline source regions can cause significant ambiguities in mineral provenance, as is the case for southern Australia's Cenozoic Eucla Basin. Here, new Hf isotope data are provided from four heavy mineral prospects ( $N = 8$ ,  $n = 844$  [ $N = \text{samples}$ ,  $n = \text{grains}$ ]). Zircon grain shape data are also presented for a suite of detrital Eucla Basin samples ( $N = 22$ ,  $n = 35,604$ ) and the basin's underlying basement, the Coompana Province ( $N = 13$ ,  $n = 824$ ). The data are integrated with published detrital and crystalline zircon U-Pb age, Hf isotope, and grain shape data to investigate the efficacy of grain shape analysis to better resolve the basin's mineral provenance. Eight shape parameters (*area*, *perimeter*, *major and minor axes*, *effective diameter*, *circularity*, *roundness*, and *aspect ratio*) are measured. Hf isotope compositions of newly analysed deposits are consistent with published placer data, indicating a primary Mesoproterozoic juvenile source for zircon melts ( $\sim 1250\text{--}1000$  Ma,  $-2.5 < \epsilon_{\text{Hf}} > \sim +5$ ) with addition of zircon grains from juvenile to evolved late Archean to Phanerozoic-aged zircon bearing magmas ( $-28.0 < \epsilon_{\text{Hf}} > +11$ ). While U-Pb geochronology and Hf-isotope geochemistry are capable of recognising the restricted western margin influence of the Albany-Fraser Orogen as a heavy mineral source, they are incapable of differentiating Mesoproterozoic-aged source rocks of the Musgrave Province to the north or the underlying Madura Province and Coompana Province for the majority of northern and eastern heavy mineral deposits. However, distinct zircon grain shapes facilitate improved differentiation across these Mesoproterozoic sources, i.e., *perimeter* (Madura and Coompana provinces vs Musgrave Province), *major axis* (Madura and Coompana provinces vs Albany-Fraser

Orogen), and *circularity* (Musgrave Province vs Albany-Fraser Orogen). Filtering of U-Pb age, Hf isotope and shape data implicate the underlying Madura and Coompana provinces as dominant sediment sources for Eucla Basin detritus aged ~1400–1000 Ma. The lack of direct sediment pathways between the underlying basement provinces and placer sediments analysed demonstrates the significance of zircon reworking from intermediate sedimentary basins in the formation of the economically significant Eucla Basin beach placers. Such multi-cyclicality is supported by the recognition of the circularity grain shape character as the most pronounced differentiation of detrital vs crystalline zircon grains.

## 1. Introduction

U-Pb geochronology of detrital zircon has become an extensively applied technique to constrain the depositional ages of sedimentary successions and to reconstruct sediment routing from age-defined crystalline source regions (e.g., Reid et al., 2013a; Gehrels, 2014). However, the efficacy of U-Pb detrital zircon fingerprinting in provenance studies may be limited where crystallisation ages of potential magmatic and metamorphic sources are insufficiently different for clear age separation (Andersen, 2005). One approach to resolve sediment provenance in studies involving crystalline source rocks with overlapping crystallisation ages is to measure additional geochemical fingerprints such as Lu-Hf isotopes (e.g., Griffin et al., 2002; Belousova et al., 2006; Gerdes & Zeh, 2006; Zeh et al., 2008; Reid et al., 2013b; Barham et al., 2018; Olierook et al., 2018; Kirkland et al., 2020; Sundell & Saylor, 2021). Isotopic fingerprinting of detrital zircon using Lu-Hf isotopes enables differentiation of whether clastic sediment was derived from a more juvenile or evolved magma and gives insight into the tectonic processes through which source rocks may have formed (i.e., continental collision zones or arc-type settings; Collins et al., 2011; Dhuime et al., 2012; Roberts, 2012). However, the integration of U-Pb geochronology and Hf isotope fingerprinting requires a larger analytical volume (potentially beyond single grain or single growth domain capabilities), is more costly, and may prove difficult for resolving sediment provenance when source regions express similarities in both age and geochemical signatures. Recently, zircon grain shape analyses have been tested for provenance significance (e.g., Markwitz & Kirkland, 2018; Makuluni et al., 2019). Previous works have established that the growth and shape of zircon may be controlled

by crystallisation processes in the original crystalline source area (Pupin, 1980; Vavra, 1990; Corfu et al., 2003), and that certain primary grain shape characteristics may be retained by detrital zircon grains through transport (Markwitz & Kirkland, 2018; Makuluni et al., 2019). Replicating past U-Pb geochronology-based provenance studies with grain shape analyses have suggested that certain grain shape parameters may be used to identify likely sediment source rocks, and that detrital grain shape analyses may help recognise geologically significant sub-populations within sedimentary systems (Makuluni et al., 2019).

The Eucla Basin along the southern Australian margin (Fig. 3.1a) offers an ideal study area for investigating detrital zircon provenance using an integrated approach of U-Pb and Lu-Hf dating techniques with additional grain shape analysis given the economic significance of sediment provenance in the region and three Mesoproterozoic-aged potential source regions (Fig. 3.1a). Better understanding of sediment provenance and routing in this region is economically significant due to its world-class heavy mineral deposits (Hou et al., 2011), two of which have been developed into the largest producing zircon mine in the world (Jacinth-Ambrosia; Iluka Resources Limited, 2021; Fig. 3.1b). Previous provenance studies on detrital zircon grains from Eucla Basin beach placer deposits incorporated U-Pb dating and some Hf isotope fingerprinting (Reid & Hou, 2006; Hou et al., 2011; Reid et al., 2013a, b; Gartmair et al., 2022). However, many aspects of the basin's source to sink routing history remain poorly understood because of the basin's bounding and underlying crystalline basements overlapping Mesoproterozoic zircon-forming ages (i.e., the Albany-Fraser Orogen, the Musgrave Province, and the Madura Province and Coompana Province; Fig. 3.1a; e.g., Edgoose et al., 2004; Spaggiari et al., 2009; Neumann & Korsch, 2014; Kirkland et al., 2015; Wingate et al., 2015; de Gromard et al., 2016; Jagodzinski et al., 2018; Wise et al., 2018). Furthermore, some of these basement regions also express similar Hf isotope compositions (i.e., Musgrave Province and Madura and Coompana provinces; Kirkland et al., 2013, 2017; Hartnady et al., 2020), stemming ultimately from a shared crustal evolution. Hf isotope analyses on detrital zircon grains from Eucla Basin placer deposits are limited (Reid et al., 2013b), and newly analysed Hf isotope data of the basin's underlying Mesoproterozoic basement (Madura Province and Coompana Province; Kirkland et al., 2017; Hartnady et al., 2020) now demonstrate

that integrated U-Pb and Hf isotope data alone may be insufficient to clearly differentiate source regions.

In this work, we present new zircon Hf isotope data for recently U-Pb dated mineral sand samples from the Eucla Basin (Gartmair et al., 2022), and apply zircon grain shape analysis to detrital and crystalline zircon grains to help refine Eucla Basin sediment provenance. Integrating archived and new U-Pb age, Hf isotope and grain shape data, we explore a novel 3G (geochronology-geochemistry-grain shape) triple-characterisation approach to constrain sediment provenance, transportation, and recycling of Eucla Basin heavy mineral beach placers, and explore the practicality of grain shape characterisation as an effective technique for detrital provenance studies in general.

## 2. Geologic Background

The southern Australian Eucla Basin is characterised by an extensive carbonate platform representing the largest Cenozoic onshore sedimentary basin globally (Benbow, 1990; Clarke et al., 2003; Li et al., 2003; Hou et al., 2006). This carbonate platform is underlain and fringed by terrigenous clastic sedimentary rocks (Lowry, 1970). Limited sedimentary sequences were preserved onshore along the central southern Australian margin prior to the opening of the Australia-Antarctica seaway during Mesozoic thinning and Cenozoic continental rifting (Brown et al., 2003). However, relative stability of principal source regions for sedimentary systems (Neoproterozoic Officer Basin, Mesozoic Madura Shelf and Cenozoic Eucla Basin shorelines; Fig. 3.1a) through deep geological time are inferred from similarities of U-Pb detrital zircon ages (Barham et al., 2018; Barham & Kirkland, 2020; Gartmair et al., 2022). During the Eocene-Miocene, major marine transgressions (that increased in magnitude) facilitated the deposition of carbonates and the development of heavy mineral prospective basin-fringing shoreline successions (Li et al., 2003). Coastal sedimentation along the southern Australian margin was halted during a period of relative sea level stability in the Oligocene before shifting to a long-term regressive period in the Miocene-Pliocene that led to the exposure of distinct highstand formations and the preservation of Eucla Basin Eocene shorelines (Hou et al., 2003, 2011). Along the Eucla Basin's margins, sediment migration and the development of progressive beach barriers in the north-east and east were directly influenced by





prevailing weather systems that facilitated a crude west to east directed longshore drift (Kemp, 1978; Beard, 1998; Gartmair et al., 2022). Ongoing northwards continent migration led to overriding of a mantle anomaly during the Cenozoic that has resulted in a significant west-up, east-down elevation difference across the Eucla Basin (Gurnis, 2001; Sandiford, 2007). This tilting motion is responsible for stratigraphically thicker sequences along the eastern basin margin, and progressive heavy mineral enrichment of the north-eastern and eastern barrier sands (i.e., Barton Barrier and Ooldea Barrier) through sediment reworking and mixing (Hou et al., 2008). Clastic sediment supply to the basin's margin was facilitated by an extensive palaeodrainage system of the bounding Precambrian hinterland (de Broekert & Sandiford, 2005; Hou & Warland, 2005; Hou & Keeling, 2008; Hou et al., 2008). Primary sediment contributions based on detrital zircon U-Pb geochronology are associated with bounding Mesoproterozoic sources (e.g., Albany-Fraser Orogen, Musgrave Province, Madura Province and Coompana Province; Fig. 3.1a), with minor detritus supplied from Archean-aged rocks (Yilgarn and Gawler cratons; Fig. 3.1a), as well as intermediate sedimentary reservoirs (e.g., Officer Basin; Fig. 3.1a; Reid & Hou, 2006; Hou et al., 2011; Reid et al., 2013a, b; Gartmair et al. 2022).

The western Eucla Basin margin is bound by magmatic and metamorphic rocks of the multi-phase Palaeoproterozoic-Mesoproterozoic Albany-Fraser Orogen (~1700–1600 Ma and ~1345–1291 Ma; Clark et al., 2000; Spaggiari et al., 2009; Kirkland et al., 2011a; Fig. 3.1a) that developed on and modified the margin of the Archean Yilgarn Craton (~3800–2620 Ma; Kinny & Nutman, 1996; Wilde & Hickman, 2001; Cassidy et al., 2006; Fig. 3.1a). The zircon Hf-signature of the Albany-Fraser Orogen is dominantly subchondritic at ~1300–1100 Ma as a result of reworking of ancient crust (Kirkland et al., 2011a, b). The northern Eucla Basin hinterland region comprises isotopically distinct juvenile magmatic and metamorphic lithologies, defining the episodically rejuvenated Palaeoproterozoic-Mesoproterozoic Musgrave Province (~1607–1052 Ma; Kirkland et al., 2013; Howard et al., 2015; Fig. 3.1a). The far eastern portion of the Eucla Basin developed adjacent to the Archean-Mesoproterozoic-aged Gawler Craton (~2640–1575 Ma; Cowley et al., 2003; Ferris & Schwarz, 2004; Fanning et al., 2007; Jagodzinski et al., 2019; Reid, 2019; Courtney-Davies et al., 2020; Reid et al., 2020; Fig. 3.1a). The recently investigated crystalline basement underlying the Eucla Basin (beneath the intervening Madura Shelf and Officer Basin;

Fig. 3.1a), reflect the evolution of juvenile Palaeoproterozoic-Mesoproterozoic crust, and have been defined as the Madura Province and Coompana Province (~1614–1074 Ma; Wingate et al., 2015; de Gromard et al., 2016; Wise et al., 2018; Fig. 3.1a). The magmatic and metamorphic units associated with the Madura and Coompana provinces developed on ~1950 Ma, early Proterozoic oceanic crust, which was only later stabilised due to emplacement of buoyant high temperature ~1200–1120 Ma magmas (Maralinga event; Spaggiari et al., 2016). The Musgrave Province and the Madura and Coompana provinces lack Archean substrate, thus exhibit more juvenile Hf isotope values as compared to those known from the Albany-Fraser Orogen (Kirkland et al., 2011a, b, 2013, 2017; Hartnady et al., 2020). The Madura Province and Coompana Province were later overlain in parts by the Proterozoic Officer Basin (~850–400 Ma; Grey et al., 2005; Fig. 3.1a) and the Cretaceous Madura Shelf (~135–70 Ma; Barham et al., 2018; Fig. 3.1a) prior to the development of the Eucla Basin (Fig. 3.1a). For the sake of simplicity, we consider the Madura Province and Coompana Province as one source region due to similarities in rock forming ages and Hf-isotopic character (described as “Madura-Coompana provinces” throughout the remainder of this text), to more easily refer to the basin’s underlying basement.

### 3. Samples and Methods

#### 3.1 Sample selection

Thirteen unconsolidated sediment samples were selected from reverse circulation and air core drilling assays acquired from recent exploration campaigns undertaken by Iluka Resources Limited. Drilling was performed along the northern and eastern Eucla Basin margins across the prospects Wanna, Tripitaka, and Gobi, and the Ambrosia and Atacama deposits (Fig. 3.1b; Table 3.1). Samples were chosen based on their received heavy mineral grades from various mineralisation zones at different drill depths (Table 3.1). For this study, we classify samples that represent the highest heavy mineral grade of a drill hole as peak mineralisation samples, and samples with lower heavy mineral concentrations as low-grade heavy mineral samples and indicate whether they were obtained from drill depths above (upper) or below (lower) the peak mineralisation zone (Table 3.1). A single sample was selected as a background sample outside the mineralisation footprint (Gobi sample AD550079; Table 3.1). Concentrated zircon grains from all 13 samples were analysed for grain shape characteristics. Samples from

Wanna, Ambrosia, Tripitaka, and Gobi were additionally analysed for their Hf isotope compositions to complement their recently published U-Pb data (Gartmair et al., 2022; Table 3.1).

*Table 3.1 Overview of heavy mineral samples analysed in this study for detrital zircon Lu-Hf geochemistry and detrital zircon grain morphology. Samples previously analysed for U-Pb geochronology in Gartmair et al. (2022). Atacama samples (marked in grey colour) analysed for grain shapes only. HM = heavy mineral*

Sample ID	Prospect/ Deposit	Latitude	Longitude	Drill Hole ID	Collar Depth (m)	HM Grade * (%)	Mineralisation Zone
<i>Eucla Basin – new heavy mineral samples</i>							
PG109105	Wanna**	-28.5116	128.0969	WE0191	27.0 - 28.5	2.5	HM mineralisation peak***
AD605589	Ambrosia	-30.8624	132.2178	AM1100	18.0 - 19.0	0.8	Upper low-grade HM****
AD605228	Ambrosia	-30.8600	132.2218	AM1089	3.0 - 4.0	0.9	Upper low-grade HM
AD605248	Ambrosia	-30.8600	132.2218	AM1089	22.0 - 23.0	21.9	HM mineralisation peak
AD605251	Ambrosia	-30.8600	132.2218	AM1089	25.0 - 26.0	1.6	Lower low-grade HM*****
AD458869	Atacama	-30.7952	132.2567	AT0926	42.0 - 43.0	38.4	HM mineralisation peak
AD443711	Atacama	-30.8167	132.2612	AT0539	29.0 - 30.0	11.6	Upper low-grade HM
AD443727	Atacama	-30.8167	132.2612	AT0539	44.0 - 45.0	14.2	HM mineralisation peak
AD443731	Atacama	-30.8167	132.2612	AT0539	48.0 - 49.0	10.9	Lower low-grade HM
AD457878	Atacama	-30.7927	132.2651	AT0918	47.0 - 48.0	39.4	HM mineralisation peak
AD376778	Tripitaka	-31.5481	132.8048	TR1078	23.0 - 24.0	9.1	HM mineralisation peak
AD550079	Gobi	-31.2267	133.1277	YE16687	24.0 - 25.5	0.3	Background HM
AD550520	Gobi	-31.2285	133.1392	YE16708	11.0 - 12.0	14.2	HM mineralisation peak

\* received heavy mineral (HM) grade

\*\* also referred to as Western Eucla prospect

\*\*\* highest recorded HM grade observed in drill hole

\*\*\*\* low-grade proportion of HM mineralisation zone found above peak mineralisation of drill hole

\*\*\*\*\* low-grade portion of HM mineralisation zone found below peak mineralisation of drill hole

Zircon grain shape was characterised for detrital and crystalline samples with published U-Pb data (and Hf data where available): i) six heavy mineral samples from the Eucla Basin (Balladonia, Cyclone, Thar, Jacinth, and Atacama prospects; Reid et al., 2013a; Fig. 3.1b; App. Table 3.1), ii) three sedimentary samples north of the Eucla Basin (Trainor Hill Sandstone and Observatory Hill Beds of the Cambrian-aged Officer Basin, and Noorina palaeochannel of probable Palaeogene age; Reid et al., 2013a; Fig. 3.1b; App. Table 3.1), and iii) thirteen crystalline samples from the Eucla Basin's underlying Coompana Province supersuites (Jagodzinski et al., 2018; Fig. 3.1b; App. Table 3.2). Published U-Pb age and Hf isotope data of five heavy mineral concentrates from the prospects Jacinth (sample 1688513), Notrab, Tripitaka (sample 1688510), Dromedary and Gullivers (Reid & Hou, 2006; Hou et al., 2011; Reid et al., 2013a, b; Fig. 3.1b; App. Table 3.1) are incorporated in the broader sediment provenance analysis without additional detrital zircon grain shape characterisation.

### 3.2 Sample preparation

Sample splitting and mineral density separation of the newly acquired drill samples was undertaken by Iluka Resources Limited at the Narngulu mineral separation plant, Western Australia. Heavy minerals  $\geq 2.86 \text{ g/cm}^3$  were separated using heavy liquid from the 53- to 1,000- $\mu\text{m}$  particle fraction. At the School of Earth and Planetary Sciences, Curtin University in Western Australia, the selected 13 heavy mineral concentrate samples (Table 3.1) were then bulk mounted on double sided tape attached to glass plates and filled with Epofix resin in 25 mm-diameter moulds. Bulk mounting was used in preference to handpicking to prevent potential bias in the zircon grain selection (Sláma & Košler, 2012; Dröllner et al., 2021; Zutterkirch et al., 2021). Detrital mineral bulk mounting and automated mineral characterisation is a valuable method in sediment provenance studies to eliminate reliance on traditional petrographic analyses of individually hand-picked minerals (and potential bias in the grain selection process), while the total grain population of a sample can be characterised more rapidly and accurately (Akinlotan & Rogers, 2021; Akinlotan et al., 2021). Grain interiors of the heavy mineral mounts were exposed through polishing with successively finer abrasive paper (up to 2,000 grit), diamond-embedded lapping film (9, 6, and 3  $\mu\text{m}$ ) and diamond suspension (1  $\mu\text{m}$ ). Scanning electron microscopy imaging of the polished samples was enabled with a final carbon coat of  $\sim 20 \text{ nm}$  (= 2,000 ms) using Emitech 950x evaporative carbon coater.

### 3.3 Analytical methodology

#### 3.3.1 Digital zircon grain extraction from bulk mounted heavy mineral samples

Mineralogical, geochronological, and geochemical analyses of the 13 heavy mineral concentrates were undertaken at the John de Laeter Centre, at Curtin University in Western Australia. Using a TESCAN integrated mineral analyser (TIMA), with integrated energy dispersive X-ray spectroscopy (EDS) and backscattered electron imaging, zircon grains within a bulk mounted sand sample were identified via mineralogical dot-mapping and mineralogically colour-coded (App. 3.1). A mineral phase filter was then applied to each of the 13 phase maps to extract zircon grains with  $> 95 \%$  zircon by mass and digital densities  $\geq 4.6$  and  $\leq 4.8 \text{ g/cm}^3$  to avoid grain aggregates containing zircon. Finally, a particle property filter was applied to exclude grains touching borders internally and externally during image stitching to avoid

truncated grains. Systematic cathodoluminescence imagery was impractical on the mixed composition bulk-mounts, with high-contrast, back-scattered electron imaging and transmitted light microscopy assisting understanding of internal grain textures for spot placement.

### 3.3.2 Geochemical composition analysis of new prospect samples

Detrital zircon grains from the prospects Wanna, Ambrosia, Tripitaka, and Gobi (Fig. 3.1b; Table 3.1; excluding Atacama prospect samples) were analysed for their Hf isotopes ( $N = 8$ ,  $n = 1,070$ ). From each of the eight chosen sample sets, individual zircon grains sufficiently large to host analytical spots within single growth phases were randomly selected for geochemical analyses using laser ablation inductively coupled plasma mass spectrometry (LA-ICPMS). Detrital zircon Hf isotope composition analysis was performed on the same zircon grain cores and the same analytical volume used for U-Pb dating and described in detail in a recent Eucla Basin provenance study (Gartmair et al., 2022). Mineral phase maps, in conjunction with light microscopy and backscatter imaging (App. 3.1) were used to guide target site selection in the zircon grains. Applying a 50- $\mu\text{m}$  laser spot size and a dynamic repetition time of 10 Hz, isotope signals for  $^{178}\text{Hf}$ ,  $^{177}\text{Hf}$ ,  $^{176}\text{Hf}$ ,  $^{176}\text{Lu}$  and  $^{176}\text{Yb}$  in each analysis were time-resolved with two cleaning laser pulses and 35 s of ablation and 60-s background capture. Ablation responses were assessed to further filter for mixed growth zone analysis. Geochemical composition data were reduced with Iolite v4.3.11 software and calculated using standard-corrected  $^{176}\text{Hf}/^{177}\text{Hf}$ , 3SD (standard deviation) outlier rejection, weighted means and 2SE (standard error). Lu-Hf fractionation calibration and monitoring of the  $^{176}\text{Hf}/^{177}\text{Hf}$  isotope ratio were achieved with the Mud Tank zircon reference material (Woodhead & Hergt, 2005). Accuracy and precision of the  $^{176}\text{Hf}/^{177}\text{Hf}$  isotope ratio were monitored with secondary zircon reference materials Plešovice ( $0.282482 \pm 12$ ; Sláma et al, 2008), 91500 ( $0.282305 \pm 6$ ; Blichert-Toft, 2008), FC1 ( $0.282184 \pm 16$ ; Woodhead and Hergt, 2005), and R33 ( $0.282767 \pm 18$ ; Vervoort, 2010). Data analyses were performed in three analytical sessions with zircon reference materials Plešovice ( $0.282488 \pm 7$ ,  $0.282484 \pm 12$  and  $0.282476 \pm 11$ ), 91500 ( $0.282320 \pm 11$ ,  $0.282304 \pm 9$  and  $0.282297 \pm 13$ ), FC1 ( $0.282191 \pm 17$ ,  $0.282215 \pm 38$  and  $0.282196 \pm 12$ ) and R33 ( $0.282765 \pm 17$ ,  $0.282764 \pm 13$  and  $0.282774 \pm 13$ ; App. Table 3.3) all within 1% of published values. To help monitor and correct for instrument drift, primary and secondary reference materials were analysed every 20 to

24 unknowns and at the start and end of each analytical session. Data assessment of the  $^{178}\text{Hf}/^{177}\text{Hf}$  stable isotope ratio was performed across the three analytical sessions, with all sample values falling between the accepted range of 1.46688 and 1.46746 (Spencer et al., 2020; Analysis Session 1: mean =  $1.46713 \pm 0.00006$ , max = 1.46721, min = 1.46706,  $n = 400$ ; Analysis Session 2: mean =  $1.46712 \pm 0.00007$ , max = 1.46722, min = 1.46701,  $n = 450$ ; Analysis Session 3: mean =  $1.46710 \pm 0.00006$ , max = 1.46717, min = 1.46701,  $n = 220$ ). The initial  $^{176}\text{Hf}/^{177}\text{Hf}$  ratio was calculated based on concordant  $^{207}\text{Pb}/^{206}\text{Pb}$  geochronology ages with 1SD from published data (Gartmair et al., 2022) and the  $^{176}\text{Lu}$  decay constant ( $1.865 \times 10^{-11}$ ; Scherer et al., 2001). Final isotope data were expressed in  $\epsilon\text{Hf}$  values (App. Table 3.4) that were calculated using parts per 10,000 deviation of the initial  $^{176}\text{Hf}/^{177}\text{Hf}$  ratio from the evolution curve for CHUR (chondritic uniform reference) after Blichert-Toft and Albarède (1997).

### *3.3.3 Zircon grain shape analysis of detrital and crystalline samples from bulk mounted and hand-picked sample sets*

From the newly acquired bulk mounted samples (Table 3.1), all zircon grains extracted from filtered TIMA phase maps (App. 3.1) were analysed for grain shape attributes (Table 3.2). The transmitted light images associated with published U-Pb analyses (Reid et al., 2013a; Jagodzinski et al., 2018) were used for hand-picked zircon grains polished to half-grain thickness from archived detrital and crystalline samples chosen for our study (App. Tables 3.1, 3.2). The methodology applied in this study to quantitatively measure morphologies of detrital and crystalline zircon grains closely follows two-dimensional image processing techniques utilised and described in detail in the recent provenance study by Markwitz and Kirkland (2018). For our analyses we used Fiji (Schindelin et al., 2012), an image processing application of ImageJ software (Schneider et al., 2012; Rueden et al., 2017), with a shape descriptor plugin (Syverud et al., 2007). Morphological attributes were extracted from the overall shape of a grain.

Transmitted light images from hand-picked samples were first scaled and non-zircon grains, where present, were manually removed. Each image was converted to an 8-bit binary image (App. Fig. 3.1a) and thresholded using the default function in Fiji to allow grain boundary information extraction (App. Fig. 3.1b). Filling of grains was performed to avoid morphological measurements of internal features (App. Fig. 3.1c), and the watershed segmentation function of the Euclidean Distance Map (EDM;

Danielsson, 1980) was applied to separate touching grains (App. Fig. 3.1d). We refrained from applying the image modelling operations of dilation/erosion and opening/closing (Serra, 1983), as used by Markwitz and Kirkland (2018) to separate touching grains, as we identified small-scale (although likely negligible) changes to the overall shape of a zircon grain. We removed grains that did not result in complete filling, or that became internally segmented after applying the watershed algorithm (App. Fig. 3.1e). Zircon grains that became artificially altered after the segmentation process or where grain boundaries could not be restored sufficiently were also excluded from further grain shape analysis (App. Fig. 3.1e).

Each zircon grain was then analysed with the Image J Particle Analyser, using area, perimeter, and shape descriptors (Fiji Image J function) to calculate shape parameters of relevance (Table 3.2). Zircon grains were analysed with an image-specific minimum particle size filter (in units [pixel]) to exclude unwanted “particle” background noise without compromising the shape of a grain (manually tested and adjusted for each image), and the pre-set Image J circularity value range (0.00 to 1.00) to account for all circularity values. The grain shape analysis output function was set to produce outline drawings of all analysed zircon grains (App. Fig. 3.1f). Zircon grains positioned on the image’s edge were excluded. Eight shape parameters were measured for each grain: *area, perimeter, major and minor axes, effective diameter, circularity, roundness, and aspect ratio* (Table 3.2; App. Table 3.5).

Filtered TIMA phase map images from bulk mounted new detrital samples were adjusted to only display zircon grains (blue phases; App. 3.1) using Image J colour thresholding. Remaining zircon grains were then analysed with the same approach as used for transmitted light images but with adjusted thresholding and a selected minimum grain (i.e., particle size of 53  $\mu\text{m}$  to capture the smallest available zircon grains of the sieved sand samples; App. Table 3.5).

Statistical analysis of shape parameters across all detrital ( $N = 22$ ,  $n = 35,604$  [bulk mounted:  $N = 13$ ,  $n = 33,702$ ; hand-selected:  $N = 9$ ,  $n = 1,902$ ]; Table 3.1; App. Tables 3.1, 3.6) and crystalline samples ( $N = 13$ ,  $n = 824$ ; App. Tables 3.2, 3.6) was performed with the univariate function of PAST Paleontological Statistics software version 3.25 (Hammer et al., 2001). Normality testing of each sample’s zircon data distribution ( $p$  – values) was achieved with the Shapiro-Wilk test, and a principal component analysis



Table 3.2 Overview and description of shape parameters used for zircon grain shape analysis

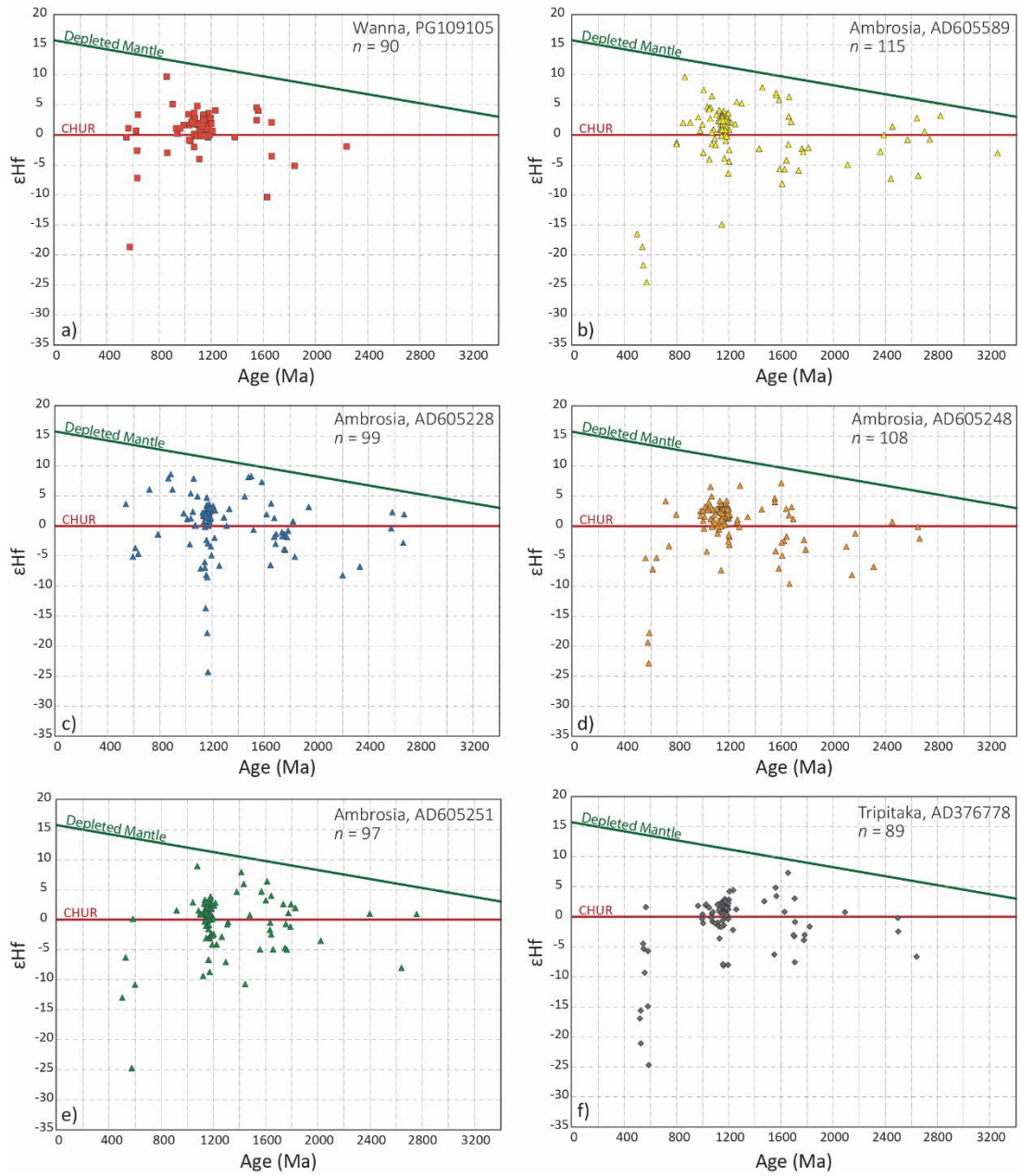
Parameter	Area	Perimeter	Major Axis	Minor Axis	Effective Diameter	Circularity	Roundness	Aspect Ratio
Abbreviation	(A)	(P)	(MaA)	(MiA)	(ED)	(Ci)	(Rn)	(AR)
Unit	$\mu\text{m}^2$	$\mu\text{m}$	$\mu\text{m}$	$\mu\text{m}$	$\mu\text{m}$	unitless	unitless	unitless
Formula	N/A	N/A	N/A	N/A	$2 \sqrt{(\text{Area} / \pi)}$	$4\pi (\text{Area} / \text{Perimeter})^2$	$4 \times \text{Area} / [\pi (\text{Major Axis})^2]$	Major Axis / Minor Axis
Range	$0.0 < A$	$0.0 < P$	$0.0 < \text{MaA}$	$0 < \text{MiA}$	Minor axis $< \text{ED} < \text{Major axis}$	$0.0 < \text{Ci} < 1.0$	$0.0 < \text{Rn} < 1.0$	$1.0 < \text{AR}$
Description	Sum of calibrated pixels within selected grain boundaries (in applicable units)	Outer length of boundary of selected grain	Long axis of representative best fit ellipse matching selected grain area, where best fit ellipse has same area, orientation, and centroid as selected grain.	Short axis of representative best fit ellipse matching selected grain area, where best fit ellipse has same area, orientation, and centroid as selected grain.	Measurement of the grain shape's average diameter, indicating the grain's approximation of a sphere, with values falling between that of the minor and major axis	Measurement of the grain shape's symmetry and surface area, where 1.0 equates to a perfect circle, while increasingly elongated irregular shapes approach 0.0	Measurement of the grain shape's surface area compared to that of a perfect circle, where 1.0 indicates a grain surface matching a perfect circle, and rougher grain surfaces approach 0.0	Measurement of the grain's length to width ratio, where 1.0 indicates even sides, with increasing elongation giving values increasingly greater than 1

(PCA; App. Fig. 3.2) was run for each zircon sample set and across all grain shape parameters (Table 3.2) to determine key parameters that best describe the shape of the zircon grains within each sample (Davis & Sampson, 1986; Legendre & Legendre, 1998; Harper, 1999).

## 4. Results

### 4.1 Detrital zircon Hf geochemistry of newly analysed prospect samples

Detrital zircon  $\epsilon\text{Hf}$  data of concordant U-Pb dated zircon grains (Gartmair et al., 2022) from Wanna, Ambrosia, Tripitaka, and Gobi express high degrees of similarity in U-Pb vs. Hf space (Figs. 3.2a-h). Overall, newly analysed  $\epsilon\text{Hf}$  values ( $N = 8$ ,  $n = 844$ ) range between -28.0 and +9.6 for the Archean to Phanerozoic-aged grains (Fig. 3.2i). Across all samples analysed a predominantly superchondritic to weakly subchondritic population is defined at ~1250–1000 Ma ( $-2.5 < \epsilon\text{Hf} > \sim +5$ ; Fig. 3.2a-h). This grain population is the most prevalent detrital zircon cluster across the new Eucla Basin heavy mineral data sets (Fig. 3.2i). From the combined data set of published and newly analysed samples, a weakly pronounced superchondritic zircon cluster is defined between ~1700 and 1500 Ma ( $+1.3 < \epsilon\text{Hf} > +7.3$ ; Fig. 3.2i). Additional distinct secondary subchondritic grain populations are evident in the data set: a sub-CHUR zircon population clusters at ~1850–1550 Ma, recording  $\epsilon\text{Hf}$  values between ~-5 and -0.5 (Fig. 3.2i). An additional predominantly subchondritic aggregation is evident for zircon grains aged ~1225–1100 Ma ( $-5 < \epsilon\text{Hf} > -2.5$ ; Fig. 3.2i) that partly overlaps with a subchondritic vertical array (~1200–1100 Ma;  $-24.3 < \epsilon\text{Hf} > \sim -5$ ; Fig. 3.2i). A further distinct vertical array of zircon grains aged ~650–500 Ma coincides with weakly superchondritic to predominantly subchondritic signatures ( $-28.0 < \epsilon\text{Hf} > +3.7$ ; Fig. 3.2i). Archean to late Palaeoproterozoic-aged detrital zircon grains are less common and express superchondritic to subchondritic signatures for grains aged ~3250–1850 Ma ( $-8.2 < \epsilon\text{Hf} < +3.2$ ; Fig. 3.2i).



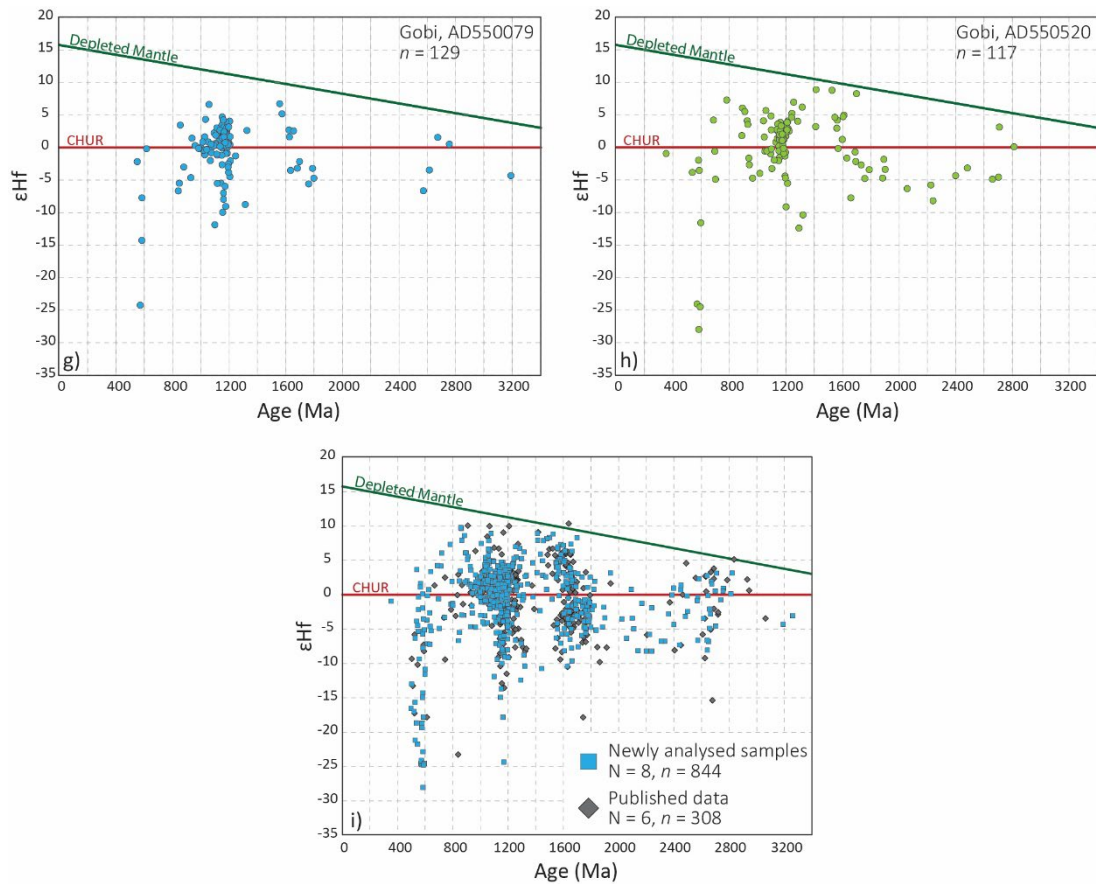


Figure 3.2 Hf isotope results from newly analysed heavy mineral samples (a-h). New Hf data overlain on published Eucla Basin heavy mineral Hf isotope data (i) (Reid et al., 2013b). Depleted mantle and chondritic uniform reference (CHUR) references from Spencer et al. (2020).

## 4.2 Zircon grain shape analyses

Nearly half of all samples and shape parameters analysed from the 13 crystalline data sets are normally distributed ( $p > 0.05$ ;  $\sim 43\%$ ; 45/104 analyses; App. Tables 3.2, 3.6), while detrital zircon grain shapes are almost exclusively non-normally distributed ( $p < 0.05$ ;  $\sim 5\%$ ; 167/176 analyses; App. Table 3.6). We therefore used median values of shape parameters to enable a more representative comparison of data sets. PCA analysis (App. Fig. 3.2) of the eight selected grain shape parameters (Table 3.2) across all sample sets identified grain area, perimeter, effective diameter, and major and minor axes to be the dominant shape characteristics for describing the dispersion of data across zircon grain shape populations, while circularity, aspect ratio, and roundness are of lesser importance (App. Fig. 3.2). A full description of the summary statistics and Shapiro-Wilk  $p$  – values of zircon shape parameters for each detrital and crystalline zircon sample set are provided in App. Table 3.6.





#### 4.2.1 Detrital zircon grain shape characterisation

Across all detrital zircon samples analysed ( $N = 22$ ,  $n = 35,604$ ; Table 3.1; App. Tables 3.1, 3.5), the smallest median values for the shape parameters *area*, *perimeter*, *major axis*, *minor axis*, and *effective diameter* are observed in the Thar prospect (sample 1841639;  $A = 2842.5 \mu\text{m}^2$ ;  $P = 210.9 \mu\text{m}$ ;  $\text{MaA} = 73.9 \mu\text{m}$ ;  $\text{MiA} = 48.2 \mu\text{m}$ ;  $\text{ED} = 60.2 \mu\text{m}$ ;  $n = 248$ ; App. Table 3.6) while the largest median values belong to the Cyclone sample (1688515;  $A = 23173.3 \mu\text{m}^2$ ;  $P = 644.8 \mu\text{m}$ ;  $\text{MaA} = 245.5 \mu\text{m}$ ;  $\text{MiA} = 127.9 \mu\text{m}$ ;  $\text{ED} = 171.8 \mu\text{m}$ ;  $n = 158$ ; App. Table 3.6). Median *circularity* values of detrital zircon grains range between  $\text{Ci} = 0.722$  (Observatory Hill Beds, sample 1661077;  $n = 138$ ; App. Table 3.6) and  $\text{Ci} = 0.809$  (Tripitaka, sample AD376778;  $n = 5251$ ; App. Table 3.6), while median *roundness* ranges from 0.532 (Cyclone, sample 1688515;  $n = 158$ ; App. Table 3.6) to 0.727 (Wanna, sample PG109105;  $n = 813$ ; App. Table 3.6). All sedimentary samples express median *aspect ratios* between  $\text{AR} = 1.376$  (Wanna) and  $\text{AR} = 1.879$  (Cyclone; App. Table 3.6). Across all shape parameters measured (Table 3.2), zircon grains from sedimentary non-heavy mineral samples (Trainor Hill Sandstone, Observatory Hill Beds and Noorina palaeochannel; App. Table 3.1) express values that are within the median grain shape data range of zircon grains from heavy-mineral bearing prospect samples (Table 3.1; App. Tables 3.1, 3.6).

#### 4.2.2 Coompana Province zircon grain shapes

The smallest median values for *area*, *perimeter*, *major axis*, *minor axis*, and *effective diameter* across crystalline zircon samples from the Coompana Province ( $N = 13$ ,  $n = 824$ ; App. Tables 3.2, 3.5) are recorded for the Koomalboogurra Suite (combined data of samples 2427076, 2425443 and 2132936;  $A = 4284.9 \mu\text{m}^2$ ;  $P = 297.0 \mu\text{m}$ ;  $\text{MaA} = 94.3 \mu\text{m}$ ;  $\text{MiA} = 58.0 \mu\text{m}$ ;  $\text{ED} = 73.9 \mu\text{m}$ ;  $n = 255$ ; Table 3.3; App. Table 3.6), while the undifferentiated Moodini Supersuite expresses the largest median values for the same shape characteristics (combined data of samples 2427070 and 2132968;  $A = 12909.4 \mu\text{m}^2$ ;  $P = 518.9 \mu\text{m}$ ;  $\text{MaA} = 163.5 \mu\text{m}$ ;  $\text{MiA} = 114.0 \mu\text{m}$ ;  $\text{ED} = 128.2 \mu\text{m}$ ;  $n = 71$ ; Table 3.3; App. Table 3.6). Younger Coompana supersuites (Moodini Supersuite and Warakurna Supersuite) express overall larger grains (i.e., age  $< 1200$  Ma; median values:  $\text{MaA} \geq 111 \mu\text{m}$ ,  $\text{MiA} \geq 74 \mu\text{m}$ ; Table 3.3; App. Tables 3.5, 3.6), while older supersuites of the basement (“unassigned supersuite” and Toolgana Supersuite) are distinct of smaller grains (i.e., age  $> 1500$  Ma; median values:  $\text{MaA} \leq 100 \mu\text{m}$ ,  $\text{MiA} \leq 62 \mu\text{m}$ ; Table 3.3; App. Tables 3.5, 3.6). Median *Circularity* values range from  $\text{Ci} =$

Table 3.3 Schematic zircon representation of crystalline basement suites using grain shape median major and minor axes values of zircon grains analysed from Coompana Province samples. Values based on all grains analysed for the geological unit, including dated and non-dated grains. Age information and geological unit categorisation from Jagodzinski et al. (2018) and after Pawley et al. (2020)

Supersuite	Unassigned	Toolgana Supersuite	Moodini Supersuite	Warakurna Supersuite
Suite	Bunburra Suite	Koomalboogurra Suite	Undifferentiated	Giants Head Suite
Formation	N/A	N/A	N/A	Mallabie Basalt
Sample IDs	2423705 2423700	2427076 2425443 2132936	2427070 2132968	2430064 2498072
Age (Ma)	1526	1618	~ 1148–1141	1074
Grains analysed (n)	208/265	255/295	71/131	202/243
Major Axis (µm)	100	94	163	111
Minor Axis (µm)	62	58	114	77
Zircon Illustrations				
	100 x 62	94 x 58	163 x 114	111 x 77
				136 x 74

0.590 for the only sample analysed from the Merdayerrah Shoshonite (sample 2425514;  $n = 69$ ; App. Tables 3.2, 3.5, 3.6) to  $C_i = 0.650$  for the combined samples 2430064 and 2498072 from the Mallabie Basalt (Giants Head Suite from the Warakurna Supersuite;  $n = 19$ ; App. Tables 3.2, 3.5, 3.6). Median *roundness* values are lowest from the Koomalboogurra Suite (samples 2427076, 2425443 and 2132936;  $R_n = 0.605$ ;  $n = 255$ ; App. Tables 3.2, 3.5, 3.6) and highest for data sampled from the undifferentiated Moodini Supersuite (samples 2427070 and 2132968;  $R_n = 0.706$ ;  $n = 71$ ; App. Tables 3.2, 3.5, 3.6), while median *aspect ratios* show the reverse trend for the same stratigraphic units (undifferentiated Moodini Supersuite,  $AR = 1.416$  and Koomalboogurra Suite,  $AR = 1.653$ ; App. Tables 3.2, 3.5, 3.6).

## 5. Discussion

### 5.1 Hf isotope composition analysis of Eucla Basin heavy mineral samples

The newly obtained detrital zircon Hf data ( $N = 8$ ,  $n = 844$ ) are similar to published data ( $N = 6$ ,  $n = 308$ ; Reid et al., 2013b; Fig. 3.2i; Table 3.1; App. Table 3.2), suggesting shared provenance histories for the majority of detrital grains in the different deposits analysed across these studies (Section 4.1; Fig. 3.2). The most prominent sub-population of grains with ages  $\sim 1250$ – $1000$  Ma, expresses  $\epsilon_{\text{Hf}}$  values between  $-2.5$  and  $\sim +5$  (Fig. 3.2i), indicative of a relatively juvenile magmatic source. These age and Hf-isotope characteristics match the Musgrave Province to the north of the Eucla Basin (Figs. 3.1a, 3.3; Kirkland et al., 2013; Reid et al., 2013b), as well as the underlying Madura-Coompana provinces (Kirkland et al., 2017; Jagodzinski et al., 2018; Hartnady et al., 2020; Figs. 3.1a, 3.3). Both regions are therefore possible sediment sources for the primary Mesoproterozoic age mode observed in Eucla Basin heavy mineral age spectra (Reid & Hou, 2006; Hou et al., 2011; Reid et al., 2013a, b; Gartmair et al., 2022). The proportions of sediment supply from each of the two regions cannot be established based on the age and Hf data present alone (Fig. 3.3e). Some degree of sediment mixing from different Mesoproterozoic-aged sources is evident from the more weakly pronounced subchondritic grain sub-population ( $\sim 1225$ – $1100$  Ma,  $-5 < \epsilon_{\text{Hf}} > -2.5$ ; Figs. 3.2i, 3.3b) and the vertical array of zircon grains ( $\sim 1200$ – $1100$  Ma;  $-24.3 < \epsilon_{\text{Hf}} > \sim -5$ ; Figs. 3.2i, 3.3b) that overlap in U-Pb age and Hf isotope characteristics with those recorded from the Albany-Fraser Orogen (Kirkland et al., 2011a; Reid et al., 2013b; Fig. 3.3). A restricted Albany-Fraser Orogen

supply to the western Eucla Basin margin (i.e., Balladonia prospect; Fig. 3.1b) with minor sediment contributions to beach placers along the northern and eastern margins is consistent with a previous Hf isotope analysis (Reid et al., 2013b).

Additional mixing of late Palaeoproterozoic to early Mesoproterozoic-aged grains defining a pronounced secondary age mode in detrital zircon age spectra across all Eucla Basin margin samples (Reid & Hou, 2006; Hou et al., 2011; Reid et al., 2013a; Gartmair et al., 2022) is identified in the broad ~1850–1400 age interval (Fig. 3.2i). These subordinate grain contributions define two sub-populations of superchondritic to subchondritic zircons (~1700–1500 Ma,  $+1.3 < \epsilon_{\text{Hf}} > +7.3$  and ~1850–1550 Ma,  $-5 < \epsilon_{\text{Hf}} > -0.5$ ; Fig. 3.2i).

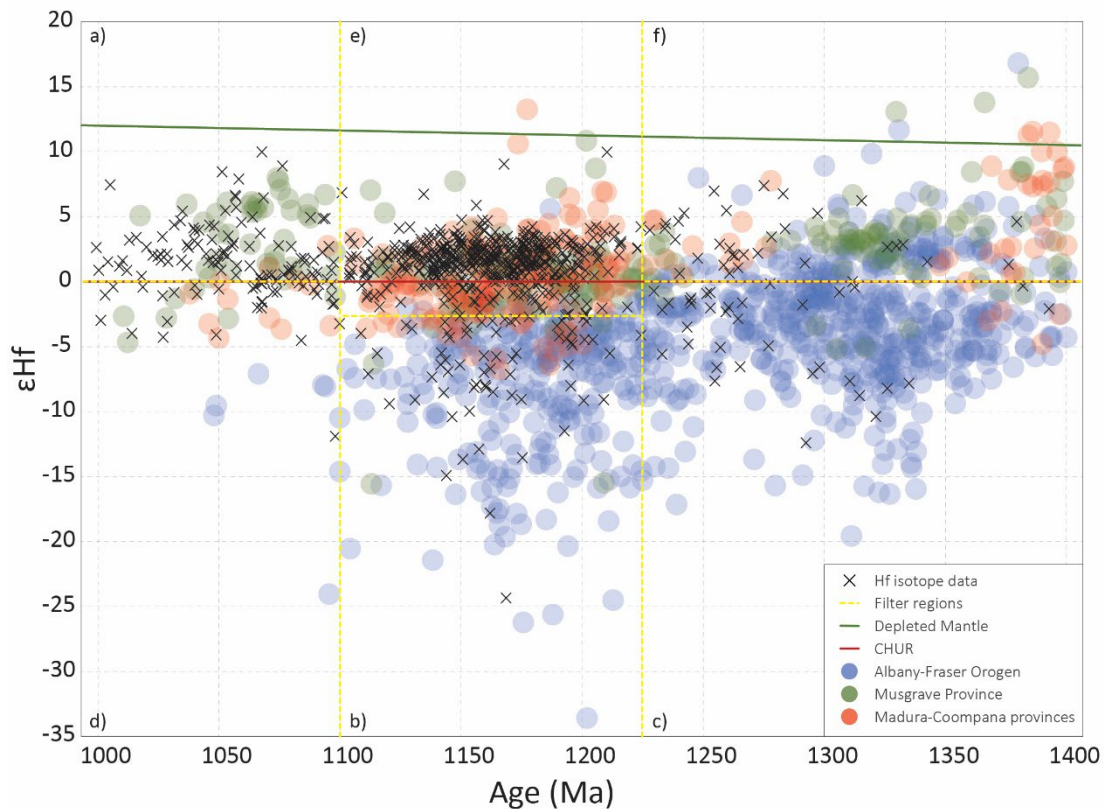


Figure 3.3 Detrital zircon Hf isotope data of Eucla Basin heavy mineral samples within the dominant age interval 1400–1000 Ma (this study; Reid et al., 2013b) overlain on published crystalline zircon Hf isotope data from the Albany-Fraser Orogen (Kirkland et al., 2011a; Spaggiari et al., 2015; Hartnady, 2019; Mole et al., 2019), the Musgrave Province (Kirkland et al., 2013), and the Madura and Coompana provinces (Kirkland et al., 2017; Hartnady et al., 2020). Regions (a - f) based on distinct U-Pb and Hf characteristics to distinguish source regions (Table 3.5).

Magmatic zircon grains of the Albany-Fraser Orogen's Biranup Zone (~1800–1625 Ma) express subchondritic to superchondritic Hf isotope values ( $-10 < \epsilon_{\text{Hf}} > +10$ ; Kirkland et al., 2011b; Spaggiari et al., 2015), that reflect mixing of juvenile mantle with evolved crust. Albany-Fraser Orogen derived zircon grains likely intermixed with



juvenile crustal zircon grains aged ~1650–1410 Ma from the Madura-Coompana provinces ( $\sim -2 < \epsilon H > +12$ ; Spaggiari et al., 2015; Kirkland et al., 2017; Hartnady et al., 2020), and zircon grains of evolved and juvenile character from Gawler Craton rocks (~1850–1605 Ma,  $\sim -8 < \epsilon H > +8$ ; Belousova et al., 2009; Reid & Payne, 2017). Minor contributions from an Archean-aged (~3000–2500 Ma) subchondritic to superchondritic source ( $\sim -10 < \epsilon H > +5$ ; Fig. 3.2i) to Eucla Basin heavy mineral placer deposits are associated with the western lying Yilgarn Craton (Kirkland et al., 2011a; Wyche et al., 2012) and the eastern lying Gawler Craton (Belousova et al., 2009; Reid & Payne; Fig. 3.1a). The significance of secondary Gawler Craton sediment supply to eastern Eucla Basin heavy mineral prospects, and a distinct Yilgarn Craton contribution restricted to the western basin margin and to the eastern lying Jacinth deposit during a Miocene enrichment phase was highlighted recently (Gartmair et al., 2022). Further sediment mixing of Eucla Basin palaeoshores is identified by the presence of detrital subchondritic zircon grains aged ~2800–1800 Ma ( $\sim -10 < \epsilon H > 0$ ; Fig. 3.2i) that match with evolved crustal components of the Gawler Craton (Belousova et al., 2009; Reid & Payne, 2017; Fig. 3.1a). The vertical array of predominantly young subchondritic detrital zircon grains dated at ~650–500 Ma ( $\sim -28 < \epsilon H > +4$ ; Fig. 3.2i) is indicative of an evolved source that experienced replenishment with juvenile magma and is likely associated with the Kuunga Orogen (Morón et al., 2019; Gartmair et al., 2022). These geologically young zircon grains are associated with long-lived fluvial transportation from Pangea-breakup to Gondwana-assembly, from where they were widely dispersed across Australian sedimentary basins (e.g., Officer Basin; Morón et al., 2019). While geochronological and geochemical analyses help resolve source specific zircon contributions to the overall detrital assemblage of Eucla Basin beach placers, ambiguities in resolving the dominant Mesoproterozoic supply source still remain.

## 5.2 Zircon grain shape analysis for sediment provenance studies

The similar spread of median grain shape values across all detrital samples (Table 3.1; App. Tables 3.1, 3.6) suggests that the data are obtained from a suite of grains expressing similar variations in shape morphologies as a result of shared hydraulic sorting processes during transportation (Schuiling et al., 1985; Komar, 2007), and that these sorting processes are not a direct function of heavy mineral upgrading. Our data set further identifies that the smallest median values recorded for the principal shape

parameters *area*, *perimeter*, *major axis*, *minor axis*, and *effective diameter* (Section 4.2; App. Fig. 3.2) express similarity between detrital and crystalline samples (sample 1841639, Thar prospect, and sample 2425443, Koomalboogurra Suite; App. Table 3.6). This similarity in grain size suggests a potential source to sink relationship between these grains, given that overall grain morphology may be retained during transportation, as previously highlighted (Morton & Hallsworth, 1999; Balan et al., 2001; Markwitz & Kirkland, 2018). It is therefore likely that the Koomalboogurra Suite may be a potential sediment supply source specifically for the north-eastern lying Thar prospect (Fig. 3.1b). Recent studies analysing potential biases in sediment provenance studies have identified that smaller zircon grains may be missed in the grain selection process during handpicking (Moecher & Samson, 2006; Zutterkirch et al., 2021), thus a contribution from the Koomalboogurra Suite to other northern and eastern Eucla Basin prospects from which samples were hand-picked (i.e., Cyclone, Jacinth, Atacama; Fig. 3.1b; App. Table 3.1) cannot be excluded. A potential bias in hand-picked samples is also identified in our analysis, as hand-picked detrital samples (App. Table 3.1) express overall larger minimum values for *area*, *perimeter*, *major axis*, *minor axis* and *effective diameter* across the data sets, compared to those from bulk-mounted detrital grains (Table 3.1; App. Tables 3.5, 3.6). We further identify from our grain shape data sets that the largest median values observed in the analysed detrital samples (sample 1688515, Cyclone; App. Table 3.6) exceed the largest median values recorded from the Coompana Province samples (App. Table 3.6), suggesting that these large zircon grains have likely originated from a source region distinct from which our crystalline basement samples were obtained (App. Table 3.2). Source rocks yielding granitic melts of low uranium content typically produce zircon grains with larger prisms (Benisek & Finger, 1993) and are likely not present within the Coompana Province lithologies analysed in this study (App. Table 3.2). The smallest median *circularity* values obtained from detrital data (sample 1661077, Observatory Hill Beds;  $C_i = 0.722$ ; App. Table 3.6) exceeds the largest median *circularity* values of Coompana Province data (sample 2427076, Koomalboogurra Suite;  $C_i = 0.654$ ; App. Table 3.6). This highlights the effects of prolonged sediment transportation on a grain's symmetry (i.e., value of 1.0 equating to a perfect circle; Table 3.2), while principal shape parameters (*area*, *perimeter*, *major axis*, *minor axis*, and *effective diameter*; App. Fig. 3.2) are overall maintained. Median *roundness* and *aspect ratio* values of detrital zircon grains are not statistically distinct from values obtained from crystalline

samples (App. Table 3.6) and are likely not subject to significant alteration during sediment sorting and transportation.

We extended the grain shape investigations by applying a Kolmogorov-Smirnov distance-based multidimensional scaling to all our samples ( $N = 35$ ,  $n = 36,428$ ; Table 3.1; App. Tables 3.1, 3.2, 3.5) to test for grain shape similarities as indicators for shared grain generation and erosion histories, and to identify unique shape descriptors that may distinguish between fresh and unweathered crystalline zircon grains from detrital transported and reworked zircon grains. The Kolmogorov-Smirnov test offers a statistical evaluation of age population similarities in cumulative distribution space (Vermeesch, 2013). More dissimilar sample pairs exhibit greater distance ( $D$ ) values and visually plot further apart in multidimensional scaling space, while sample pairs with more similar shape population characteristics have lower  $D$ -values and cluster more closely together. Our multidimensional scaling analysis of zircon populations across heavy mineral enriched and detrital non-heavy mineral samples exhibit great consistency in grouping, irrespective of which shape descriptors were deemed relevant through PCA (i.e., *area*, *perimeter*, *major axis*, *minor axis* and *effective diameter*; App. Figs. 3.2, 3.3). Each principal shape descriptor is therefore capable of identifying similarity trends related to grain size across detrital zircon populations, potentially broadening the scope of shape characteristics used in future studies (c.f., highlighted major and minor axes, effective diameter of Makuluni et al., 2019). Analysis of *circularity* does not show any conclusive clustering across zircon populations from our detrital data sets (App. Fig. 3.3), whereas *roundness* and *aspect ratio* indicate a clear distinction between bulk mounted samples (median  $R_n > 0.690$  and median  $AR < 1.450$ ; Table 3.1; App. Fig. 3.3) and hand-picked grain mount samples (median  $R_n < 0.690$  and median  $AR > 1.450$ ; App. Tables 3.1, 3.3). The differentiation in roundness and aspect ratio between bulk mounted and hand-picked samples may be associated with the mounting technique where bulk mounting and polishing of more randomly orientated zircon grains may result in 3-dimensional rotation of the grains (which may affect true measurements of roundness and aspect ratios; Table 3.2), or that handpicking of zircon grains (with mounting of the grains parallel to the grain's long-axis; e.g., Markwitz and Kirkland, 2018) results in a biased selection of less rounded, more elongated and overall larger grains (i.e., Dröllner et al., 2021; Zutterkirch et al., 2021).

Irrespective of the grain selection method chosen, none of the shape parameters analysed (Table 3.2) show distinct zircon population groupings across detrital samples associated with i) varying heavy mineral grades (i.e., peak heavy mineral samples compared to low-grade heavy mineral samples across deposits and within the same deposit; Table 3.1; App. Fig. 3.3), ii) between heavy mineral enriched prospect samples (irrespective of their heavy mineral grade) to non-enriched sedimentary samples from the basin's associated sedimentary hinterland region (Table 3.1; App. Table 3.1; App. Fig. 3.3), iii) across heavy mineral samples from varying basin margins (i.e., western, northern and eastern margins; Fig. 3.1b; Table 3.1; App. Tables 3.1; App. Fig. 3.3), or iv) across deposit samples associated with different Eocene and Miocene strandline settings (Gartmair et al., 2022; Table 3.1; App. Table 3.1; App. Fig. 3.3). We therefore interpret that differentiation of transportation modes, the degree of reworking, and processes necessary for heavy mineral maturation and upgrading cannot be obtained from detrital zircon grain shape analysis alone.

*Circularity* is the only shape parameter that conclusively distinguishes crystalline and detrital zircon populations (Fig. 3.4; App. Fig. 3.4), despite not being recognised as a principal shape parameter by PCA (App. Fig. 3.2). The fundamentals of a PCA analysis are based on a reduction method in order to determine key parameters of dimensionally large data sets while reducing the number of variables (Davis & Sampson, 1986; Legendre & Legendre, 1998; Harper, 1999). Our analysis indicates that grain shape characteristics not recognised as principal components through PCA (i.e., *circularity*; this study; Makuluni et al., 2019; App. Fig. 3.2) may be important in better resolving detrital source to sink patterns by indicating the degree of transportation a detrital zircon grain may have undergone from source to sink. Here, median *circularity* values of Coompana Province basement samples are smaller ( $C_i < 0.700$ ; App. Table 3.6) compared to median values of any detrital zircon samples analysed (i.e., heavy mineral enriched and sedimentary non-enriched detrital zircon samples;  $C_i > 0.700$ ; App. Table 3.6). Based on algebraic calculations using the equation  $Circularity = 4 \pi \left( \frac{Area}{Perimeter} \right)^2$ , the increased *circularity* values of detrital zircon grains are associated with greater surface area (i.e., values of 1.0 equate to a perfect circle; Table 3.2), while smaller values (i.e., values closer to 0.0) represent more euhedral and elongated zircon grains (Table 3.2), indicating that all sedimentary samples have undergone extended transportation and grain shape modification. This

distinction in grain circularity between crystalline and sedimentary samples may prove beneficial in detrital provenance studies incorporating grain morphologies.

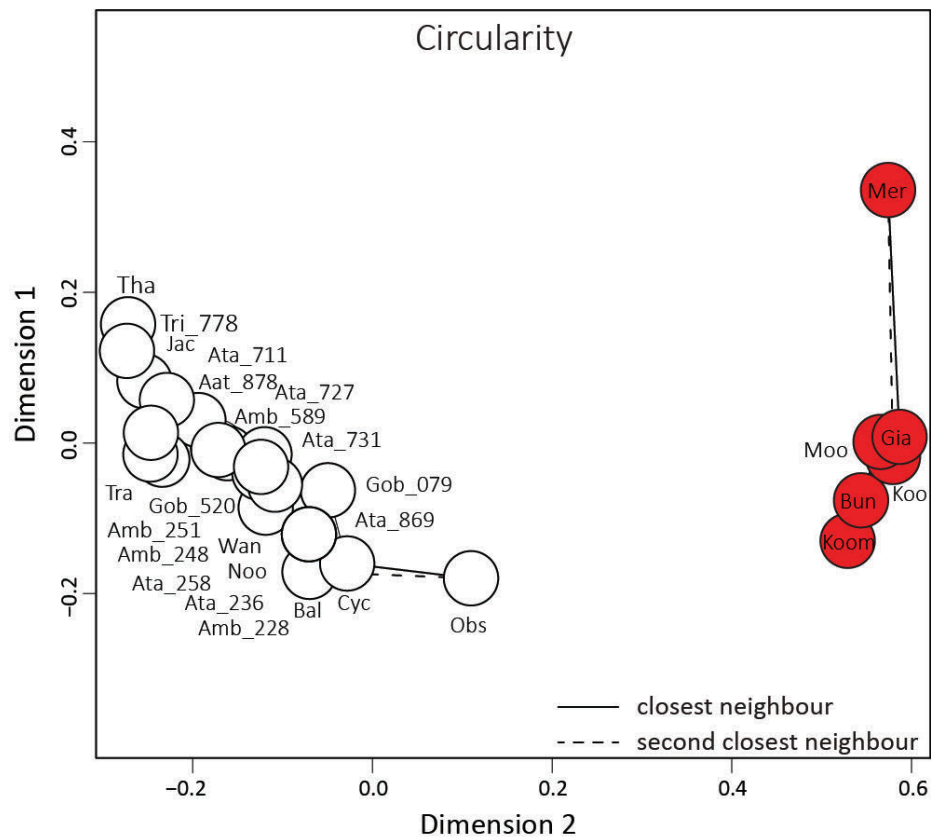


Figure 3.4 Kolmogorov-Smirnov distance-based multidimensional scaling (MDS) analysis of circularity shape parameter analysed from detrital and crystalline zircon samples (Tables 3.1, 3.2, 3.3). Unfilled circles represent detrital zircon samples, red circles indicate crystalline Coompana Province zircon grains. Amb\_228 = Ambrosia AD605228, Amb\_248 = Ambrosia AD605248, Amb\_251 = Ambrosia AD605251, Amb\_589 = Ambrosia AD605589, Ata\_236 = Atacama 1924236, Ata\_258 = Atacama 1924258, Ata\_711 = Atacama AD443711, Ata\_727 = Atacama AD443727, Ata\_731 = AD443731, Ata\_869 = Atacama AD458869, Ata\_878 = Atacama AD457878, Bal = Balladonia, Bun = Bunburra Suite (2423700, 2423705), Cyc = Cyclone, Gia = Giants Head Suite (2430064, 2498072), Gob\_079 = Gobi AD550079, Gob\_520 = Gobi AD550520, Jac = Jacinth, Koo = Koonalda Suite (2423713, 2423713\_534, 2423713\_828), Koom = Koomalboogurra Suite (2132936, 2425443, 2427076), Mer = Merdayerrah Shoshonite (2425514), Moo = Undifferentiated Moodini Supersuite (2132968, 2425514, 2427070), Noo = Noorina palaeochannel, Obs = Observatory Hill Beds, Tha = Thar, Tra = Trainor Hill Sandstone, Tri\_778 = Tripitaka AD376778, Wan = Wanna.

### 5.3 Refined mineral system approach using integrated U-Pb, Hf isotopes and grain shape analysis

Analysed samples were first screened for zircon grains that fall within the dominant Mesoproterozoic interval (~1400–1000) of Eucla Basin deposits (Fig. 3.3). From the chosen crystallisation interval, we only selected grains for which Hf isotope data and grain shape characteristics are also measured (Balladonia, Wanna, Cyclone, Ambrosia,

Gobi and Tripitaka;  $N = 10$ ,  $n = 229$ ; Reid et al., 2013b; this study; Fig. 3.1b; Table 3.1; App. Tables 3.1, 3.5). Published zircon U-Pb, Hf, and grain shape data from Mesoproterozoic source regions (i.e., Albany-Fraser Orogen, Musgrave Province, Madura-Coompana provinces; Kirkland et al., 2011a, 2013, 2017; Spaggiari et al., 2015; Markwitz & Kirkland, 2018; Hartnady, 2019; Makuluni et al., 2019; Mole et al., 2019; Hartnady et al., 2020) were extracted from literature sources and incorporated with new zircon grain shape data from the Coompana Province (App. Table 3.5). Samples 2430064 and 2498072 from the Mallabie Basalt of the Giants Head Suite (App. Tables 3.2, 3.5) were excluded in the following analysis due to a lack of grain shape, U-Pb, and Hf data. All other crystalline samples were then grouped into province-specific data sets. Data from the Eucla Basin's underlying Madura-Coompana basement (Kirkland et al., 2017; Jagodzinski et al., 2018; Makuluni et al., 2019; Hartnady et al., 2020; this study) were combined into one sample suite as some supersuites span both regions (i.e., Moodini Supersuite from the western Madura Province and the eastern Coompana Province; Jagodzinski et al., 2018) and to better capture the data spread of the underlying crystalline basement. Box and whisker plots (Fig. 3.5; App. Fig. 3.5) and Kolmogorov-Smirnov tests (Table 3.4) were calculated for the eight shape parameters (Table 3.2) across all three potential Mesoproterozoic source regions.

Table 3.4 Kolmogorov-Smirnov distance matrix comparing grain shape populations between source regions specifically for grains aged 1400–1000 Ma from the Albany-Fraser Orogen (Makuluni et al., 2019), the Musgrave Province (Markwitz & Kirkland, 2018) and the Madura and Coompana provinces (this study; Makuluni et al., 2019). Values in bold represent the most significant distance and probability values of distinct shape parameters to differentiate source regions.  $D$  = Distance values,  $p$  = Probability values. Giants Head Suite samples (2430064 and 2498072) excluded from analysis

	<i>Area</i>	<i>Perimeter</i>	<i>Major Axis</i>	<i>Minor Axis</i>	<i>Effective Diameter</i>	<i>Circularity</i>	<i>Roundness</i>	<i>Aspect Ratio</i>	
Madura-Coompana provinces	<b>Musgrave Province</b>								
	0.570	<b>0.610</b>	0.570	0.531	0.477	0.506	0.187	0.187	D
	< 0.05	< <b>0.05</b>	< 0.05	< 0.05	< 0.05	< 0.05	0.065	0.065	<i>p</i>
Albany-Fraser Orogen	<b>Madura-Coompana provinces</b>								
	0.550	0.426	<b>0.644</b>	0.441	0.550	0.570	0.490	0.433	D
	< 0.05	< 0.05	< <b>0.05</b>	< 0.05	< 0.05	< 0.05	< 0.05	< 0.05	<i>p</i>
Musgrave Province	<b>Albany-Fraser Orogen</b>								
	0.270	0.406	0.193	0.322	0.217	<b>0.643</b>	0.346	0.298	D
	< 0.05	< 0.05	< 0.05	< 0.05	< 0.05	< <b>0.05</b>	< 0.05	< 0.05	<i>p</i>

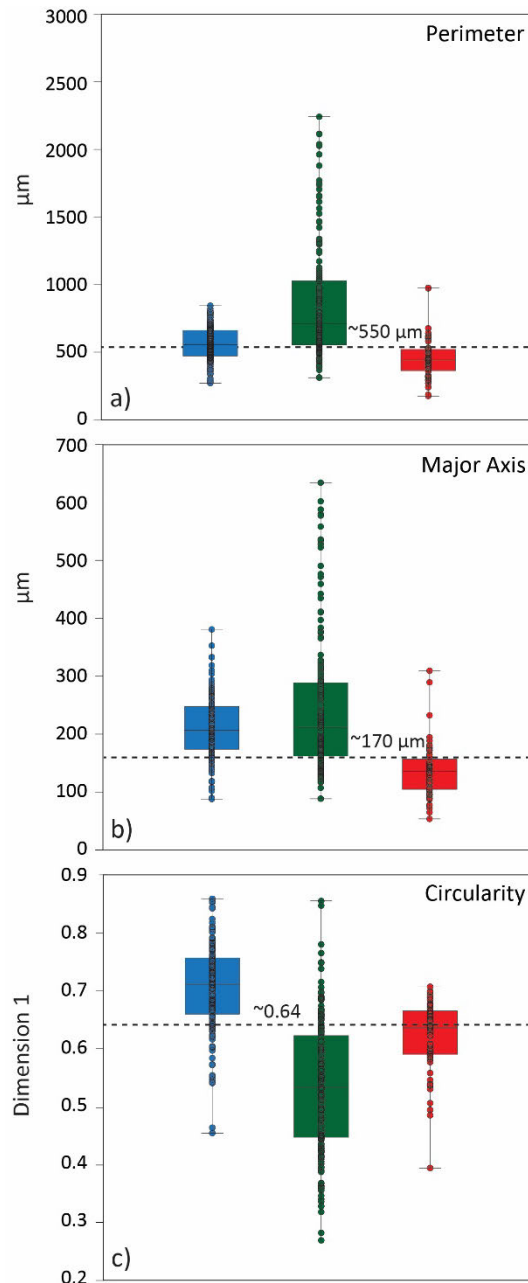


Figure 3.5 Box and whisker plots of grain shape parameters perimeter (a), major axis (b) and circularity (c) measured from 1400–1000 Ma dated crystalline zircon grains from the Albany-Fraser Orogen (Makuluni et al., 2019), Musgrave Province (Markwitz & Kirkland, 2018) and Madura and Coompana provinces (this study; Makuluni et al., 2019). Box outlines show the 25 – 75 percentiles of shape data for each provenance-specific sample set. Median values of data are presented as horizontal lines inside the box. Short horizontal lines ('whiskers') outside the box outlines represent minimal and maximal values of data sets. Values from grain shape data (App. Table 3.5). Giants Head Suite samples (2430064 and 2498072) excluded from analysis.

Mesoproterozoic source region zircon grains aged 1400–1000 Ma express variation in shape characteristics (Fig. 3.5a-c; Table 3.4; App. Fig. 3.5). Grains from the Madura-Coompana provinces (MCP) exhibit greatest dissimilarity to Musgrave Province (MP) zircon populations in *perimeter* values ( $D = 0.610$ ,  $p < 0.05$ ;  $MCP < 550 \mu\text{m} > MP$ ;

Fig. 3.5a; Table 3.4). The Madura-Coompana provinces (MCP) express greatest distinction in *major axis* of zircon grains to that of grains from the Albany-Fraser Orogen (AFO;  $D = 0.644$ ,  $p < 0.05$ ;  $MCP < 170 \mu m > AFO$ ; Fig. 3.5b; Table 3.4 [and  $MCP < 170 \mu m > MP$ ; Fig. 3.5b], while differentiation of the Musgrave Province (MP) and the Albany-Fraser Orogen (AFO) is most pronounced in grain *circularity* ( $D = 0.643$ ,  $p < 0.05$ ;  $MP < 0.64 > AFO$ ; Fig. 3.5c; Table 3.4).

A filtering approach based on the principles of elimination was then applied to the zircon grains of the selected heavy mineral samples (Balladonia, Wanna, Cyclone, Ambrosia, Gobi, and Tripitaka), integrating U-Pb, Hf isotope composition, and grain shape characteristics (Fig. 3.3; Table 3.5) to help more accurately constrain sediment provenance. Zircon grains from each individual heavy mineral sample set was first filtered for U-Pb and Hf characteristics that coincide with only one specific source region (Fig. 3.3a-c; Table 3.5). The remaining data were then screened for overlapping U-Pb and Hf signatures of likely source regions that could be further distinguished through shape-specific parameters identified from Kolmogorov-Smirnov analysis (Fig. 3.3d-f; Tables 3.4, 3.5).

The combined approach of U-Pb geochronological, Hf isotope geochemical, and grain morphological investigation of Eucla Basin deposit samples (Fig. 3.3; Table 3.5) indicates that the Madura-Coompana provinces are the dominant zircon contributors for heavy mineral accumulations along northern and north-eastern Eucla Basin palaeoshorelines (between 57% in Ambrosia AD605228 and 89% in Ambrosia AD605589; excluding Cyclone; Fig. 3.6; Table 3.5). Grain-shape indicated contributions from the Musgrave Province range from 0% (Ambrosia AD605251; Fig. 3.6; Table 3.5) to 29% (Gobi AD550079; Fig. 3.6; Table 3.5) for the same deposits. The northern positioned Cyclone deposit (Fig. 3.1b) exhibits a sediment signature that is unique to that observed in other northern and north-eastern beach placers (Fig. 3.6, Table 3.5), highlighted by a predominant sediment supply from the Musgrave Province (86%; Fig. 3.6; Table 3.5) and a low contribution from the Madura-Coompana provinces (9%; Fig. 3.6; Table 3.5). A high Musgrave Province signature in Cyclone's heavy mineral spectrum is plausible due to the placer deposit's location near the mouth of a large channel system draining from the Musgrave Province (Wanna palaeodrainage; Hou et al., 2011).



Table 3.5 Detrital provenance filter analysis using integrated U-Pb, Hf isotope and grain shape data. Filtering of data based on Fig. 3.3 and Table 3.4. Cells with bold text indicate detrital grains matching with data from Mesoproterozoic source regions. Percentages of grain contributions rounded to whole number. Filter = filter regions identified from integrated U-Pb, Hf isotope and grain shape filter analysis (Fig. 3.3). AFO = Albany-Fraser Orogen, Ci = circularity, MaA = major axis, MCP = Madura-Coompana provinces, MP = Musgrave Province. P = perimeter

Sample, ID	Filter	U-Pb	eHF	Source Region	Number of Grains (n)	Shape Distinction	Source Region	Number of Grains (n)	Shape Distinction	Source Region	Number of Grains (n)	Provenance Number of Grains (n/N, %)
Balladonia 1688514	a)	1100–1000 Ma	> 0	MP	0							Albany-Fraser Orogen 19/23, 83
	b)	1225–1100 Ma	< -2.5	AFO	3							Musgrave Province 1/23, 4
	c)	1400–1225 Ma	< 0	AFO	13							Madura-Coompana provinces 3/23, 13
	d)	1100–1000 Ma	< 0	MP	0	P > 550 µm	MP	0				
	e)	1225–1100 Ma	> -2.5	MP	1	P < 550 µm	MP	0				
	f)	1400–1225 Ma	> 0	AFO MP MCP	6 6 6	MaA > 170 µm MaA < 170 µm	AFO MP MCP	4 4 2	Ci > 0.64 Ci < 0.64	AFO MP	3 1	
Wanna PC109105	a)	1100–1000 Ma	> 0	MP	2							Albany-Fraser Orogen 0/24, 0
	b)	1225–1100 Ma	< -2.5	AFO	0							Musgrave Province 5/24, 21
	c)	1400–1225 Ma	< 0	AFO	0							Madura-Coompana provinces 19/24, 79
	d)	1100–1000 Ma	< 0	MP	2	P > 550 µm	MP	0				
	e)	1225–1100 Ma	> -2.5	MP	20	P < 550 µm	MP	3				
	f)	1400–1225 Ma	> 0	AFO MP MCP	0 0 7	MaA > 170 µm MaA < 170 µm	AFO MP MCP	0 0 0	Ci > 0.64 Ci < 0.64	AFO MP	0 0	
Cyclone 1688515	a)	1100–1000 Ma	> 0	MP	7							Albany-Fraser Orogen 1/22, 5
	b)	1225–1100 Ma	< -2.5	AFO	0							Musgrave Province 19/22, 86
	c)	1400–1225 Ma	< 0	AFO	1							Madura-Coompana provinces 2/22, 9
	d)	1100–1000 Ma	< 0	MP	1	P > 550 µm	MP	1				
	e)	1225–1100 Ma	> -2.5	MP	13	P < 550 µm	MP	11				
	f)	1400–1225 Ma	> 0	AFO MP MCP	0 0 0	MaA > 170 µm MaA < 170 µm	AFO MP MCP	0 0 0	Ci > 0.64 Ci < 0.64	AFO MP	0 0	
Ambrosia AD605228	a)	1100–1000 Ma	> 0	MP	2							Albany-Fraser Orogen 4/14, 29
	b)	1225–1100 Ma	< -2.5	AFO	4							Musgrave Province 2/14, 14
	c)	1400–1225 Ma	< 0	AFO	0							Madura-Coompana provinces 8/14, 57
	d)	1100–1000 Ma	< 0	MP	0	P > 550 µm	MP	0				
	e)	1225–1100 Ma	> -2.5	MP	8	P < 550 µm	MP	8				
	f)	1400–1225 Ma	> 0	AFO MP MCP	0 0 0	MaA > 170 µm MaA < 170 µm	AFO MP MCP	0 0 0	Ci > 0.64 Ci < 0.64	AFO MP	0 0	

Sample ID	Filter	U-Pb	eHf	Source Region	Number of Grains (n)	Shape Distinction	Source Region	Number of Grains (n)	Shape Distinction	Source Region	Number of Grains (n)	Provenience Number of Grains (n/N, %)
Ambrosia AD605248	a)	1100–1000 Ma	> 0	MP	3							Albany-Fraser Orogen 1/12, 8
	b)	1225–1100 Ma	< -2.5	AFO	1							Musgrave Province 3/12, 25
	c)	1400–1225 Ma	< 0	AFO	0							Madura-Coompana provinces 8/12, 67
	d)	1100–1000 Ma	< 0	MCP	0	P > 550 µm	MP	0				
	e)	1225–1100 Ma	> -2.5	MP	7	P > 550 µm	MP	0				
	f)	1400–1225 Ma	> 0	MCP	1	P < 550 µm	MCP	7				
Ambrosia AD605251	a)	1100–1000 Ma	> 0	MP	1	MaA > 170 µm	AFO	0	CI > 0.64	AFO	0	
	b)	1225–1100 Ma	> 0	MP	0	MaA < 170 µm	MP	0	CI < 0.64	MP	0	
	c)	1400–1225 Ma	< 0	AFO	0							Albany-Fraser Orogen 2/14, 14
	d)	1100–1000 Ma	< 0	MP	0	P > 550 µm	MP	0				Musgrave Province 0/14, 0
	e)	1225–1100 Ma	> -2.5	MCP	12	P < 550 µm	MP	0				Madura-Coompana provinces 12/14, 86
	f)	1400–1225 Ma	> 0	MCP	0	P < 550 µm	MCP	12				
Ambrosia AD605589	a)	1100–1000 Ma	> 0	MP	1	MaA > 170 µm	AFO	0	CI > 0.64	AFO	0	
	b)	1225–1100 Ma	< -2.5	AFO	2	MaA < 170 µm	MP	0	CI < 0.64	MP	0	
	c)	1400–1225 Ma	< 0	AFO	0							Albany-Fraser Orogen 2/28, 7
	d)	1100–1000 Ma	< 0	MCP	2	P > 550 µm	MP	0				Musgrave Province 1/28, 4
	e)	1225–1100 Ma	> -2.5	MCP	23	P < 550 µm	MCP	2				Madura-Coompana provinces 25/28, 89
	f)	1400–1225 Ma	> 0	MCP	0	P < 550 µm	MCP	23				
Gobi AD550079	a)	1100–1000 Ma	> 0	MP	5	MaA > 170 µm	AFO	0	CI > 0.64	AFO	0	
	b)	1225–1100 Ma	< -2.5	AFO	5	MaA < 170 µm	MP	0	CI < 0.64	MP	0	
	c)	1400–1225 Ma	< 0	AFO	1							Albany-Fraser Orogen 6/52, 11
	d)	1100–1000 Ma	< 0	MCP	3	P > 550 µm	MP	0				Musgrave Province 15/52, 29
	e)	1225–1100 Ma	> -2.5	MCP	38	P < 550 µm	MCP	3				Madura-Coompana provinces 31/52, 60
	f)	1400–1225 Ma	> 0	MCP	0	P > 550 µm	MCP	38				

Sample ID	Filter	U-Pb	eHF	Source Region	Number of Grains (n)	Shape Distinction	Source Region	Number of Grains (n)	Shape Distinction	Source Region	Number of Grains (n)	Provenance Number of Grains (n/N, %)
Gobi AD550520	a)	1100–1000 Ma	> 0	MP	2							Albany-Fraser Orogen 2/20, 10
	b)	1225–1100 Ma	< -2.5	AFO	2							Musgrave Province 2/20, 10
	c)	1400–1225 Ma	< 0	AFO	0							Madura-Coompana provinces 16/20, 80
	d)	1100–1000 Ma	< 0	MCP	3	P > 550 $\mu$ m	MP	0				
	e)	1225–1100 Ma	> -2.5	MCP	12	P < 550 $\mu$ m	MP	0				
	f)	1400–1225 Ma	> 0	MCP	1	Maa > 170 $\mu$ m	AFO	0	Ci > 0.64	AFO	0	
Irritator AD376778	a)	1100–1000 Ma	> 0	MP	1	Maa < 170 $\mu$ m	MCP	1				Albany-Fraser Orogen 4/20, 20
	b)	1225–1100 Ma	< -2.5	AFO	4							Musgrave Province 1/20, 5
	c)	1400–1225 Ma	< 0	AFO	0							Madura-Coompana provinces 15/20, 75
	d)	1100–1000 Ma	< 0	MCP	2	P > 550 $\mu$ m	MP	0				
	e)	1225–1100 Ma	> -2.5	MCP	13	P < 550 $\mu$ m	MCP	13				
	f)	1400–1225 Ma	> 0	MCP	0	Maa > 170 $\mu$ m	MP	0	Ci > 0.64	AFO	0	
				MCP	0	Maa < 170 $\mu$ m	MCP	0	Ci < 0.64	MP	0	

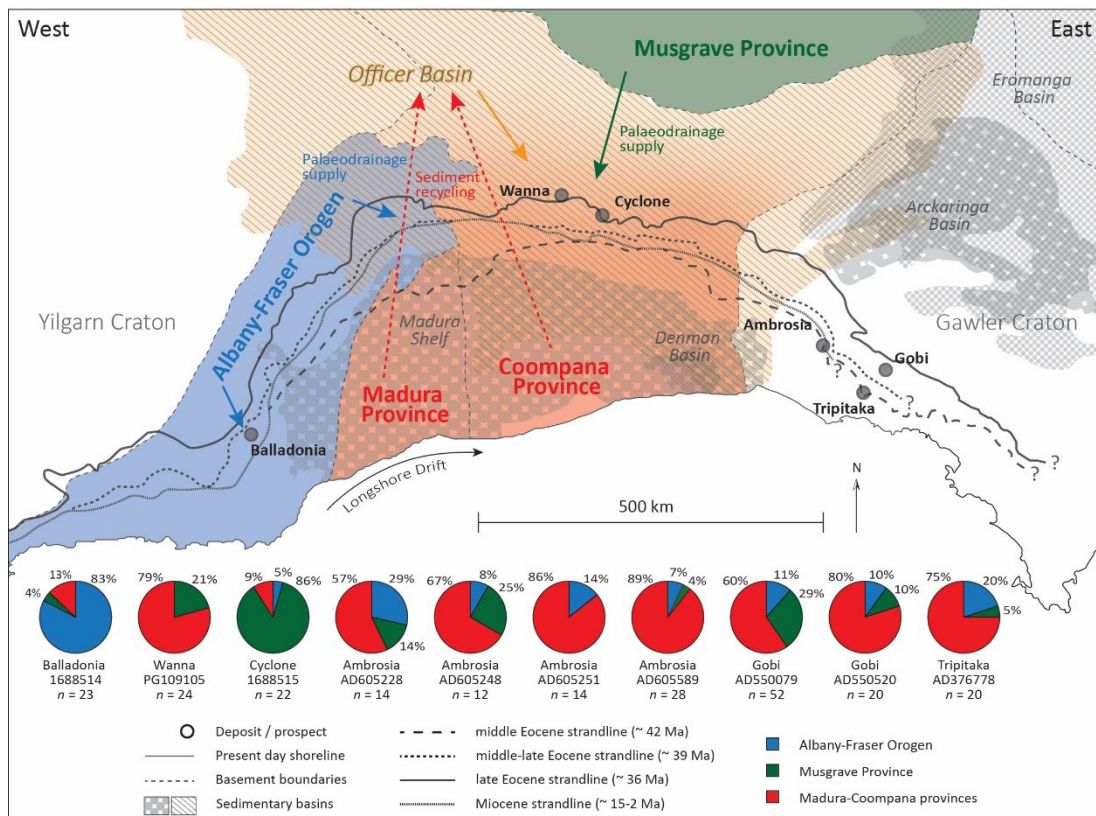


Figure 3.6 Schematic summary figure and pie chart representation of dominant Mesoproterozoic source region contribution to Eucla Basin heavy mineral placer deposits based on integrated geochronology, Hf isotope and grain shape filtering (Fig. 3.3; Table 3.5).

However, a biased selection of larger grains from handpicking cannot be entirely excluded (*perimeter* > 550  $\mu\text{m}$ ; Fig. 3.5a; Table 3.5; Zutterkirch et al., 2021). It is therefore possible that contributions from the Madura-Coompana provinces to Cyclone may in fact be higher than our analysis from the available sample indicates. The far western Balladonia sample (Fig. 3.1b) is distinctive from all other samples analysed (Wanna, Cyclone, Ambrosia, Gobi and Tripitaka; Figs. 3.1b, 3.6; Table 3.5) and indicates a dominant Albany-Fraser Orogen detrital provenance (83%; Fig. 3.6; Table 3.5), supporting previous interpretations (based on U-Pb data, proximity and longshore drift direction; Reid et al., 2013a, b; Gartmair et al. 2022). Balladonia's detrital signature further indicates minor detrital contributions from the underlying Madura-Coompana provinces (13% of the total analysed zircon grains in Balladonia; Fig. 3.6; Table 3.5). Sediment may have been supplied from the far western portion of the Madura Province to the western basin margin by ocean swells. However, given the low number of grains involved, the single grain associated with the Musgrave Province (Fig. 3.6; Table 3.5) may be an outlier or reflect recycling through intermediate sedimentary basins (i.e., Officer Basin; Gartmair et al., 2022).

#### **5.4 Implications for future sediment provenance studies and heavy mineral prospectivity models**

While our study highlights the efficacy and low-cost potential of integrating zircon grain shape analysis with traditional U-Pb and Hf investigation in sediment provenance studies, we acknowledge that our analysis (Section 5.3) is based on the overall shape of a grain, irrespective of potential internal growth zones. The integrated analysis is also based on a restricted number of grain counts across the data sets ( $N = 10$ ,  $n = 229$ ; Fig., 3.6; Table 3.5) due to a reliance on comprehensive geochronological, geochemical, and shape data for each grain. The total number of grains available for our provenance analysis (Section 5.3) was also affected by grains deemed unsuitable due to insufficient or altered grain boundary extraction (Section 3.3.3). Nonetheless, it is clear the methodology we have advocated has advantages for resolving ambiguities in conventional provenance studies where source regions overlap in either or both age and geochemical composition. Specifically for mineral systems models (e.g., Wyborn et al., 1994; Porwal et al., 2010; McCuaig & Hronsky, 2014; Joly et al., 2015; Li et al., 2018; Mao et al., 2019) an advanced understanding of unique sediment sourcing and varying supply regimes responsible for enriching palaeoshorelines is crucial to minimise potential risks in exploration targeting. The integrated triple-characterisation approach (geochronology-geochemistry-grain shape) demonstrates the importance of the newly identified sediment supply regime from the Eucla Basin's underlying Madura-Coompana basement through Officer Basin recycling. The results of our analysis indicate that the dominant detrital supply may not be restricted to presently elevated hinterland regions via palaeodrainage, and that detrital recycling through older sedimentary basins (i.e., Officer Basin) may be much more important for enriching prospective palaeoshorelines than previously thought. Although recycling of older sedimentary units has been implicated as a mechanism of sediment supply to Eucla Basin heavy mineral placers (e.g., Reid et al., 2013a), this sediment recycling was associated with the basin's bounding source rocks, rather than it's directly underlying crust. Our results further support recent investigations, where such sourcing from underlying basement units (i.e., Madura-Coompana provinces; Fig. 3.1a) into overlying basins has been recognised (i.e., Madura Shelf; Fig. 3.1a; Makuluni et al., 2019). We therefore suggest that future exploration targeting (in the Eucla Basin and globally) may benefit from directing a palaeodrainage-barrier system-

heavy mineral trap site focus into a broader regional play that incorporates intermediate older sedimentary reservoirs and non-exposed crystalline basements in their source to sink prospectivity analyses. To mitigate some of the limitations encountered in our study and to further enhance the application of grain shape analysis as an additional tool for sediment provenance studies globally, we suggest that future analyses would benefit from bulk mounting samples from which grain shape data can be extracted prior to geochronological and geochemical analysis. Additional age and geochemical profiling of various grain growth zones may help further refine sediment provenance investigations, as well as the incorporation of cathodoluminescence imagery obtained from bulk-mounted samples.

## 6. Conclusions

Eucla Basin heavy mineral placer deposits are characterised by grain contributions associated with mixing of late Archean to early Palaeoproterozoic-aged source rocks that are characteristic of juvenile and magmatically evolved compositions. A dominant supply of Mesoproterozoic-aged zircon grains of weakly subchondritic to superchondritic Hf isotope composition ( $\sim -2.5 < \epsilon_{\text{Hf}} > \sim +5$ ) is identified in the crystalline regional basement, that matches the age and geochemistry to that of both the basin's northern Musgrave Province and the underlying Madura-Coompana provinces. Grain shape analysis of detrital and crystalline zircon samples helps resolve U-Pb age and Hf-isotope ambiguities within the sediment source to sink record by providing a third distinctive grain characteristic. Mesoproterozoic sources bounding and underlying the Eucla Basin are uniquely distinguished in specific grain shape characteristics. Median *perimeter* values of Madura-Coompana zircon grains are typically smaller ( $< 550 \mu\text{m}$ ) than those from the Musgrave Province ( $> 550 \mu\text{m}$ ). Median *major axis* values of zircon grains are distinct between the Madura-Coompana provinces ( $< 170 \mu\text{m}$ ) and the Albany-Fraser Orogen and Musgrave Province (both  $> 170 \mu\text{m}$ ), and *circularity* of grains differ between the Musgrave Province ( $< 0.64$ ) and the Albany-Fraser Orogen ( $> 0.64$ ). Stepwise filtering of U-Pb age, Hf-isotope, and unique grain shape characteristics identifies the Madura-Coompana provinces as the likely dominant sediment source for the Eucla Basin heavy mineral placers. Reworking and recycling of underlying crystalline basement zircon grains through intermediate sedimentary reservoirs (e.g., Officer Basin, Madura Shelf, etc.) is

recognised as an important mechanism for Eucla Basin heavy mineral placer formation. Multi-dimensional scaling analysis of zircon grain shape characteristics identifies *circularity* as a unique shape distinguisher between detrital and crystalline samples, indicating increased transportation and abrasion of grains from their original source to their final sink locality. Integration of a triple-characterisation approach, utilising geochronology and geochemistry with integrated grain shape analysis, provides an additional dimension for sediment provenance studies currently hindered by limitations encountered in conventional U-Pb age and Hf-isotope investigations.

### **Acknowledgements**

The authors would like to express their gratitude to Iluka Resources Ltd. for the provision of sample material. Dr. Anthony Reid from the Geological Survey of South Australia is greatly acknowledged for providing samples images. Noreen Evans and Bradley McDonald from the John de Laeter Centre at Curtin University are thanked for facilitating laser ablation measurements. We further thank the Mineral Research Institute of Western Australia (MRIWA) for grant M551, and Curtin University for providing financial support with the Master of Research Stipend Scholarship.

### Chapter Three Reference List

- Akinlotan, O. O., & Rogers, G. H. (2021). Heavy mineral constraints on the provenance evolution of the English Lower Cretaceous (Wessex Basin). *Marine and Petroleum Geology*, *127*, 104952. <https://doi.org/10.1016/j.marpetgeo.2021.104952>
- Akinlotan, O. O., Rogers, G. H., & Okunuwadje, S. E. (2021). Provenance evolution of the English Lower Cretaceous Weald Basin and implications for palaeogeography of the northwest European massifs: constraints from heavy mineral assemblages. *Marine and Petroleum Geology*, *127*, 104953. <https://doi.org/10.1016/j.marpetgeo.2021.104953>
- Andersen, T. (2005). Detrital zircons as tracers of sedimentary provenance: limiting conditions from statistics and numerical simulation. *Chemical Geology*, *216*(3-4), 249-270. <https://doi.org/10.1016/j.chemgeo.2004.11.013>
- Balan, E., Neuville, D. R., Trocellier, P., Fritsch, E., Muller, J.-P., & Calas, G. (2001). Metamictization and chemical durability of detrital zircon. *American Mineralogist*, *86*(9), 1025-1033. <https://doi.org/10.2138/am-2001-8-909>
- Barham, M., & Kirkland, C. L. (2020). Changing of the guards: Detrital zircon provenance tracking sedimentological reorganization of a post-Gondwanan rift margin. *Basin Research*, *32*, 854-874. <https://doi.org/10.1111/bre.12403>
- Barham, M., Reynolds, S., Kirkland, C. L., O'Leary, M. J., Evans, N. J., Allen, H. J., . . . McDonald, B. J. (2018). Sediment routing and basin evolution in Proterozoic to Mesozoic east Gondwana: A case study from southern Australia. *Gondwana Research*, *58*, 122-140. <https://doi.org/10.1016/j.gr.2018.03.006>
- Beard, J. (1998). Position and developmental history of the central watershed of the Western Shield, Western Australia. *Journal of the Royal Society of Western Australia*, *81*, 157-164.
- Belousova, E. A., Griffin, W. L., & O'Reilly, S. Y. (2006). Zircon Crystal Morphology, Trace Element Signatures and Hf Isotope Composition as a Tool for Petrogenetic Modelling: Examples From Eastern Australian Granitoids. *Journal of Petrology*, *47*, 329-353. <https://doi.org/10.1093/petrology/egi077>
- Belousova, E. A., Reid, A. J., Griffin, W. L., & O'Reilly, S. Y. (2009). Rejuvenation vs. recycling of Archean crust in the Gawler Craton, South Australia: evidence from U–Pb and Hf isotopes in detrital zircon. *Lithos*, *113*(3-4), 570-582.
- Benisek, A., & Finger, F. (1993). Factors controlling the development of prism faces in granite zircons: a microprobe study. *Contributions to mineralogy and petrology*, *114*(4), 441-451. <https://doi.org/10.1007/bf00321749>
- Blichert-Toft, J., & Albarède, F. (1997). The Lu-Hf isotope geochemistry of chondrites and the evolution of the mantle-crust system. *Earth and Planetary Science Letters*, *148*(1), 243-258. [https://doi.org/10.1016/S0012-821X\(97\)00040-X](https://doi.org/10.1016/S0012-821X(97)00040-X)



- Brown, B., Müller, R., Gaina, C., Struckmeyer, H., Stagg, H., & Symonds, P. (2003). Formation and evolution of Australian passive margins: Implications for locating the boundary between continental and oceanic crust. *Special Papers - Geological Society of America*, 372, 223-243. <https://doi.org/10.1130/0-8137-2372-8.223>
- Cassidy, K., Champion, D., Krapez, B., Barley, M., Brown, S., Blewett, R., . . . Tyler, I. (2006). A revised geological framework for the Yilgarn Craton, Western Australia. *Geological Survey of Western Australia, Record 2006/8*, 8.
- Clark, D. J., Hensen, B. J., & Kinny, P. D. (2000). Geochronological constraints for a two-stage history of the Albany–Fraser Orogen, Western Australia. *Precambrian Research*, 102(3), 155-183. [https://doi.org/10.1016/S0301-9268\(00\)00063-2](https://doi.org/10.1016/S0301-9268(00)00063-2)
- Collins, W. J., Belousova, E. A., Kemp, A. I. S., & Murphy, J. B. (2011). Two contrasting Phanerozoic orogenic systems revealed by hafnium isotope data. *Nature Geoscience*, 4(5), 333-337. <https://doi.org/10.1038/ngeo1127>
- Corfu, F., Hanchar, J. M., Hoskin, P. W. O., & Kinny, P. (2003). Atlas of Zircon Textures. *Reviews in Mineralogy and Geochemistry*, 53(1), 469-500. <https://doi.org/10.2113/0530469>
- Courtney-Davies, L., Ciobanu, C. L., Tapster, S. R., Cook, N. J., Ehrig, K., Crowley, J. L., . . . Condon, D. J. (2020). Opening the magmatic-hydrothermal window: High-precision U-Pb geochronology of the Mesoproterozoic Olympic Dam Cu-U-Au-Ag deposit, South Australia. *Economic Geology*, 115(8), 1855-1870. <https://doi.org/10.5382/econgeo.4772>
- Cowley, W., Connor, C., & Zang, W. (2003). New and revised Proterozoic stratigraphic units on northern Yorke Peninsula. *MESA Journal*, 29, 46-58.
- Danielsson, P.-E. (1980). Euclidean distance mapping. *Computer Graphics and Image Processing*, 14(3), 227-248. [https://doi.org/10.1016/0146-664X\(80\)90054-4](https://doi.org/10.1016/0146-664X(80)90054-4)
- Davis, J. C., & Sampson, R. J. (1986). *Statistics and data analysis in geology* (Vol. 646): Wiley New York.
- de Broekert, P., & Sandiford, M. (2005). Buried inset-valleys in the Eastern Yilgarn Craton, Western Australia: geomorphology, age, and allogenic control. *The Journal of Geology*, 113(4), 471-493. <https://doi.org/10.1086/430244>
- de Gromard, R. Q., Wingate, M. T. D., Kirkland, C., Smithies, R., & Howard, H. (2016). Geology and U-Pb Geochronology of the Warlawurru Supersuite and MacDougall Formation in the Mitika and Wanarn Areas, West Musgrave Province. *Geological Survey of Western Australia, Record 2016/4*, 29. Retrieved from <http://hdl.handle.net/20.500.11937/55206>
- Dhuime, B., Hawkesworth, C. J., Cawood, P. A., & Storey, C. D. (2012). A change in the geodynamics of continental growth 3 billion years ago. *Science*, 335(6074), 1334-1336. <https://doi.org/10.1126/science.1216066>
- Dröllner, M., Barham, M., Kirkland, C., & Ware, B. (2021). Every zircon deserves a date: selection bias in detrital geochronology. *Geological Magazine*, 158, 1-8. <https://doi.org/10.1017/S0016756821000145>

- Edgoose, C., Scrimgeour, I., & Close, D. (2004). Geology of the Musgrave Block, Northern Territory. *Northern Territory Geological Survey, Report 15*, 48.
- Fanning, C., Reid, A., & Teale, G. S. (2007). A geochronological framework for the Gawler Craton, South Australia. *South Australia Geological Survey. Bulletin 55*, 258.
- Ferris, G., & Schwarz, M. (2004). Definition of the Tunkillia Suite, western Gawler craton. *MESA Journal*, 34, 32-41.
- Gartmair, G., Barham, M., & Kirkland, C. L. (2022). Detrital Zircon Perspectives on Heavy Mineral Sand Systems, Eucla Basin, Australia. *Economic Geology*. <https://doi.org/10.5382/econgeo.4871>
- Gehrels, G. (2014). Detrital zircon U-Pb geochronology applied to tectonics. *Annual Review of Earth and Planetary Sciences*, 42, 127-149. <https://doi.org/10.1146/annurev-earth-050212-124012>
- Gerdes, A., & Zeh, A. (2006). Combined U–Pb and Hf isotope LA-(MC-)ICP-MS analyses of detrital zircons: Comparison with SHRIMP and new constraints for the provenance and age of an Armorican metasediment in Central Germany. *Earth and Planetary Science Letters*, 249(1), 47-61. <https://doi.org/10.1016/j.epsl.2006.06.039>
- Grey, K., Hocking, R., Stevens, M., Bagas, L., Carlsen, G., Irimies, F., . . . Apak, S. (2005). Lithostratigraphic nomenclature of the Officer Basin and correlative parts of the Paterson Orogen, Western Australia. *Western Australia Geological Survey, Report, 93*, 89.
- Griffin, W., Wang, X., Jackson, S., Pearson, N., O'Reilly, S. Y., Xu, X., & Zhou, X. (2002). Zircon chemistry and magma mixing, SE China: in-situ analysis of Hf isotopes, Tonglu and Pingtan igneous complexes. *Lithos*, 61(3-4), 237-269. [https://doi.org/10.1016/S0024-4937\(02\)00082-8](https://doi.org/10.1016/S0024-4937(02)00082-8)
- Gurnis, M. (2001). Sculpting the Earth from inside out. *Scientific American*, 284(3), 40-47. <https://www.jstor.org/stable/10.2307/26059128>
- Hammer, Ø., Harper, D. A., & Ryan, P. D. (2001). PAST: Paleontological statistics software package for education and data analysis. *Palaeontologia electronica*, 4(1), 9. Retrieved from [http://palaeo-electronica.org/2001\\_1/past/issue1\\_01.htm](http://palaeo-electronica.org/2001_1/past/issue1_01.htm).
- Harper, D. A. (1999). *Numerical palaeobiology: computer-based modelling and analysis of fossils and their distributions*. John Wiley & Sons Inc.
- Hartnady, M. I. H. (2019). *Crustal Evolution of the Albany-Fraser Orogen, Western Australia* (Doctoral dissertation, Perth, Curtin University).
- Hartnady, M. I. H., Kirkland, C. L., Dutch, R. A., Bodorkos, S., & Jagodzinski, E. A. (2020). Evaluating zircon initial Hf isotopic composition using a combined SIMS–MC–LASS–ICP–MS approach: A case study from the Coompana Province in South Australia. *Chemical geology*, 558, 119870. <https://doi.org/10.1016/j.chemgeo.2020.119870>
- Hou, B., Frakes, L., Alley, N., & Heithersay, P. (2003). Evolution of beach placer shorelines and heavy-mineral deposition in the eastern Eucla Basin, South Australia. *Australian Journal of Earth Sciences*, 50(6), 955-965. <https://doi.org/10.1111/j.1400-0952.2003.01036.x>

- Hou, B., Frakes, L., Sandiford, M., Worrall, L., Keeling, J., & Alley, N. (2008). Cenozoic Eucla Basin and associated palaeovalleys, southern Australia—climatic and tectonic influences on landscape evolution, sedimentation and heavy mineral accumulation. *Sedimentary Geology*, 203(1-2), 112-130. <https://doi.org/10.1016/j.sedgeo.2007.11.005>
- Hou, B., & Keeling, J. (2008). Eucla basin, emerging as a new heavy mineral province of global significance: Old province—new ideas. *MESA Journal*, 49, 20-26.
- Hou, B., Keeling, J., Reid, A., Fairclough, M., Warland, I., Belousova, E., . . . Hocking, R. (2011). Heavy mineral sands in the Eucla Basin, southern Australia: deposition and province-scale prospectivity. *Economic Geology*, 106(4), 687-712. <https://doi.org/10.2113/econgeo.106.4.687>
- Hou, B., & Warland, I. (2005). Heavy mineral sands potential of the Eucla Basin in South Australia—a world-class palaeobeach placer province. *MESA Journal*, 37, 4-12.
- Howard, H., Smithies, R., Kirkland, C., Kelsey, D., Aitken, A., Wingate, M., . . . Maier, W. D. (2015). The burning heart—the Proterozoic geology and geological evolution of the west Musgrave Region, central Australia. *Gondwana Research*, 27(1), 64-94. <https://doi.org/10.1016/j.gr.2014.09.001>
- Iluka Resources Limited. (2021). Jacinth-Ambrosia Overview. <https://iluka.com/operations-resource-development/operations/jacinth-ambrosia>. Retrieved from <https://www.iluka.com/operations-resource-636-development/operations/jacinth-ambrosia>
- Jagodzinski, E. A., Bodorkos, S., & Crowley, J. L. (2018). PACE Copper Coompana Drilling Project: U-Pb Dating of Basement and Cover Rocks. *Department for Energy and Mining, South Australia, Report Book 2018/00028*, 211.
- Jagodzinski, E. A., Reid, A., & Gribbin, G. (2019). U-Pb geochronological data from the Fowler Domain, western Gawler Craton. *Department for Energy and Mining, South Australia, Report Book 2019/00018*, 58.
- Joly, A., Porwal, A., McCuaig, T. C., Chudasama, B., Dentith, M. C., & Aitken, A. R. (2015). Mineral systems approach applied to GIS-based 2D-prospectivity modelling of geological regions: Insights from Western Australia. *Ore Geology Reviews*, 71, 673-702. <https://doi.org/10.1016/j.oregeorev.2015.06.007>
- Kemp, E. M. (1978). Tertiary climatic evolution and vegetation history in the southeast Indian Ocean region. *Palaeogeography, Palaeoclimatology, Palaeoecology*, 24(3), 169-208. [https://doi.org/10.1016/0031-0182\(78\)90042-1](https://doi.org/10.1016/0031-0182(78)90042-1)
- Kinny, P.D., & Nutman, A.P.(1996). Zirconology of the Meeberrie gneiss, Yilgarn craton, Western Australia: An early Archaean migmatite. *Precambrian Research*, 78, 165-178. [https://doi.org/10.1016/0301-9268\(95\)00076-3](https://doi.org/10.1016/0301-9268(95)00076-3)
- Kirkland, C. L., Barham, M., & Danišik, M. (2020). Find a match with triple-dating: Antarctic sub-ice zircon detritus on the modern shore of Western Australia. *Earth and Planetary Science Letters*, 531, 115953. <https://doi.org/10.1016/j.epsl.2019.115953>

- Kirkland, C. L., Smithies, R., & Spaggiari, C. (2015). Foreign contemporaries—Unravelling disparate isotopic signatures from Mesoproterozoic Central and Western Australia. *Precambrian Research*, 265, 218-231.  
<https://doi.org/10.1016/j.precamres.2014.12.001>
- Kirkland, C. L., Smithies, R. H., Spaggiari, C. V., Wingate, M., De Gromard, R. Q., Clark, C., . . . Belousova, E. A. (2017). Proterozoic crustal evolution of the Eucla basement, Australia: Implications for destruction of oceanic crust during emergence of Nuna. *Lithos*, 278, 427-444.  
<https://doi.org/10.1016/j.lithos.2017.01.029>
- Kirkland, C. L., Smithies, R. H., Woodhouse, A. J., Howard, H. M., Wingate, M. T., Belousova, E. A., . . . Spaggiari, C. V. (2013). Constraints and deception in the isotopic record; the crustal evolution of the west Musgrave Province, central Australia. *Gondwana Research*, 23(2), 759-781.  
<https://doi.org/10.1016/j.gr.2012.06.001>
- Kirkland, C. L., Spaggiari, C. V., Pawley, M., Wingate, M., Smithies, R. H., Howard, H., . . . Poujol, M. (2011a). On the edge: U–Pb, Lu–Hf, and Sm–Nd data suggests reworking of the Yilgarn craton margin during formation of the Albany-Fraser Orogen. *Precambrian Research*, 187(3-4), 223-247.  
<https://doi.org/10.1016/j.precamres.2011.03.002>
- Kirkland, C., Spaggiari, C., Wingate, M., Smithies, R., Belousova, E., Murphy, R., & Pawley, M. (2011b). Inferences on crust–mantle interaction from Lu–Hf isotopes: a case study from the Albany–Fraser Orogen. *Geological Survey of Western Australia, Record*, 2011/12, 25.
- Komar, P. D. (2007). The entrainment, transport and sorting of heavy minerals by waves and currents. *Developments in Sedimentology*, 58, 3-48.  
[https://doi.org/10.1016/S0070-4571\(07\)58001-5](https://doi.org/10.1016/S0070-4571(07)58001-5)
- Legendre, P., & Legendre, L. (1998). *Numerical Ecology*. (2nd English ed.). In: Elsevier Science, Amsterdam.
- Li, N., Xiao, K., Sun, L., Li, S., Zi, J., Wang, K., . . . Li, C. (2018). Part I: A resource estimation based on mineral system modelling prospectivity approaches and analogical analysis: A case study of the MVT Pb-Zn deposits in Huayuan district, China. *Ore Geology Reviews*, 101, 966-984.  
<https://doi.org/10.1016/j.oregeorev.2018.02.014>
- Li, Q., James, N., & McGowran, B. (2003). Middle and Late Eocene Great Australian Bight lithostratigraphy and stepwise evolution of the southern Australian continental margin. *Australian Journal of Earth Sciences*, 50(1), 113-128. <https://doi.org/10.1046/j.1440-0952.2003.00978.x>
- Lowry, D. C. (1970). Geology of the Western Australian part of the Eucla Basin. *Geological Survey of Western Australia. Bulletin* 122, 201.
- Makuluni, P., Kirkland, C., & Barham, M. (2019). Zircon grain shape holds provenance information: a case study from southwestern Australia. *Geological Journal*, 54(3), 1279-1293. <https://doi.org/10.1002/gj.3225>
- Mao, X., Ren, J., Liu, Z., Chen, J., Tang, L., Deng, H., . . . Liu, C. (2019). Three-dimensional prospectivity modeling of the Jiaojia-type gold deposit, Jiaodong Peninsula, Eastern China: A case study of the Dayingezhuang deposit.

- Journal of Geochemical Exploration*, 203, 27-44.  
<https://doi.org/10.1016/j.gexplo.2019.04.002>
- Markwitz, V., & Kirkland, C. (2018). Source to sink zircon grain shape: Constraints on selective preservation and significance for Western Australian Proterozoic basin provenance. *Geoscience Frontiers*, 9(2), 415-430.  
<https://doi.org/10.1016/j.gsf.2017.04.004>
- McCuaig, T. C., & Hronsky, J. M. (2014). The mineral system concept: the key to exploration targeting. *Society of Economic Geologists Special Publication*, 18, 153-175. <https://doi.org/10.5382/SP.18.08>
- Moecher, D. P., & Samson, S. D. (2006). Differential zircon fertility of source terranes and natural bias in the detrital zircon record: Implications for sedimentary provenance analysis. *Earth and Planetary Science Letters*, 247(3), 252-266. <https://doi.org/10.1016/j.epsl.2006.04.035>
- Mole, D. R., Kirkland, C. L., Fiorentini, M. L., Barnes, S.J., Cassidy, K.F., Isaac, C., Belousova, E.A., Hartnady, M., and Thebaud, N. (2019). Time-space evolution of an Archean craton: A Hf-isotope window into continent formation. *Earth-Science Reviews*, 196, 102831.  
<https://doi.org/10.1016/j.earscirev.2019.04.003>
- Morón, S., Cawood, P. A., Haines, P. W., Gallagher, S. J., Zahirovic, S., Lewis, C. J., & Moresi, L. (2019). Long-lived transcontinental sediment transport pathways of East Gondwana. *Geology*, 47(6), 513-516.  
<https://doi.org/10.1130/g45915.1>
- Morton, A. C., & Hallsworth, C. R. (1999). Processes controlling the composition of heavy mineral assemblages in sandstones. *Sedimentary Geology*, 124(1), 3-29. [https://doi.org/10.1016/S0037-0738\(98\)00118-3](https://doi.org/10.1016/S0037-0738(98)00118-3)
- Neumann, N., & Korsch, R. J. (2014). SHRIMP U-Pb zircon ages for Kutjara 1 and Mulyawara 1, Northwestern South Australia. *Geoscience Australia, Canberra, Record 2014/5*, p. 18.
- Olierook, H., Barham, M., Fitzsimons, I., Timms, N., Jiang, Q., Evans, N., & McDonald, B. (2018). Tectonic controls on sediment provenance evolution in rift basins: Detrital zircon U-Pb and Hf isotope analysis from the Perth Basin, Western Australia. *Gondwana Research*, 66.  
<https://doi.org/10.1016/j.gr.2018.11.002>
- Porwal, A., González-Álvarez, I., Markwitz, V., McCuaig, T., & Mamuse, A. (2010). Weights-of-evidence and logistic regression modeling of magmatic nickel sulfide prospectivity in the Yilgarn Craton, Western Australia. *Ore Geology Reviews*, 38(3), 184-196. <https://doi.org/10.1016/j.oregeorev.2010.04.002>
- Pupin, J. (1980). Zircon and granite petrology. *Contributions to mineralogy and petrology*, 73(3), 207-220. <https://doi.org/10.1007/BF00381441>
- Reid, A. J. (2019). The Olympic Cu-Au province, Gawler craton: A review of the lithospheric architecture, geodynamic setting, alteration systems, cover successions and prospectivity. *Minerals*, 9, 371.  
<https://doi.org/10.3390/min9060371>

- Reid, A. J., & Hou, B. (2006). Source of heavy minerals in the Eucla Basin palaeobeach placer province, South Australia: age data from detrital zircons. *MESA Journal*, 42, 10-14.
- Reid, A. J., Keeling, J. L., & Belousova, E. A. (2013b). Hf isotopic investigation into the provenance of zircons in heavy mineral sands of the Eucla Basin. *MESA Journal*, 68, 17-24.
- Reid, A. J., Keeling, J. L., Boyd, D., Belousova, E. A., & Hou, B. (2013a). Source of zircon in world-class heavy mineral placer deposits of the Cenozoic Eucla Basin, southern Australia from LA-ICPMS U–Pb geochronology. *Sedimentary Geology*, 286-287, 1-19.  
<https://doi.org/10.1016/j.sedgeo.2012.10.008>
- Reid, A. J., Pawley, M., Wade, C., Jagodzinski, E., Dutch, R., & Armstrong, R. (2020). Resolving tectonic settings of ancient magmatic suites using structural, geochemical and isotopic constraints: the example of the St Peter Suite, southern Australia. *Australian Journal of Earth Sciences*, 67(1), 31-58.  
<https://doi.org/10.1080/08120099.2019.1632224>
- Reid, A. J., & Payne, J. L. (2017). Magmatic zircon Lu–Hf isotopic record of juvenile addition and crustal reworking in the Gawler Craton, Australia. *Lithos*, 292, 294-306. <https://doi.org/10.1016/j.lithos.2017.08.010>
- Roberts, N. M. (2012). Increased loss of continental crust during supercontinent amalgamation. *Gondwana Research*, 21(4), 994-1000.  
<https://doi.org/10.1016/j.gr.2011.08.001>
- Rueden, C. T., Schindelin, J., Hiner, M. C., DeZonia, B. E., Walter, A. E., Arena, E. T., & Eliceiri, K. W. (2017). ImageJ2: ImageJ for the next generation of scientific image data. *BMC bioinformatics*, 18(1), 529.  
<https://doi.org/10.1186/s12859-017-1934-z>
- Sandiford, M. (2007). The tilting continent: a new constraint on the dynamic topographic field from Australia. *Earth and Planetary Science Letters*, 261(1-2), 152-163. <https://doi.org/10.1016/j.epsl.2007.06.023>
- Schindelin, J., Arganda-Carreras, I., Frise, E., Kaynig, V., Longair, M., Pietzsch, T., . . . Schmid, B. (2012). Fiji: an open-source platform for biological-image analysis. *Nature methods*, 9(7), 676-682. <https://doi.org/10.1038/nmeth.2019>
- Schneider, C. A., Rasband, W. S., & Eliceiri, K. W. (2012). NIH Image to ImageJ: 25 years of image analysis. *Nature methods*, 9(7), 671-675.  
<https://doi.org/10.1038/nmeth.2089>
- Schuilting, R., Scholten, M., de Meijer, R., & Riezebos, H. (1985). Grain size distribution of different minerals in a sediment as a function of their specific density. *Geologie en Mijnbouw*, 64(2), 199-203. Retrieved from [https://inis.iaea.org/search/search.aspx?orig\\_q=RN:18055974](https://inis.iaea.org/search/search.aspx?orig_q=RN:18055974)
- Serra, J. (1983). *Image analysis and mathematical morphology*: Academic Press, Inc.
- Sláma, J., & Košler, J. (2012). Effects of sampling and mineral separation on accuracy of detrital zircon studies. *Geochemistry, Geophysics, Geosystems*, 13(5), 1525-2027. <https://doi.org/10.1029/2012GC004106>
- Spaggiari, C. V., Bodorkos, S., Barquero-Molina, M., Tyler, I., & Wingate, M. (2009). Interpreted bedrock geology of the south Yilgarn and central Albany-

- Fraser orogen, Western Australia. *Geological Survey of Western Australia, Record*, 2009/10, 84.
- Spaggiari, C. V., Kirkland, C. L., Smithies, R. H., Wingate, M., & Belousova, E. A. (2015). Transformation of an Archean craton margin during Proterozoic basin formation and magmatism: The Albany–Fraser Orogen, Western Australia. *Precambrian Research*, 266, 440-466.  
<https://doi.org/10.1016/j.precamres.2015.05.036>
- Spaggiari, C. V., Smithies, R. H., Kirkland, C. L., Wingate, M. T. D., England, R. N., & Lu, Y.-J. (2018). Buried but preserved: The Proterozoic Arubiddy Ophiolite, Madura Province, Western Australia. *Precambrian Research*, 317, 137-158. <https://doi.org/10.1016/j.precamres.2018.08.025>
- Spaggiari, C. V., Smithies, R.H., Wingate, M., Kirkland, C. L., & England, R. N. (2016). Exposing the Eucla basement: what separates the Albany–Fraser Orogen and the Gawler Craton. *GSWA 2016 extended abstracts: promoting the prospectivity of Western Australia. Geological Survey of Western Australia*, 36-41.
- Spencer, C. J., Kirkland, C. L., Roberts, N. M. W., Evans, N. J., & Liebmann, J. (2020). Strategies towards robust interpretations of in situ zircon Lu–Hf isotope analyses. *Geoscience Frontiers*, 11(3), 843-853.  
<https://doi.org/10.1016/j.gsf.2019.09.004>
- Sundell, K. E., & Saylor, J. E. (2021). Two-Dimensional Quantitative Comparison of Density Distributions in Detrital Geochronology and Geochemistry. *Geochemistry, Geophysics, Geosystems*, 22(4), e2020GC009559.  
<https://doi.org/10.1029/2020GC009559>
- Syverud, K., Chinga Carrasco, G., Johnsen, O., Leirset, I., & Wiik, K. (2007). Analysis of lint particles from full-scale printing trials. *Appita Journal*, 60, 286-290.
- Vavra, G. (1990). On the kinematics of zircon growth and its petrogenetic significance: a cathodoluminescence study. *Contributions to mineralogy and petrology*, 106(1), 90-99. <https://doi.org/10.1007/BF00306410>
- Vermeesch, P. (2013). Multi-sample comparison of detrital age distributions. *Chemical geology*, 341, 140-146.  
<https://doi.org/10.1016/j.chemgeo.2013.01.010>
- Wilde, S., & Hickman, A. H. (2001). Jimperding and Chittering metamorphic belts, southwestern Yilgarn Craton, Western Australia: a field guide. *Geological Survey of Western Australia, Record* 2001/12, 24.
- Wingate, M., Kirkland, C., Spaggiari, C., & Smithies, R. (2015). U–Pb geochronology of the Forrest Zone of the Coompana Province. *Eucla basement stratigraphic drilling results release workshop: extended abstracts compiled by CV Spaggiari and RH Smithies: Geological Survey of Western Australia, Record* 2015/10, 37-40.
- Wise, T., Dutch, R., Pawley, M., Foss, C., & Thiel, S. (2018). Building the Coompana Province. *MESA Journal*, 88, 25-37.
- Woodhead, J. D., & Hergt, J. M. (2005). A preliminary appraisal of seven natural zircon reference materials for in situ Hf isotope determination. *Geostandards*

and *Geoanalytical Research*, 29(2), 183-195. <https://doi.org/10.1111/j.1751-908X.2005.tb00891.x>

- Wyborn, L., Heinrich, C., & Jaques, A. (1994). Australian Proterozoic mineral systems: essential ingredients and mappable criteria. *Australasian Institute of Mining and Metallurgy Publication Series 5/94*, 109-115.
- Wyche, S., Kirkland, C., Riganti, A., Pawley, M., Belousova, E., & Wingate, M. (2012). Isotopic constraints on stratigraphy in the central and eastern Yilgarn Craton, Western Australia. *Australian Journal of Earth Sciences*, 59(5), 657-670. <https://doi.org/10.1080/08120099.2012.697677>
- Zeh, A., Gerdes, A., Klemm, R., & Barton, J. M. (2008). U–Pb and Lu–Hf isotope record of detrital zircon grains from the Limpopo Belt – Evidence for crustal recycling at the Hadean to early-Archean transition. *Geochimica et Cosmochimica Acta*, 72(21), 5304-5329. <https://doi.org/10.1016/j.gca.2008.07.033>
- Zutterkirch, I. C., Kirkland, C. L., Barham, M., & Elders, C. (2021). Thin-section detrital zircon geochronology mitigates bias in provenance investigations. *Journal of the Geological Society*.



## CHAPTER FOUR

### Research Conclusions

Beach heavy mineral placer deposits from the Cenozoic Eucla Basin express polymodal detrital zircon age spectra that indicate sediment sourcing primarily originated from Mesoproterozoic sources with minor detritus from various regionally specific late Archean to early Phanerozoic-aged crustal units. The western Eucla Basin indicates a more restricted sediment sourcing (Albany-Fraser Orogen and Yilgarn Craton), while northern and eastern margins show increased intermixing of Mesoproterozoic sources (Musgrave, Madura and Coompana provinces and Albany-Fraser Orogen) with minor Archean contributions (Gawler Craton and Yilgarn Craton). Depositional shoreline settings of Eucla Basin placer deposits are reinterpreted with digital elevation modelling and integrated similarity testing of heavy mineral U-Pb age spectra, identifying a unique Miocene enrichment phase with restricted Yilgarn Craton sediment supply to the eastern Jacinth deposit at an intersection of Miocene and Eocene shoreline trends. Heavy mineral assemblages and grades of placer deposits vary along the basin margins from west to east, expressing increased retention of resistate over labile minerals (a function of mineral reworking) and progressive heavy mineral enrichment. This heavy mineral upgrading is correlated to the time minerals were transported, intermixed, and recycled within a sedimentary system, and can be quantified using a Shannon-Weaver heterogeneity test on detrital zircon age spectra. Heterogeneity analysis on detrital zircon age spectra gives an indication of the degree of sediment mixing and the maturation zircon populations have undergone by quantitatively measuring the number and distribution of varying zircon ages present within a sample. Detrital zircon age spectra similarities across different placer deposits indicates that detrital supply from proximal source regions is temporally non-unique, and differently aged barrier systems (Ooldea and Barton barriers) were affected by similar sediment supply regimes. Hf isotope analysis on Eucla Basin heavy mineral samples offers a more refined sediment provenance interpretation that highlights a dominant juvenile magmatic Mesoproterozoic source for northern and eastern lying beach placers (northern lying Musgrave Province or the underlying Madura and Coompana provinces). Implementation of additional grain

shape characterisations on detrital and crystalline samples demonstrate that U-Pb and Hf-isotope source rock ambiguities can be resolved. Eucla Basin Mesoproterozoic sources impart unique shape characteristics that are identified through Kolmogorov-Smirnov dissimilarity tests and visualised with box and whisker plots. Median *perimeter* and median *major axis* values of zircon grains are overall smaller for the Madura and Coompana province zircons ( $P < 550 \mu\text{m}$ ,  $\text{MaA} < 170 \mu\text{m}$ ) compared to those sampled from the Musgrave Province ( $P > 550 \mu\text{m}$ ) and Albany-Fraser Orogen ( $\text{MaA} > 170 \mu\text{m}$ ), while zircon grains from the Musgrave Province are overall less circular ( $C_i < 0.64$ ) than those sampled from the Albany-Fraser Orogen ( $C_i > 0.64$ ). Through stepwise filtering of U-Pb, Hf isotope and grain shape analysis, a dominant Madura and Coompana provinces' supply to northern and eastern Eucla Basin palaeoshorelines, through extensive reworking of older sedimentary systems, is identified. While this analysis is basin-specific and requires extensive sets of U-Pb age, Hf isotope, and grain shape data for detrital and crystalline zircon grains, the approach offers readily employed and cheap advances for conventional sediment provenance studies where source regions may be best distinguished by shape characteristics, or where this additional fingerprinting tool can differentiate otherwise geochronologically or geochemically identical but geographically distinct zircon grain sources. Future sediment provenance investigations utilising grain shape analysis may benefit from bulk mounting of detrital samples from which grain shape analysis should be performed prior to U-Pb and Hf isotope composition analyses. This ensures greater grain yields that are necessary for more nuanced sediment provenance interpretations and prevents potential grain size bias introduced from hand-selecting of zircon grains.